On exploration of Mechanical Insights into Bipedal Walking: Gait Characteristics, Energy Efficiency, and Experimentation

by

Mansoor Alghooneh

A Thesis submitted to the Faculty of Graduate Studies of

The University of Manitoba

in partial fulfilment of the requirements of the degree of

Doctor of Philosophy

Department of Mechanical Engineering

University of Manitoba

Abstract

Human walking is dynamic, stable, and energy efficient. To achieve such remarkable legged locomotion in robots, engineers have explored bipedal robots developed based on two paradigms: trajectory-controlled and passive-based walking. Trajectory-controlled bipeds often deliver energy-inefficient gaits. The reason is that these bipeds are controlled via high-impedance geared electrical motors to accurately follow predesigned trajectories. Such trajectories are designed to keep a biped locally balanced continually while walking.

On the other hand, passive-based bipeds provide energy-efficient gaits. The reason is that these bipeds adapt to their natural dynamics[1]. Such gaits are stable limit-cycles through entire walking motion, and do not require being locally balanced at every instant during walking. However, passive-based bipeds are often of round/point foot bipeds that are not capable of achieving and experiencing standing, stopping, and some important bipedal gait phases and events, such as the double support phase. Therefore, the goals of this thesis are established such that the aforementioned limitations on trajectory-controlled and passive-based bipeds are resolved.

Toward the above goal, comprehensive simulation and experimental explorations into bipedal walking have been carried out. Firstly, a novel systematic trajectory-controlled gait-planning framework has been developed to provide mechanical insights into bipedal walking in terms of gait characteristics and energy efficiency. For the same purpose, a

[1]Natural dynamics of a mechanism is the result of movement of passive components such as mass, geometry, and spring.

novel mathematical model of passive-based bipedal walking with compliant hip-actuation and compliant-ankle flat-foot has been developed. Finally, based on mechanical insights that have been achieved by the aforementioned passive-based model, a physical prototype of a passive-based bipedal robot has been designed and fabricated. The prototype experimentally validates the importance of compliant hip-actuation in achieving a highly dynamic and energy efficient gait.

This thesis has concluded that:

1. The systematic trajectory-controlled gait-planning framework has improved the walking speed and the energy efficiency of bipedal gaits, relative to available trajectory-controlled approaches [1–11].

2. Passive-based bipedal walking with compliant hip-actuation and compliant-ankle flat-foot can deliver more dynamic and energy efficient bipedal gaits, relative to current trajectory-controlled and passive-based gaits in the literature [4, 12–19]. They are also close to human walking. Such gaits have then been used to achieve invaluable mechanical insights into bipedal walking:

    - the first major finding is that two-sided ankle compliance (stiffer backside stiffness than frontside) can improve the performance of bipedal walking in terms of gait properties and energy efficiency, as compared with uniform ankle compliance (the same backside stiffness to frontside).
    - the second major finding is that single-support heel-off, which occurs when the heel of the stance leg has been lifted from the ground, while the swing leg is still swinging forward, is a crucial gait event which can significantly improve the performance of bipedal walking in terms of gait properties and energy efficiency.

3. Based on mechanical insights that have been achieved by the aforementioned passive-based model, a physical prototype of a passive-based bipedal robot has shown a

highly dynamic and energy efficient gait, relative to available walking prototypes in the literature [4, 12–19]. The prototype experimentally validated the important role of compliant hip-actuation in achieving such a walking gait on the flat ground. Note that the inclusion of compliant-ankle flat-foot in the physical prototype remains as future work.

To my parents

and

to my love

Masoumeh

Acknowledgments

I would like to thank my thesis adviser, Professor Christine Q. Wu, for her invaluable advice, support, guidance, patience, and friendship during my Ph. D. study at the Nonlinear Systems Research Laboratory. She has taught me to be a better communicator, both in publications and in presentations. She has always encouraged me to pursue novel intuitive ideas that will have impact and significance. I am deeply grateful for her faith and trust that the bipedal prototype would always work better, particularly when I was struggling to design, build, and improve the prototype.

One of my unique opportunity at the University of Manitoba, indeed, was to work with Professor Subramaniam Balakrishnan (Bala) as his Teaching Assistant for the Design and Manufacturing course. He generously shared with me his excellent experimental/pragmatic visions into the design and manufacturing of Mechatronic systems, during all discussions we had.

I sincerely appreciate all of considerations of my advisory committee members, Professors Bala, Anderson, and Park for their careful review, comments, and suggestions.

I wish to thank all my lab mates for being a good ally during my Ph.D. study, specially unforgettable kindness and support of Alireza.

I wish to send my gratitude to my brothers and sisters for their constant support and encouragement, and to my parents who have always supported me, and have made it possible for me to start this journey.

Lastly and most importantly to my love, Masoumeh; I give my deepest appreciation to her, as in spite of all uncertainties in life, she is always the constant. We have started our Ph.D. together, and during this time, she has been both the best friend and the best fellow for me. She is the greatest inspirational person I have ever known, and I will be thankful of her for sharing her knowledge and futuristic vision with me through my Ph.D., career, and life.

Co-Authorship

Chapters 2 and 4 contain contents from two journal papers[2] [20] and [21], and two conference papers[3] [22] and [23]. The papers were written by the author, and were reviewed by Dr. Christine Q. Wu.

Chapter 4 is in preparation to be submitted to ASME Transactions - Journal of Mechanisms and Robotics.

[2]International Journal of Humanoid Robotics, 2012 and Robotica - Cambridge Journals, 2014.
[3]CSME international conference, 2012 and Dynamic Walking Conference, 2013.

Contents

List of Figures

List of Tables

Chapter 1

Introduction

1.1 Motivation

This thesis provides mechanical insights into bipedal (human-like) walking, aiming at improving the design and development of bipedal robots and rehabilitation devices. Bipedal robots are one of the best alternatives to humans to perform difficult tasks in environments designed for humans. The reconfigurable structure of the legs of these robots allows to traverse rough terrains, such as stairs and uneven pathways. In addition, rehabilitation devices, such as intelligent prostheses and exoskeletons, are another motivation of this research. Such devices are considered as assisting tools to restore/recover the functionality of damaged/dysfunctional lower-body limbs.

Issues with available bipedal robots and rehabilitation devices in the literature are that these machines cannot exhibit dynamic, energy efficient, and versatile walking simultaneously. Bipedal robots can mostly be categorized into two paradigms: trajectory-controlled and passive-based walking [4,12–19]. Trajectory-controlled bipeds are fully actuated based on controlling high-impedance geared electrical motors to accurately follow predesigned gaits. Passive-based bipeds are semi (low-impedance) actuated based on the concept of

passive dynamic gaits. Predesigned gaits are locally balanced at every instant during walking, while passive dynamic gaits are stable limit-cycles through entire walking motion.

Trajectory-controlled bipeds are versatile to walk on uneven terrains with different walking speed, but are energy inefficient. Passive-based bipeds are energy efficient, but not versatile to walk on uneven terrains with different speed. On the other hand, rehabilitation devices such as intelligent lower-body prostheses mostly are not dextrous enough to be equipped with some important joints such as the ankle joints. As a result, the outcome of this thesis can significantly improve the performance of bipedal robots and rehabilitation devices in terms of gait characteristics and energy efficiency.

1.2 Basics of a gait cycle

1.2.1 Gait phases

A bipedal gait cycle consists of two phases [29]: the single-support and the double-support phases. During the single-support phase, one leg is the stance, and is always in contact with the ground via heel, toe, or both, while the other leg is swinging forward. During the double-support phase, however, both legs are the stance legs, and are in contact with the ground via heel, toe, or both, such that the body can be moving forward. The transition between the single-support phase to the double-support phase is the strike phase. The strike transition can be either heel-strike or foot-strike. Heel-strike is when the heel hits the ground, and foot-strike is when the entire foot hits the ground.

1.2.2 Gait planes

Bipedal walking can be projected into two planes, the sagittal plane and the frontal plane. The sagittal plane is a vertical plane which passes from anterior to posterior, dividing the body into right and left halves, and is often used when the gait properties in 2D walking

are to be explored [29]. The frontal plane is any vertical plane that divides the body into ventral and dorsal (belly and back) sections, and is often used when the gait properties in 3D walking are to be studied [29].

1.2.3 Gait characteristics and energy efficiency

Gait characteristics in bipedal walking are defined as the step length, step period, and walking speed [29]. The step length is defined as the distance between two successive placements of the same foot. The step period is defined as the time period during which the step length occurs [29]. The walking speed is defined as the speed of the center mass of the body when it is moving forward [29]. Energy efficiency is evaluated based on the cost of transport, and is a normalized energy cost. The cost of transport is defined as the amount of power consumption per weight per walking speed for each gait cycle [29].

1.3 Background and related work

Engineers have explored bipedal walking through two different walking categories: trajectory-controlled and passive-based walking. The advantages and disadvantages of each category will be discussed in the following sections.

1.3.1 Trajectory-controlled bipedal walking

Trajectory-controlled bipeds are controlled via high-impedance geared electrical motors to accurately follow predesigned trajectories. Such trajectories are designed to keep a biped locally balanced continually, while walking. ASIMO [13], HRP [24], WABIAN [16], Jennifer [30], and Nao [31] are examples of trajectory-controlled walking machines, shown in Figure 1.1. These robots show bipedal gaits that are versatile to perform difficult tasks such as climbing stairs [14] or ice skating [30], but are energy inefficient.

(a) (b) (c) (d)

Figure 1.1: Examples of trajectory-controlled bipedal robots: (a) ASIMO [13], (b) HRP [24], (c) WABIAN [16], (d) Jennifer [25].

1.3.1.1 Control strategies for trajectory-controlled bipeds

A common characteristic of trajectory-controlled bipedal robots is that all joints are controlled by high-impedance geared electrical motors to accurately follow predesigned trajectories. These trajectories are designed such that zero-moment-point (ZMP[1]) of a biped stays within the support-polygon[2] [29, 32–34]. As a result, the biped can be locally balanced, while walking. Because of the ZMP constraint, and since the controllers of these bipeds need to follow precisely the aforementioned trajectories, their energy consumption is unreasonably high [20, 27, 35].

Another issue with trajectory-controlled bipeds is that most of them walk with bent knees. Such a walking style allows the controllers to have authority over the entire upper-body dynamics, and helps to provide postural balance via upper body degrees of freedom. In addition, the aforementioned walking style allows these bipeds to avoid the control complexity due to heel-toe gait phases, which finally lead to unnatural walking [10, 21, 28, 36–38].

To improve the walking speed of trajectory-controlled bipeds, the modified ZMP has been applied to a bipedal robot, Jennifer [25]. The modified ZMP allows a bipedal robot to traverse indoor and outdoor ice surfaces more stably, as compared with a classic inverted pendulum-based walking concept [39]. As a result, a bipedal robot can perform ice skating [30], entirely based on the frontal plane movement to propel the robot forward.

To improve high energy cost of trajectory-controlled bipeds, researchers have designed and developed various optimal predesigned trajectories in joint space or task space [1, 3, 5–7, 11, 40–43]. Different control strategies have also been used to accurately follow the aforementioned "optimal" trajectories. Examples are Sliding Mode Control (SMC) [44], and Hybrid Zero Dynamic (HZD) [45], among others. However, the high-impedance

[1]The ZMP is a point on the ground where the moment of the total inertia forces including the gravitational forces, projected on the ground, becomes zero.

[2]Support polygon is the convex hull of the foot-support area.

hardware of a trajectory-controlled biped requires high controller gains to follow those "optimal" trajectories, finally leading to low energy efficiency [21, 28].

Furthermore, to improve the gait characteristics and the energy efficiency of trajectory-controlled bipeds, researchers have developed different actuation systems, while using the same control strategy [37, 46]. A bipedal robot named Lucy has been designed and built by the Vrije Universiteit Brussel [46]. The unique feature of this robot is its actuation system. The robot is actuated via pleated pneumatic artificial muscles which allow both the torque and the compliance to be controllable. The control strategy is, however, to follow predesigned trajectories to keep the robot locally balanced. Such a control suppresses the natural dynamics of the robot, and eventually leads to slow and energy inefficient bipedal walking.

1.3.1.2 Balance strategies for trajectory-controlled bipeds

Human walking is the main source of inspiration for the design and development of bipedal gaits. Observing natural human walking, researchers have proposed three biomechanically motivated characteristics for bipedal gaits: the gait repeatability, [47–49] postural balance, [50–52] highly regulated centroidal angular momentum (CAM) [52, 53].

Each individual walks in a fairly repeatable way. Gait repeatability is generally divided into two parts: postural and velocity repeatability. In distinction to postural repeatability, to satisfy velocity repeatability, gait-planning strategies require dealing with two-point boundary value problems (BVPs), which are a much more challenging issue than initial value problems [29, 48]. Non-zero impact[3] also causes BVPs to be more complex, since it causes discontinuity in velocity repeatability [48]; even though, non-zero impact provides faster locomotion for a biped.

Bipedal gaits are inherently unstable, so there is a strong need to negotiate their pos-

[3]The non-zero impact means that the foot hits the ground at non-zero velocity.

tural stability/balance. Elftman et al. [32] found that postural balance of natural bipedal walking is somehow related to the location of the ground reaction force, which was revised later by Vukobratovic et al. [51] as the Zero-Moment point (ZMP) measure. The ZMP is a point on the ground where the moment of the total inertia force consisting of inertia and gravitational forces, projected on the ground, becomes zero [29, 51]. The postural balance of bipedal walking is guaranteed, provided that the support polygon of the biped covers the ZMP. The support polygon is the convex hull of the foot-support area. In addition to the ZMP, a few postural balance measures [36, 50] have then been presented, among others, Goswami [50] developed the Foot-Rotation Indicator (FRI) measure to monitor the severity of the postural instability of bipedal gaits.

Popovic et al. [53] reported that centroidal angular momentum (CAM) of natural human walking remains highly regulated by the central nervous system. The physical concept behind the regulation of CAM is about rotational equilibrium condition for the body [52, 54]. To quantify the regulation of CAM, some measures have recently been proposed such as the Zero Rate of Angular Momentum (ZRAM), [55] the Zero Spin Center of Pressure (ZSCP), [56] and the Centroidal Moment Pivot (CMP) [52]. These measures do not monitor postural balance, yet a condition for the body rotational equilibrium [52]. The CMP, defined by Popovic et al. [52], is a point where the ground reaction force would have to apply to keep CAM conserved. It is important to point out that CAM is considered highly regulated for bipedal walking during the single-support phase, provided that the CMP-ZMP separation distant normalized by foot length is less than 14% [52].

Bipedal robots possess highly nonlinear multi-link dynamics, that causes satisfying dynamic-based characteristics of a biped, such as the ZMP and the CAM, complex [29,48]. In order to reduce the complexity, researchers have employed inverted pendulum models (IPMs) instead of original multi-link bipedal robots for gait planning since IPMs present conceptual insights into the dynamics of bipeds. IPMs consist of a single mass representing

the center of mass of a biped, which is connected to the Center of Pressure (COP) of a biped by a virtual link [8, 43]. The ZMP and the CAM of a biped cannot be negotiated by both the hip and the swing ankle using conventional IPMs since their CAM is always zero due to their concentrated mass at the center of mass [57]. However, referring to the Gravity-Compensated Inverted Pendulum Model (GCIPM) introduced by Park [58], which involves the dynamics of the swing ankle and the hip, the ZMP and the CAM of a biped can be negotiated by both the hip and the swing ankle. Note that the GCIPM consists of three single concentrated masses placed at the hip and the ankles. The masses are connected together to the supporting foot of the biped by virtual links.

Although all the aforementioned biomechanically motivated characteristics have been reported and explored individually in the literature, there is no trajectory-controlled gait-planning framework available to negotiate all three in the process of design a bipedal gait simultaneously.

1.3.2 Passive-based bipedal walking

Passive-based bipeds adapt to their natural dynamics[4], and are semi (low-impedance) actuated based on the concept of passive dynamic gaits. Such gaits are stable limit-cycles through entire walking motion, and do not require being locally balanced at every instant during walking. In comparison to trajectory-controlled bipedal walking, passive-based bipedal walking is energy efficient [12, 15, 18, 35, 59–64], but not versatile to walk on uneven terrains with different speed.

An example of passive-based bipeds is a passive dynamic walker that mostly is achieved when a biped is walking down a gentle slope, entirely driven by the gravitational forces [12] with no controlled actuation. Several passive-based bipedal walkers are shown in Figure

[4]Natural dynamics of a mechanism is the result of passive components such as mass, geometry, and spring.

(a) 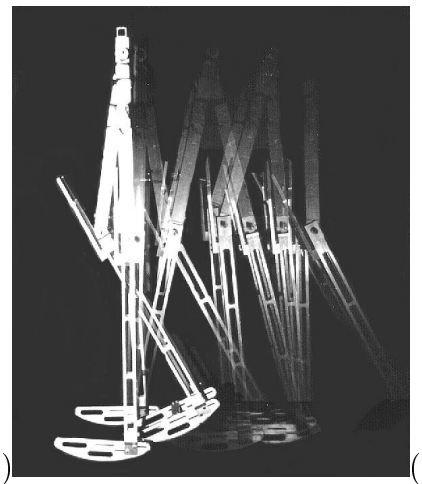 (b)  (c) 

Figure 1.2: Passive bipedal walkers: (a) McGeer's [12], (b) Cornell's [15], and (c) Dexter III [26].

1.2. The reason, why passive-based bipedal walking is dynamic, is because of their unique inherent cyclic stability. Such a gait is a stable limit-cycle [12,15,60]. As a result, a passive gait does not require local balance (ZMP) at every instant during walking [12,33].

One of the reasons for a passive-based walker to be energy efficient is that low impedance at their joints helps their natural dynamics to drive the machine forward. Such low impedance allows these walking machines to adapt to their natural dynamics quite well. In addition, since there are mostly no controlled actuation systems in such systems, there is no energy dissipation due to gearbox friction and inertia.

To achieve passive-based bipedal walking on the flat ground, there is a need to replace the gravitational source of energy by an active source of energy input. However, such a replacement is very challenging and if it is not performed properly, it will not lead to a walking machine with the same level of speed and energy efficiency as a passive-based walking machine driven by the gravitational source of energy [12].

There are two points that need to be considered when passive-based bipedal walking is modified to walk on the flat ground: actuation mechanisms which are in charge of active energy input, and numbers of passive/underactuated degrees of freedom. If the actuation

mechanism has high-impedance due to the high gearbox ratio, it will lead to energy-inefficiency and slow bipedal walking. In addition, if all degrees of freedom are actively assisted, it will again lead to an energy-inefficient bipedal walking. In other words, more actively-assisted degrees of freedom mean less energy efficiency for a biped. Therefore, there is a need to carefully select numbers of the active and passive degrees of freedom.

There are a few passive-based bipedal machines walking on flat ground, shown in Figure 1.3, which show both energy efficiency and dynamic gaits [17–19, 28]. All of these robots use active power sources to walk on the flat ground, by compensating the energy loss due to foot strikes and joint friction. The key of an acceptable performance for these walking robots is to take advantage of their natural dynamics to contribute to their motion.

The efficiencies of the above machines are evaluated via a dimensionless number named the cost of transport which is the amount of energy used per weight per distance traveled. To isolate the effectiveness of the mechanical design and the actuation, sensing, and control of a bipedal machine, there are two different costs of transport; the total cost of transport is all electrical energy (actuation, sensing, and control) that a bipedal machine uses to walk, and the mechanical cost of transport is only mechanical work of the actuators that a bipedal machine uses to walk.

The Spring Flamingo, shown in Figure 1.3, allows natural dynamics to contribute to its walking motion, using series elastic actuators [27]. As a result, the mechanical cost of transport of this machine is low. However, the aforementioned series elastic actuators used for force control produce and absorb mechanical work internally, so that the total cost of transport of this machine remains high. T.U. Delft's Denise, shown in Figure 1.3, harnesses natural dynamics, and uses pneumatic McKibben muscle actuators with high efficiency. It makes this machine to have an acceptable mechanical cost of transport. However, the onboard CO2 storage system requires an inefficient down-regulation of pressure, so the total cost of transport remains high. Cornell's two robots, shown in Figure 1.3, use

(a)  (b) 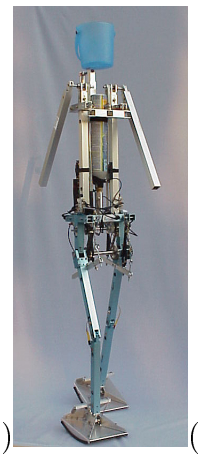 (c) 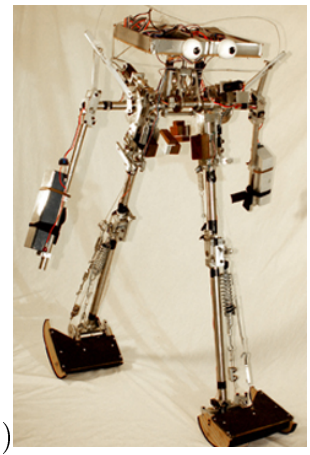 (d) 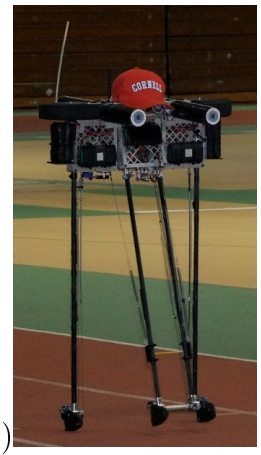

Figure 1.3: Passive-based bipedal robots walking on the flat ground: (a) MIT's Spring Flamingo [27], (b) T.U. Delft's Denise [19], (c and d) Cornell's [18], and Cornell's Ranger [28].

natural dynamics to keep their mechanical cost of transport low, and a zero-negative work actuation scheme, in which the actuation system only performs positive work, implemented with electric motors to keep the total cost of transport low as well.

Despite the advantages of the aforementioned bipedal robots, none of these robots have both low total and mechanical cost of transport, except Cornell's two machines. It shows that there is a need to explore new actuation strategies to coordinate natural dynamics and active energy input, with aiming at achieving higher energy efficient and dynamic gaits on the flat ground.

Despite the aforementioned advantages of passive-based bipedal robots, they are mostly of point/round feet that are not capable of achieving safe standing and experiencing foot strike, heel-off, and even double support phase. More importantly, their gait is mostly a sequence of the single support and the single impact. This makes their step length and walking speed fixed for a determined set of hip actuation, mass, and geometrical parameters. As a result, they are deprived of mechanical insights into the interaction between the ankle-foot and the ground. Such mechanical insights are significantly important in the design and development of efficient robotic lower-body prostheses.

To resolve the above limitations, a flat foot with a compliant ankle has recently been used [65–67]. A limited number of studies have explored the effects of the compliant ankles on bipedal walking in terms of energy consumption and gait selection [65–69]

Hobbelen and Wisse [68] explored the effects of ankle actuation on the energy efficiency of bipedal walking. They used a 2D flat-feet limit-cycle model actuated at the hip and the ankles. The hip was actuated to move the swing leg based on a predesigned motion, while the ankles were actuated to mimic the behavior of a torsional spring. As a result, they attained limit-cycle gaits of a fixed walking speed, and concluded that actuated-ankle flat-foot improves the energy efficiency of bipedal walking.

Following the aforementioned work, with a similar model, Huang et al. [65] applied torsional stiffness at the ankles where the ratio of the backside and the frontside ankle stiffness remains unchanged. For five different values of stiffness at the ankles, and five different torque profiles at the hip, they attained five flat-feet limit-cycle gaits. By comparing these limit-cycle gaits, they concluded that compliant-ankle flat-foot is very effective on gait selection of bipedal walking.

However, there are some deficiencies associated with the above studies. Firstly, it has not been demonstrated how a flat-feet limit-cycle gait exhibits versatile gait postures and events, as well as how flat-feet limit-cycle gaits were attained for a very limited range of ankle stiffness. Secondly, important questions about compliant ankle-foot remains unanswered, such that how two-sided ankle compliance influences bipedal walking, as compared with uniform ankle compliance. Single-support heel-off [5], a crucial gait event during human walking, has not been explored yet.

[5]Single-support heel-off occurs when the heel of the stance leg has been lifted from the ground, while the swing leg is still swinging forward.

1.4 Thesis objectives

The objective of this thesis is to provide mechanical insights into bipedal walking which can ultimately lead to dynamic, energy-efficient, and versatile bipedal gaits. Towards this goal, three major tasks have been carried out, listed as follows:

- A novel systematic trajectory-controlled gait-planning framework, which has been established based on biomechanically motivated gait characteristics, has been developed to improve the performance of bipedal walking in terms of gait characteristics (dynamic gait) and energy efficiency.
- A novel mathematical model of passive-based bipedal walking with compliant hip-actuation and compliant-ankle flat-foot, has been developed to improve the performance of bipedal walking in terms of gait characteristics (dynamic gait) and energy efficiency. The aforementioned model has then been used to reveal invaluable mechanical insights into bipedal walking about two-sided ankle compliance and single-support heel-off.
- A physical prototype of a bipedal walking robot has been designed and built to show a highly dynamic and energy-efficient gait. The prototype experimentally validates the importance of compliant hip-actuation in achieving such a walking gait. The inclusion of compliant-ankle flat-foot in the prototype remain as future work.

1.5 Thesis challenges

There is a number of challenges involved in this thesis, among which the major ones are as follows:

- Most conventional trajectory-controlled gait-planning approaches [3, 10, 24, 39, 42, 43, 70–72] are not established based on biomechanically motivated requirements. De-

velopment of a biomechanically motivated systematic gait-planning approach is a highly challenging task. The reason is that such a framework needs to be established based on a reduced-order simplified model that represents a realistic model accurately.

- Compared to point/round feet passive-based gaits in the literature [12, 15, 17, 19, 26] which possess one single gait series, passive-based bipedal walking with compliant hip-actuation and compliant-ankle flat-foot produces highly versatile limit-cycle gaits, comprised of a number of gait series, each of which is dictated by the kinetics of the unilateral constraints at the heel, toe, or both. Therefore, extracting such gaits becomes a highly challenging task, and requires a rigorous gait-detection algorithm.

- Design and development of a highly dynamic and energy-efficient bipedal walking robot requires the coordination between natural dynamics and active energy input, which is a very challenging task. The reason is that, geared electromechanical actuation systems cannot provide the aforementioned coordination. Hence, there is a need to develop a new custom-designed actuation system. Secondly, to have dynamic and energy-efficient bipedal walking on the flat ground, there is a need to have some passive joints such as passive knee joints. Thus, monitoring and tune such passive joints with least energy cost is a highly challenging task, and requires a custom-designed mechanism.

1.6 Thesis Outlines

Chapter 2 presents the development of a novel systematic trajectory-controlled gait-planning framework that negotiate biomechanically motivated gait characteristics. This chapter includes the development procedures of the framework, and simulation results that demonstrate how this framework works. Finally, the advantages and disadvantages

of such a framework are discussed, and concluding remarks are made.

Chapter 3 explains the development of a novel mathematical model of passive-based bipedal walking with compliant-ankle flat-foot, which is actively assisted via compliant hip-actuation to walk on the flat ground. This chapter demonstrates and discusses the properties of novel limit-cycle gaits. Such properties are compared with those of trajectory-controlled bipedal gaits achieved in Chapter 2. Finally, and more importantly, Chapter 3 is focused to answer two crucial questions about bipedal walking: firstly, how two-sided ankle compliance improves the performance of bipedal walking, as compared with uniform ankle compliance. Secondly, how single-support heel-off [6] helps improving the performance of bipedal walking.

Chapter 4 makes efforts to experimentally validate the importance of compliant hip-actuation in achieving a highly dynamic and energy efficient gait on the flat ground. For the proof of this concept, a physical prototype of a passive-based bipedal robot, equipped with custom-designed compliant hip-actuation and custom-designed spring-loaded knee-latch, has been designed and built. This chapter explains the mechanical design, actuation, sensing, coordination, and experimentation of the physical bipedal robot. Finally, it demonstrates and discusses a bipedal gait of the physical robot, followed by all steps taken in experimentation to reach such a gait. The inclusion of compliant-ankle flat-foot in the physical prototype remains as future work.

At the end, Chapter 5 presents the concluding remarks of this thesis, and discusses future work.

[6] Single-support heel-off occurs when the heel of the stance leg has been lifted from the ground, while the swing leg is still swinging forward.

Chapter 2

A systematic trajectory-controlled gait-planning framework

In this chapter, a novel systematic trajectory-controlled gait-planning framework is presented to provide mechanical insights into bipedal walking in terms of gait characteristics and energy efficiency. This is done by negotiating three biomechanically motivated characteristics: the gait repeatability, postural balance, and highly regulated centroidal angular momentum (CAM).

The framework is applied to a five-degrees-of-freedom bipedal model. Gaits designed by the framework consist of the single support and single impact phases. The framework employs a set of task-space variables and a set of gait parameters. Five kinematic and dynamic objective functions are selected, corresponding to the five degrees of freedom of the bipedal walking model. These objective functions negotiate the above three characteristics.

Combining the equations of the above five objective functions together, two ordinary differential equations called the framework equations are derived. They are being integrated through the gait cycle. The results are the motion profiles of the hip and the ankles.

The joint-motion profiles of the biped are then calculated via the inverse kinematics equations. The gait characteristics and energy efficiency of the biped for different gaits are calculated to draw conclusions.

2.1 Bipedal model

Figure 2.1 shows a five-link bipedal model which has a torso and two identical lower links with each link representing a thigh and a shank. The bipedal model has two hip joints, two knee joints, and two ankles. There is an actuator located at each joint and all of the joints are considered rotating only in the sagittal plane and friction free. Massless feet are assumed for the model. The biped can still apply torques at the ankles, even if the dynamics of the feet is neglected.

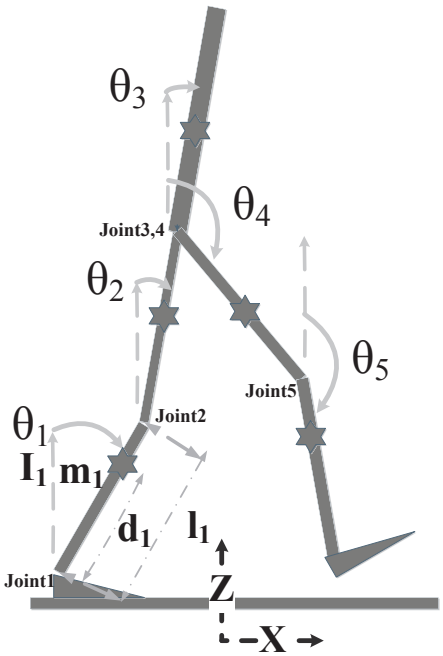

Figure 2.1: The five-link planar bipedal model.

In Figure 2.1, m_i and I_i are the mass and the mass inertia of link i, respectively. d_i, the location of the center of mass of link i, is measured as the distance between the center of

mass of link i to joint i. θ_i is also denoted as the angle of link i with respect to the vertical axis through joint i. d_i and θ_i have both been defined with respect to its lower joint. It is noteworthy that the coordinate system is attached to the ankle of the supporting foot.

The biped is studied during: the single support phase, and single impact phase. The single support phase is characterized by a supporting leg standing on the ground, while the other leg swings forward. The single impact phase is characterized by the fact that the impulsive force is only exerted to the tip of the swing link as it contacts the ground, while the stance link lifts immediately from the ground and does not receive external impulsive forces. Impact happens in an infinitesimal period of time as the swing link collides with the ground plastically, that is, when the single impact is completed, the swing link sticks on the ground, and the stance link lifts from the ground. At the end of each step, the swing link and the stance link exchange the role as is called switching to avoid repeated work of mathematical modeling.

2.1.1 Dynamic model of the biped

2.1.1.1 Dynamic equations for the single support phase

The dynamic model for the five-link bipedal robot during the single support phase is derived as the following form:

$$D(\theta)\ddot{\theta} + H(\theta, \dot{\theta})\dot{\theta} + G(\theta) = T_\theta \tag{2.1}$$

where, $D(\theta)$ is the 5×5 positive definite inertia matrix; $H(\theta, \dot{\theta})$ is the 5×5 matrix related to centrifugal and Coriolis terms, and $G(\theta)$ is the 5×1 vector of gravity terms. D, H, and G are presented in details in Appendix A. θ, $\dot{\theta}$, $\ddot{\theta}$, and T_θ are the 5×1 vectors of generalized coordinates, velocities, accelerations, and torques, respectively. T_θ represents the generalized torques, while τ_θ is the driving torques, which are applied to each joint.

The relation between $T_{\theta i}$ and $\tau_{\theta i}$ is obtained, defining the relative angle displacements (q_i):

$$q_1 = \theta_1$$

$$q_2 = 2\pi - \theta_1 + \theta_2$$

$$q_3 = -\theta_2 + \theta_3 \tag{2.2}$$

$$q_4 = 2\pi + \theta_4 - \theta_3$$

$$q_5 = -\theta_4 + \theta_5$$

Now, the relation is as follows: [73]

$$T_{\theta i} = \sum_{j=1}^{5} \tau_j \frac{\partial q_j}{\partial \theta_i} \qquad i = 1,\ 2,\ ...,\ 5 \tag{2.3}$$

The generalized torques are mapped to the driving torques, applying the following Matrix:

$$M = \begin{bmatrix} 1 & -1 & 0 & 0 & 0 \\ 0 & 1 & -1 & 0 & 0 \\ 0 & 0 & 1 & -1 & 0 \\ 0 & 0 & 0 & 1 & -1 \\ 0 & 0 & 0 & 0 & 1 \end{bmatrix} \tag{2.4}$$

The dynamic model is then rewritten as:

$$D(\theta)\,\ddot{\theta} + H(\theta, \dot{\theta})\,\dot{\theta} + G(\theta) = M\,\tau_\theta \tag{2.5}$$

2.1.1.2 Dynamic equations for the single Impact phase

The impact equations are derived, using Newtonian approach, applying the principle of conservation of impulse and momentum. The details of the derivation are presented in Appendix A. The impact phase is to establish a relation between the instant after the impact and the instant right before the impact. The relation is mathematically presented as follows: [20, 49]

$$\dot{\theta}^{t=T^-} = A\,\dot{\theta}^{t=T^+} \tag{2.6}$$

where, A is a 5×5 matrix with each element as a function of angular positions, and is full-ranked and is revertible. T^- and T^+ denote the instant right before impact and the instant after impact, respectively.

2.1.1.3 Switching phase

To ensure that the dynamic model is valid for the next step, there is a need to switch the role of the stance leg and the swing leg. The physical displacements do not change, but the link member used in the dynamic modeling, needs relabeling. The relabeling happens after impact since it is the beginning of a new step as follows:

$$\begin{bmatrix} \theta^{t=T_S^+} \\ \dot{\theta}^{t=T_S^+} \end{bmatrix} = \begin{bmatrix} \widetilde{T} & 0_{5\times5} \\ 0_{5\times5} & \widetilde{T} \end{bmatrix} \begin{bmatrix} \theta^{t=T^-} \\ \dot{\theta}^{t=T^+} \end{bmatrix} + \Pi \tag{2.7}$$

$$\widetilde{T} = \begin{bmatrix} 0 & 0 & 0 & 0 & 1 \\ 0 & 0 & 0 & 1 & 0 \\ 0 & 0 & 1 & 0 & 0 \\ 0 & 1 & 0 & 0 & 0 \\ 1 & 0 & 0 & 0 & 0 \end{bmatrix}$$

$$\Pi = \begin{bmatrix} \pi & \pi & 0 & \pi & \pi & 0 & 0 & 0 & 0 & 0 \end{bmatrix}^T$$

T^-, T^+, and T_S^+ have been represented the instant right before impact, after impact, and after switching, respectively. Combining Eqs. 2.6 and 2.7, the instant right before impact is mapped to the instant after switching or the beginning of the next gait cycle:

$$\begin{aligned} \theta^{t=T^-} &= \theta^{t=T_S^+} \\ \dot{\theta}^{t=T^-} &= (A\widetilde{T})\dot{\theta}^{t=T_S^+} \end{aligned} \tag{2.8}$$

2.2 Systematic trajectory-controlled gait-planning framework

The systematic trajectory-controlled gait-planning framework is presented to negotiate the three biomechanically motivated characteristics throughout the gait cycle for the five-link bipedal model. The three characteristics are cast into five kinematic and dynamic objective functions, corresponding to the five degrees of freedom of the biped. The framework employs a set of variables in the task space ($\mathbb{X}$) and a set of gait parameters (ω).

$$\begin{aligned} \mathbb{X} &= [X_{hip}, Z_{hip}, x_{ankle}, z_{ankle}, \theta_3] \\ \omega &= [S_L, Z^*_{hip}, H_m, T, \dot{\mathbb{X}}^{t=0}] \end{aligned} \tag{2.9}$$

The task-space variables consist of the horizontal and vertical displacements of the hip (X_{hip} and Z_{hip}), the horizontal and vertical displacements of the swing ankle (x_{ankle} and z_{ankle}), and the trunk motion (θ_3). The gait parameters contain the step length (S_L), initial height of the hip (Z^*_{hip}), maximum height of the swing ankle (H_m), step period of the gait (T), and initial velocity of the task-space variables ($\dot{\mathbb{X}}^{t=0}$). The gait parameters

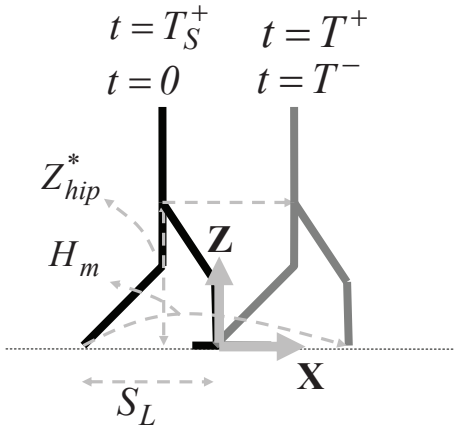

Figure 2.2: The gait parameters are illustrated on the biped during the single support phase, impact phase, and switching. T^-, T^+, and T_S^+ have been represented the instant right before impact, after impact, and after switching, respectively.

(ω) are defined, such that desired kinematic and dynamic features can be incorporated into the gait. Figure 2.2 illustrates the gait parameters on the bipedal model. It is important to point out that T^-, T^+, and T_S^+ have been represented the instant right before impact, after impact, and after switching, respectively. In addition, the step length is defined as a positive parameter.

The kinematic and dynamic objective functions consist of: the erected body posture, trajectory of the hip, trajectory of the swing ankle, postural balance, and regulation of centroidal angular momentum (CAM). The Gravity-Compensated Inverted Pendulum Model (GCIPM), shown in Figure 2.3, is applied to avoid the complexity of the multi-link dynamics of the biped through the equations of the objective functions related to the postural balance and the regulation of CAM. The GCIPM allows that the aforementioned equations are explicitly derived based on the displacements, velocities, and accelerations of the hip and the ankles.

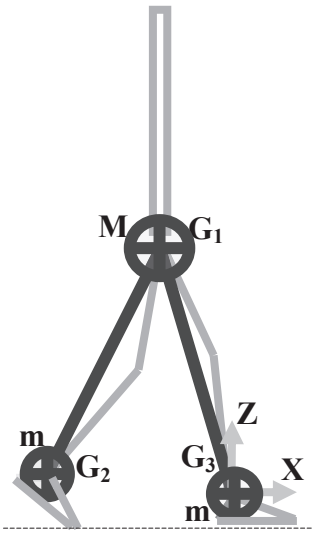

Figure 2.3: The GCIPM represents the biped. Three single concentrated masses are placed at the hip and the ankles. The GCIPM allows the framework having access to the displacements, velocities, and accelerations of the hip and ankles. M is the mass of the trunk and the hip. m is the mass of each leg. Each leg of the GCIPM is a virtual link, so their length could be variable. The coordinate system is attached to the supporting ankle.

2.2.1 Erected body posture

A bipedal robot requires a vision system in order to avoid obstacle and navigation through the environment. The vision system is mostly installed on the tip of the trunk [4]. The motion of the trunk seriously deteriorates the calibration of the system. The erected body posture then improves the navigation performance of the biped. This objective function describes as follows:

$$\theta_3 = 0 \tag{2.10}$$

where, θ_3 representing the trunk motion was already defined in Figure 2.1.

2.2.2 Trajectory of the hip

The motion of the hip significantly affects the motion of the biped in terms of smooth walking and postural balance [43]. This section constitutes a relation between X_{hip} and Z_{hip}, using the task-space variables and the gait parameters. The impact phase establishes a nonlinear relation between the hip velocity at the instants after impact (the beginning of the new step) and before impact, which dictates the horizontal and the vertical velocities of the hip. To satisfy such relationships, a 3^{rd} order polynomial is selected for the hip motion. The relation is described as follows:

$$Z_{hip} = A\,X_{hip}^3 + B\,X_{hip}^2 + C\,X_{hip} + D \tag{2.11}$$

A, B, C, and D are determined, satisfying the boundary conditions, presented in Section 2.2.6.1.

$$A = \frac{2Z_{hip}^{t=0}}{S_L^3} - \frac{2Z_{hip}^{t=T^-}}{S_L^3} + \frac{\dot{Z}_{hip}^{t=T^-}}{S_L^2\dot{X}_{hip}^{t=T^-}} + \frac{\dot{Z}_{hip}^{t=0}}{S_L^2\dot{X}_{hip}^{t=0}} \tag{2.12}$$

$$B = \frac{\dot{Z}_{hip}^{t=T^-}}{2S_L\dot{X}_{hip}^{t=T^-}} - \frac{\dot{Z}_{hip}^{t=0}}{2S_L\dot{X}_{hip}^{t=0}}$$

$$C = \frac{3Z_{hip}^{t=T^-}}{2S_L} - \frac{3Z_{hip}^{t=0}}{2S_L} - \frac{\dot{Z}_{hip}^{t=T^-}}{4\dot{X}_{hip}^{t=T^-}} - \frac{\dot{Z}_{hip}^{t=0}}{4\dot{X}_{hip}^{t=0}}$$

$$D = \frac{Z_{hip}^{t=T^-}}{2} + \frac{Z_{hip}^{t=0}}{2} - \frac{S_L\dot{Z}_{hip}^{t=T^-}}{8\dot{X}_{hip}^{t=T^-}} + \frac{S_L\dot{Z}_{hip}^{t=0}}{8\dot{X}_{hip}^{t=0}}$$

2.2.3 Trajectory of the swing ankle

The ankle of the swing leg is taken off the ground at the start of the single support phase, and lands back at the end of the single support phase, causing the impact event. Then,

it is switched to the ankle of the support leg. Here, a relation between x_{ankle} and z_{ankle} is constituted based on the task-space variables and the gait parameters. The impact phase establishes a nonlinear relation between the swing ankle velocity at the instants after impact and before impact, which dictates the horizontal and the vertical velocities of the swing ankle. Satisfying such relationships as well as achieving the prescribed maximum clearance height (H_m) of the swing ankle, a 4^{th} order polynomial is selected for the swing ankle trajectory. The maximum height can be wherever along the single support phase. In Eq. 2.13, it is considered in the middle of the gait.

$$z_{ankle} = A^{'} x_{ankle}^4 + B^{'} x_{ankle}^3 + C^{'} x_{ankle}^2 + D^{'} x_{ankle} + E^{'} \tag{2.13}$$

$A^{'}$, $B^{'}$, $C^{'}$, $D^{'}$ and $E^{'}$ are determined, satisfying the boundary conditions, presented in Section 2.2.6.1.

$$\begin{aligned}
A^{'} &= \frac{H_m}{S_L^4} + \frac{\dot{Z}_{ankle}^{t=T^-}}{4S_L^3 \dot{X}_{ankle}^{t=T^-}} - \frac{\dot{Z}_{ankle}^{t=0}}{4S_L^3 \dot{X}_{ankle}^{t=0}} \\
B^{'} &= \frac{\dot{Z}_{ankle}^{t=T^-}}{4S_L^2 \dot{X}_{ankle}^{t=T^-}} + \frac{\dot{Z}_{ankle}^{t=0}}{4S_L^2 \dot{X}_{ankle}^{t=0}} \\
C^{'} &= \frac{\dot{Z}_{ankle}^{t=0}}{4S_L \dot{X}_i^{t=0}} - \frac{\dot{Z}_{ankle}^{t=T^-}}{4S_L \dot{X}_i^{t=T^-}} - \frac{2H_m}{S_L^2} \\
D^{'} &= \frac{\dot{Z}_{ankle}^{t=T^-}}{4\dot{X}_{ankle}^{t=T^-}} - \frac{\dot{Z}_{ankle}^{t=0}}{4\dot{X}_{ankle}^{t=0}} \\
E^{'} &= H_m
\end{aligned} \tag{2.14}$$

2.2.4 Postural balance

One main goal of the framework is to negotiate postural balance and to tie that to the motion profiles of the hip and the ankles. The ZMP measure is considered to negotiate

the postural balance of the biped [33]. The ZMP equation is implemented on the GCIPM instead of the biped in order to avoid the complexity of the multi-link dynamics of the biped through the ZMP equation. The postural balance of the biped is guaranteed, provided that the support polygon covers the ZMP profile. It is important to point out that the supporting foot area during the single support phase is considered as the support polygon. The objective function related to the postural balance is as follows:

$$X_{zmp} = a\,t + b$$
$$X_{zmp} \in the\,support\,foot \tag{2.15}$$

where, X_{zmp} is the X-component of the ZMP. The Z-component of the ZMP is zero since walking is on the flat ground, and there is no Y-component of the ZMP since walking is in the sagittal plane. The ZMP is progressing in a linear form, presented by Eq. 2.15, from the heel towards the toe as same as human walking [43, 52, 74].

The equation of the ZMP, presented in Appendix. B, is derived for the GCIPM:

$$\begin{aligned}&\overrightarrow{r_{zmp}G_1} \times M\,(\ddot{X}_{hip}\ \overrightarrow{i} + \ddot{Z}_{hip}\ \overrightarrow{k}) + \overrightarrow{r_{zmp}G_2} \times m(\ddot{x}_{ankle}\ \overrightarrow{i} + \ddot{z}_{ankle}\ \overrightarrow{k})\\ &= \overrightarrow{r_{zmp}G_1} \times M\,\overrightarrow{g} + \overrightarrow{r_{zmp}G_2} \times m\,\overrightarrow{g} + \overrightarrow{r_{zmp}G_3} \times m\,\overrightarrow{g}\end{aligned} \tag{2.16}$$

where, $\overrightarrow{r_{zmp}}$ is the position of the ZMP; M is the mass of the trunk and the hip; m is the mass of each leg; $\overrightarrow{G_i}$ is the position of each GCIPM's single mass. As a result, Eqs. 2.15 and 2.16 tie the postural balance to the motion profiles of the hip and the ankles.

2.2.5 Regulation of centroidal angular momentum

The other biomechanically motivated characteristic that the framework negotiates is the regulation of CAM. The framework is to tie these characteristics to the motion profiles of the hip and the ankles. The regulation of CAM makes rotational equilibrium condition for the biped [52]. For natural walking during the single support phase, CAM is defined highly regulated. It means that the CMP-ZMP separation distant normalized by foot length is less than 14% [52]. The objective function of the regulation of CAM is presented as follows:

$$\begin{aligned} \dot{H}_{Gy} &= c\,t + d \\ \left|\frac{X_{cmp} - X_{zmp}}{foot\,length}\right| &< 0.14 \end{aligned} \tag{2.17}$$

where, $\dot{H}_{Gy}$ is the Y-component of the rate of change in CAM, and X_{cmp} is the X-component of the CMP. There is no X- and Z-component of the rate of change in CAM since walking is in the sagittal plane. The Z-component of the CMP is zero since walking is on the flat ground, and there is no Y-component of the CMP since walking is in the sagittal plane. To reduce the separation error of the ZMP-CMP, $\dot{H}_{Gy}$ is also considered in a linear form, presented by Eq. 2.17. In order to compute Eq. 2.17, the rate of change in CAM is derived for the GCIPM as:

$$\overrightarrow{\dot{H}_G} = \overrightarrow{GG_1} \times M\,(\ddot{X}_{hip}\,\overrightarrow{i} + \ddot{Z}_{hip}\,\overrightarrow{k}) + \overrightarrow{GG_2} \times m(\ddot{x}_{ankle}\,\overrightarrow{i} + \ddot{z}_{ankle}\,\overrightarrow{k}) \tag{2.18}$$

where, $\overrightarrow{\dot{H}_G}$ is the rate of change of CAM; M is the mass of the trunk and the hip; m is the mass of each leg; $\overrightarrow{G}$ is the position of the center of mass of the GCIPM; $\overrightarrow{G_i}$ is the position of each single mass of the GCIPM. The CMP-ZMP separation distant normalized by the foot length is also as follows:

$$\left| \frac{X_{cmp} - X_{zmp}}{foot\,length} \right| = \frac{\dot{H}_{Gy}}{R_z} \tag{2.19}$$

where, R_z is the Z-component of the ground reaction force. Eqs. 2.17 and 2.18 then tie the regulation of CAM to the motion profiles of the hip and the ankles.

2.2.6 The framework equations

Combining the equations of the five objective functions together, two ordinary differential equations are derived, founded on X_{hip} and x_{ankle}. The equations, which contain information about the three biomechanical characteristics, are called the framework equations henceforth, and presented as follows:

$$\begin{bmatrix} M^*_{11} & M^*_{12} \\ M^*_{21} & M^*_{22} \end{bmatrix} \begin{bmatrix} \ddot{X}_{hip} \\ \ddot{x}_{ankle} \end{bmatrix} + \begin{bmatrix} C^*_{11} & C^*_{12} \\ C^*_{21} & C^*_{22} \end{bmatrix} \begin{bmatrix} \dot{X}^2_{hip} \\ \dot{x}^2_{ankle} \end{bmatrix} + \begin{bmatrix} G^*_{11} \\ G^*_{21} \end{bmatrix} = \begin{bmatrix} 0 \\ 0 \end{bmatrix} \tag{2.20}$$

M^*_{ij}, C^*_{ij} and G^*_{ij} are presented in Appendix. B in details.

2.2.6.1 Boundary conditions for the framework

The equations of the framework, presented by Eq. 2.20, are integrated across the gait cycle to satisfy the boundary conditions, presented by Eq. 2.21 and 2.23. These boundary conditions are referred to the repeatability at the beginning and the instant right before impact of the gait cycle, which are for the entire framework equations. This way, the postural and velocity repeatability do not involve discontinuities due to the switching phase and the impact phase. The boundary conditions, related to the postural repeatability, are written in the task space as follows:

Table 2.1: The relation between postural repeatability and the gait parameters.

$t = 0\, t = T_S^+$	$t = T^-\, t = T^+$
$X_{hip} = -\frac{S_L}{2}$	$X_{hip} = -\frac{S_L}{2}$
$Z_{hip} = Z_{hip}^*$	$Z_{hip} = Z_{hip}^*$
$x_{ankle} = -S_L$	$x_{ankle} = S_L$
$z_{ankle} = 0$	$z_{ankle} = 0$
$\theta_3 = 0$	$\theta_3 = 0$

$$\begin{cases} \mathbb{X}_i^{t=0} = -\mathbb{X}_i^{t=T^-} \; i = 1, ..., 4 \\ \\ \mathbb{X}_i^{t=0} = \mathbb{X}_i^{t=T^-} \quad i = 5 \end{cases} \tag{2.21}$$

A theorem developed by the authors [47] is used to satisfy Eq. 2.21, incorporating the gait parameters. That results in Table. 2.1, which guarantees the postural repeatability. The theorem employs only two gait parameters, S_L and Z_{hip}^*. Two other gait parameters, H_m and T, are assigned, such that the biped possesses desired maneuverability through the environment.

The boundary conditions, related to the velocity repeatability, are derived in the task space, using the rest of the gait parameters $\dot{\mathbb{X}}^{t=0}$, as follows:

$$\dot{\theta}^{t=T^-} = A\theta^{t=T_S^+} \tag{2.22}$$

$$\dot{\mathbb{X}}^{t=T^-} = \left(J^* A \widetilde{T} J^{*-1}\right) \dot{\mathbb{X}}^{t=T_S^+} = \left(J^* A J^{*-1}\right) \dot{\mathbb{X}}^{t=0} \tag{2.23}$$

where, A is a matrix that maps the initial angular velocities to the angular velocities at instant right before impact. J^* is Jacobian matrix that maps the hip, ankles, and trunk to the join-space variables. Eq. 2.23 is used to calculate the velocity boundary conditions at the instant right before impact based on those at the beginning.

2.2.6.2 Solving the framework equations

The boundary conditions referring to the repeatability have been determined by Table. 2.1 and Eq. 2.23. The boundary conditions for the framework equations, presented by Eq. 2.20, are also rewritten in the following brief form:

$$\begin{aligned}
X_{hip}^{t=0} &= -\tfrac{S_L}{2} \quad & X_{hip}^{t=T^-} &= \tfrac{S_L}{2} \\
x_{ankle}^{t=0} &= -S_L \quad & x_{ankle}^{t=T^-} &= S_L \\
\dot{X}_{hip}^{t=0} &= \mathbb{A} \quad & \dot{X}_{hip}^{t=T^-} &= \mathbb{B} \\
\dot{x}_{ankle}^{t=0} &= \mathbb{C} \quad & \dot{x}_{ankle}^{t=T^-} &= \mathbb{D}
\end{aligned} \tag{2.24}$$

where, $\mathbb{A}$ and $\mathbb{B}$ are of $\dot{\mathbb{X}}^{t=0}$, which are of the gait parameters, shown in Eq. 2.9. $\mathbb{C}$ and $\mathbb{D}$ are then computed by Eq. 2.23 based on the values of $\mathbb{A}$ and $\mathbb{B}$. Therefore, the framework equations has to satisfy eight boundary conditions, while the equations are the fourth order differential equations. Four unknowns are required within the framework equations to have a unique solution. The coefficients of the ZMP and $\dot{H}_{Gy}$ provide four unknowns for the framework equations. In order to solve the framework equations, the two-point boundary value problem (BVP) solvers available in MATLAB are used [42]. An

BVP-solver algorithm is searching to find a solution for the aforementioned equations.

In summary, the framework contains the following steps in order to design a gait: (1) assigning desired values to the gait parameters, presented by Eq. 2.9; (2) calculating the boundary conditions referring to the repeatability using Table. 2.1 and Eq. 2.23; (3) solving the framework equations, presented by Eq. 2.20; (4) calculating the other task-space variables (Z_{hip} and z_{ankle})[1] by Eqs. 2.11 and 2.13; (5) obtaining the joint-space variables (θ) from the motion profiles of the hip, ankles, and trunk by the inverse kinematics equations of the biped.

2.3 Simulation results and discussions

In this section, firstly, an example of a gait designed by the framework is presented to demonstrate how the framework negotiates the three biomechanically motivated characteristics. Secondly, the gait characteristics and energy efficiency of the gait are calculated to draw a conclusion.

The gait characteristics are evaluated based on the Froude number, a normalized walking speed. The energy efficiency is evaluated based on the cost of transport, a normalized energy cost. Both the Froude number and cost of transport are explained in details in the next section.

2.3.1 A gait designed by the framework

The geometrical and mass parameters of the biped are presented in Table. 2.2. Following the five-step gait-planning procedure explained in the previous section, the gait parameters are firstly assigned as follows:

[1] The trunk motion (θ_3) is straightforward calculated by Eq. 2.10.

$$S_L = 0.15\,(m),\ Z^*_{hip} = 0.65\,(m),\ H_m = 0.1\,(m)$$

$$T = 1.5\,(s),\ \dot{\mathbb{X}}^{t=0} = [0.01,\ 0.01,\ 0.05,\ 0.05,\ 0]^T\,(\tfrac{m}{s}) \tag{2.25}$$

The second step is to calculate the boundary conditions referring to the repeatability based on Table. 2.1 and Eq. 2.23 at the beginning and the instant right before impact. The boundary conditions are presented in Table. 2.3.

The third step is to solve the framework equations, presented by Eq. 2.20, to find the horizontal motion profiles of the hip and the swing ankle, which are shown in Figs. 2.4(a) and (b). Figure 2.4(a) shows that the horizontal displacement of the hip varies from $-0.075\,(m)$ to $0.075\,(m)$, and the horizontal displacement of the swing ankle varies from $-0.15\,(m)$ to $0.15\,(m)$. Figure 2.4(b) presents that the horizontal velocity of the hip varies from $0.01\,(\frac{m}{s})$ to $-0.02\,(\frac{m}{s})$, and the horizontal velocity of the swing ankle varies from $0.05\,(\frac{m}{s})$ to $-0.01\,(\frac{m}{s})$. Thereby, the postural and the velocity boundary conditions, shown in Table. 2.3, were satisfied.

In the fourth step, the vertical displacements of the hip and the swing ankle are calculated by Eqs. 2.11 and 2.13. Figure 2.5 illustrates the displacements of the hip and the swing ankle. Figure 2.5(a) shows that the hip height is not restricted to a constant height in comparison to other gait-planning strategies [44, 58]. The hip height rises during the first half of the gait, and lowers during the second half of the gait, similar to that of human walking [75]. The displacement of the swing ankle was designed to pass an obstacle up to H_m height, assigned as $0.1\,(m)$ in Eq. 2.25, at the middle of the gait cycle. Figure 2.5(b) confirms that the ankle is capable of passing the obstacle of $0.1\,(m)$ height at the middle of the gait cycle.

The fifth step is to apply the inverse kinematics equations to the task-space variables to determine the joint angle profiles as defined in Figure 2.1. The phase portraits of the joint

angle profiles are presented in Figure 2.6, in which A and B denote the beginning and the instant right before impact of the gait cycle, respectively. The angular displacements and velocities at A and B are presented in Table. 2.4, which shows how the repeatability is mapped from the task space into the joint space. Having known the motion profiles of the joint-space variables, Figure 2.7 shows an animation of the biped walking forward.

As a conclusion, the above results demonstrated that the designed gait successfully negotiates the postural and the velocity repeatability, defined by Table. 2.1 and Eq. 2.23.

Table 2.2: The geometrical and mass parameters of the bipedal robot.

	Link 1	Link 2	Link 3	Link 4	Link 5
$l_i\,(m)$	0.4	0.3	0.4	0.3	0.4
$d_i\,(m)$	0.2	0.15	0.2	0.15	0.2
$m_i\,(kg)$	0.5	0.5	3	0.5	0.5
$I_i\,(kg.m^2)$	0.002	0.001	0.01	0.001	0.002

Table 2.3: The boundary conditions referring to repeatability.

	$t=0$	$t=T^-$	$t=T_S^+$
$X_{hip}(m)$	-0.075	0.075	0.075
$Z_{hip}(m)$	0.65	0.65	0.65
$x_{ankle}(m)$	-0.15	0.15	0.15
$z_{ankle}(m)$	0	0	0
$\dot{X}_{hip}(m/s)$	0.01	-0.02	0.01
$\dot{Z}_{hip}(m/s)$	0.01	-0.03	0.01
$\dot{x}_{ankle}(m/s)$	0.05	-0.01	0.05
$\dot{z}_{ankle}(m/s)$	0.05	0.00	0.05

The framework also negotiates the postural balance and the regulation of CAM of the gait, satisfying Eqs. 2.15 and 2.17, respectively. The profiles of the ZMP and the rate

Table 2.4: The joint angular displacements and velocities at the beginning, the instant right before impact, and the instant after switching.

	A	B
$\theta_1(rad)$	0.20	0.43
$\theta_2(rad)$	-0.53	-0.31
$\theta_4(rad)$	-3.45	-3.68
$\theta_5(rad)$	-2.72	-2.94
$\dot{\theta_1}(rad/s)$	-0.01	0.10
$\dot{\theta_2}\,(rad/s)$	0.06	-0.20
$\dot{\theta_4}\,(rad/s)$	-0.26	-0.18
$\dot{\theta_5}\,(rad/s)$	0.10	0.08

of change in CAM ($\dot{H}_{Gy}$) for the GCIPM are computed by the BVP-solver algorithm, presented in Section 2.2.6.2, as follows:

$$\begin{aligned} X_{zmp} &= 0.14\,t - 0.09 \\ & \qquad\qquad 0 < t < T^{-} \\ \dot{H}_{Gy} &= -0.09\,t + 0.06 \end{aligned} \tag{2.26}$$

The horizontal length of the supporting foot is considered as $0.25\,(m)$. The horizontal distant from the heel to the supporting ankle is considered as $0.10\,(m)$, and that from the supporting ankle to the toe is considered as $0.15\,(m)$. Worth mentioning is that the reference coordinate system is attached to the supporting ankle. The ZMP is progressing from heel-side to toe-side from $-0.09\,(m)$ to $0.12\,(m)$, respectively. The supporting foot of the GCIPM covers the ZMP, which means that the postural balance is guaranteed, referring to Eq. 2.15. In distinction to the fixed ZMP [7, 70], the moving ZMP provides the smooth and natural walking for the biped as it does for human [43, 52, 74]. $\dot{H}_{Gy}$ is

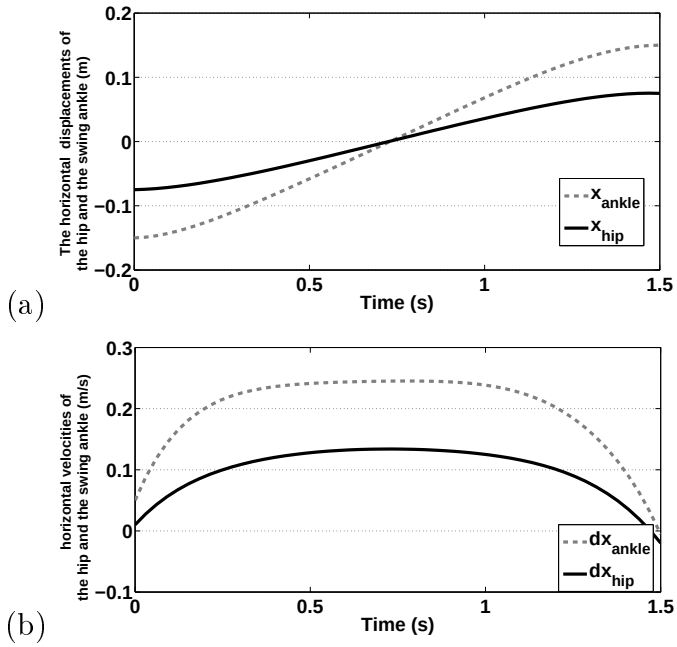

Figure 2.4: (a) The horizontal displacement of the hip and the swing ankle. (b) The horizontal velocity of the hip and the swing ankle.

varying from $0.06(N.m)$ to $-0.08(N.m)$; consequently, the ZMP-CMP separation distant normalized by the foot length stays less than 1%, which is interpreted as the regulation of CAM for the GCIPM, referring to Eq. 2.17.

Since the GCIPM simplifies the multi-link dynamics of the original biped, it is desirable to investigate the effect of that simplification on the ZMP and $\dot{H}_{Gy}$ profiles. The profiles computed on the original biped are compared with that computed on the GCIPM. Figs. 2.8(a) and (b) confirm that the errors are acceptable due to the fact that the ZMP profile computed on the original biped is still within the support polygon. Figure 2.8(a) illustrates that the supporting foot covers the ZMP profile, progressing from heel-side to toe-side from $-0.08\,(m)$ to $0.13\,(m)$, respectively. Referring to Eq. 2.15, it guarantees the postural balance of the biped. Figure 2.9 shows that the normalized separation of the CMP-ZMP stays less than 2% for the biped. Referring to Eq. 2.17, it guarantees the regulation of CAM of the biped [52].

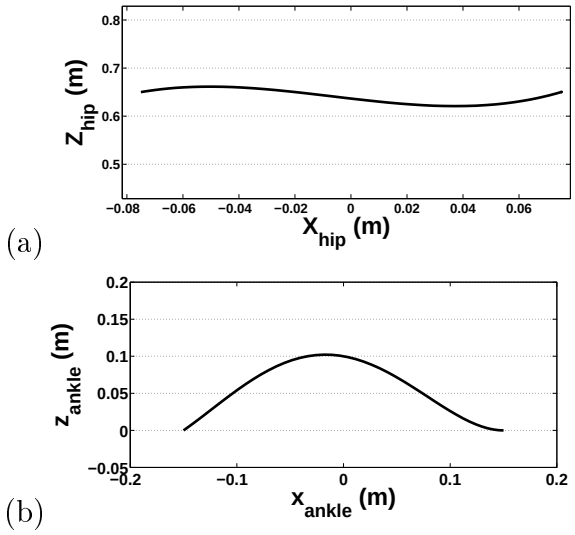

Figure 2.5: (a) The motion profile of the hip. (b) The motion profile of the swing ankle.

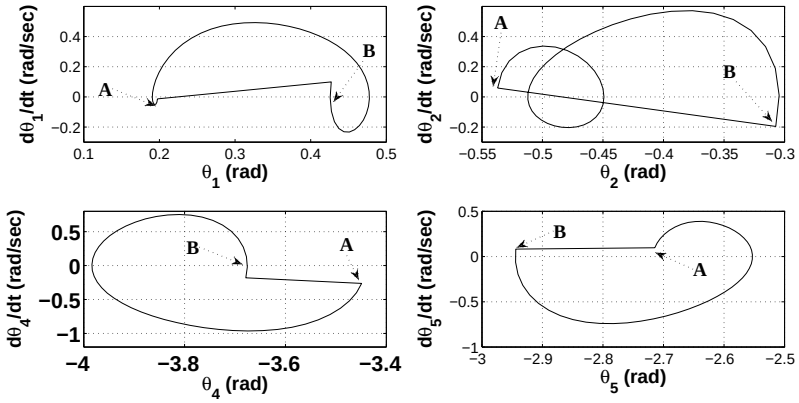

Figure 2.6: The phase portraits of the joint-space variables.

To assure that the supporting foot does not slip, the reaction force normalized to the weight of the biped is shown in Figure 2.10. For this case study, the biped will never slip on the ground, provided that the ground-friction coefficient stays more than 0.1. It is noteworthy that the normal ground-friction coefficient is between 0.1 to 0.7 [76].

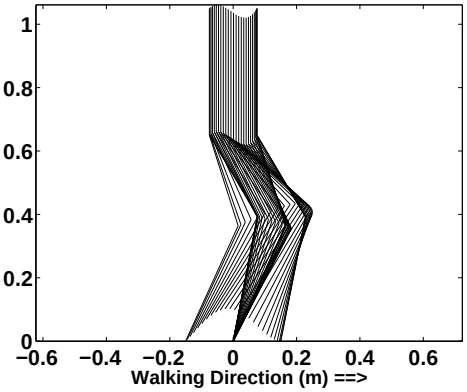

Figure 2.7: An animation of the bipedal robot.

2.3.1.1 Mechanical cost of transport and Froude number

The aforementioned section presented a gait designed by the framework. It was already checked that the designed gait successfully negotiated all the three biomechanically motivated characteristics. Now, the gait is explored via its energy efficiency and walking speed, relative to bipedal robots/models in the literature [4, 18]..

The energy efficiency is defined by the mechanical cost of transport, and the walking speed is defined by the Froude number. The mechanical cost of transport is the amount of active mechanical work performed by the actuators per weight per distance traveled. High cost of transport means low energy efficiency, and vice versa. The Froude number is the walking speed normalized by the root square of the leg length times the gravitational acceleration. High Froude number means high walking speed.

For the designed gait in the previous section, the mechanical cost of transport is about 0.50, and the Froude number is about 0.08. Note that the mechanical cost of transport of ASIMO [4] is about 1.6 and that of a passive-based walker [12] is about 0.04. The Froude number of ASIMO is about 0.11 and that of a passive-based walker is about 0.21. Accordingly, although the framework improves the cost of transport to some extent, relative to ASIMO's, the Froude number of the gait still is lower than ASIMO's. It

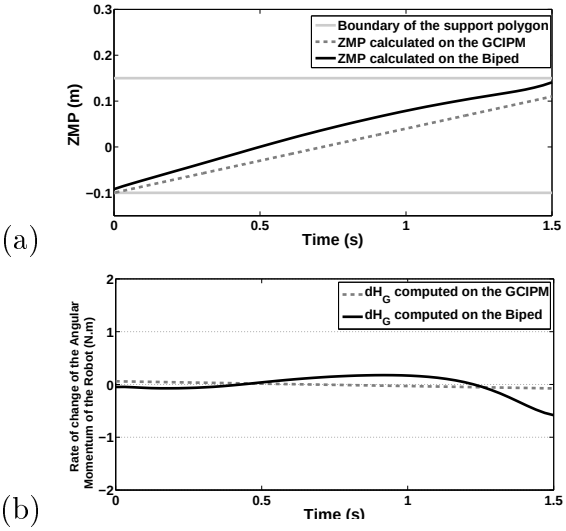

Figure 2.8: (a) Comparison between the ZMP profile computed on the biped with that computed on the GCIPM. (b) Comparison between the rate of CAM profile computed on the biped with that computed on the GCIPM.

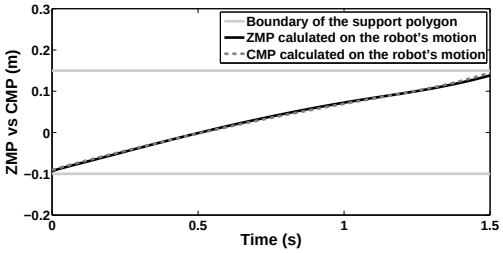

Figure 2.9: The CMP and ZMP profiles computed on the original biped.

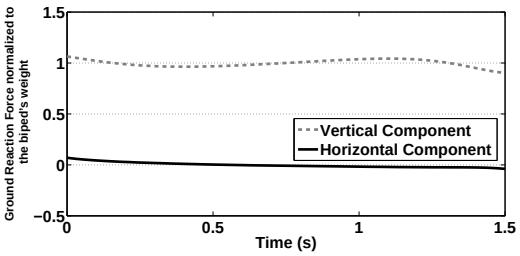

Figure 2.10: The ground reaction force normalized to the biped weight.

is important to point out that both the energy efficiency and the walking speed of the designed gait are considerably lower than a passive-based walking machine [12].

To achieve the Froude number of 0.12 (the same as ASIMO's), the step period of 1 (s) for a constant step length of 0.3 (m) is considered. The designed gait of the previous section is considered as a reference case. The horizontal foot length of the biped is 0.25 (m), and the reference coordinate system is attached to the supporting ankle. For the Froude number of 0.12 , the ZMP range increases, so the foot length needs to increase for about 20%, which lead to a foot length of 0.3 (m).

2.4 Summary

In this chapter, a novel systematic trajectory-controlled gait-planning framework was presented to provide mechanical insights into bipedal walking in terms of gait characteristics and energy efficiency. The framework negotiates three biomechanically motivated characteristics: the gait repeatability, postural balance, and highly regulated centroidal angular momentum (CAM) throughout the gait cycle. The gait cycle consists of the single support and the single impact phases. Dynamic modeling of a five-link bipedal robot was derived over the two phases.

The framework employed a set of task-space variables and a set of gait parameters. Five objective functions were defined corresponding to the five degrees of freedom of the biped to negotiate the three characteristics. The GCIPM was presented to derive the equations of the ZMP and the highly regulated CAM of the biped, based on the displacements, velocities, and accelerations of the hip and the swing ankle, and also to avoid the complexity of multi-link dynamics. Combining the equations of the five objective functions together, two ordinary differential equations were derived. The equations were integrated across the gait cycle, governed by the boundary conditions referring to gait

repeatability. The results consisted of the motion profiles of the hip and the ankles, from which the joint-space variables were calculated by the inverse kinematics equations.

Simulation results showed that the framework can present a gait that successfully satisfies the three biomechanical characteristics. The framework improved the energy efficiency to a mechanical cost of transport of 0.50, relative to ASIMO's mechanical cost of transport of 1.6. The framework also improved the walking speed, and achieved a Froude number of 0.12, similar to ASIMO's Froude number. However, the aforementioned mechanical cost of transport and the Froude number can still be improved to reach the mechanical cost of transport and the Froude number of a passive-based bipedal walker [12, 15].

Therefore, in the next chapter, a novel passive-based bipedal walking model is introduced to provide mechanical insights into bipedal walking in terms of gait characteristics and energy efficiency. It is then explored how much the mechanical cost of transport and the Froude number can be improved, relative to passive-based bipedal walkers in the literature.

Chapter 3

A passive-based bipedal model with compliant hip-actuation and compliant-ankle flat-foot

In the previous chapter, a novel systematic trajectory-controlled gait-planning framework was presented to provide mechanical insights into bipedal walking, and to improve its performance. The mechanical cost of transport and the Froude number of bipedal walking were improved, relative to the literature of trajectory-controlled walking paradigm [38]. However, the measures can still be improved to reach the mechanical cost of transport and the Froude number of a passive-based bipedal walker or a human.

Therefore, in this chapter, a novel mathematical model of a passive-based bipedal walking robot with compliant hip-actuation and compliant-ankle flat-foot is presented to provide mechanical insights into bipedal walking in terms of gait characteristics and energy efficiency. Compliant hip-actuation helps the model to enable walking on the flat ground, and compliant-ankle flat-foot helps the model to experience various limit-cycle gaits with different gait characteristics and energy efficiency.

This is done by developing a flat-feet bipedal model with two springs at each ankle at the back-side and the front-side, actuated by a compliant hip torque only during the single support phase to walk on the flat ground. It is found that such a novel model has more versatile gait sequences, in comparison to that of point/round feet, which can be detected among twelve gait postures based on unilateral constraints between the feet and the ground.

This chapter explores firstly whether inclusion of both compliant hip-actuation and ankle improves the performance of bipedal walking, in comparison with conventional passive-based bipedal models or humans [12,60,63]. Secondly, it studies how two-sided ankle stiffness (the stiffer backside than frontside stiffness) influences the performance of bipedal walking in terms of the gait characteristics and the energy efficiency, as compared with uniform ankle stiffness (the same backside and frontside stiffness). Finally, this chapter studies a crucial gait event named single-support heel-off[1], specifically in how it influences the gait characteristics and the energy efficiency of bipedal walking.

3.1 Bipedal model

The passive-based bipedal model with compliant-ankle flat-foot and compliant hip-actuation is developed and shown in Figure 3.1a. The concentrated masses of the hip, leg, and foot are denoted as m_h, m_l, and m_f, respectively. The leg length and the distance from the hip to the mass center of each leg are indicated as l and l_c, respectively. The distance of the sole to the ankle, distance from the ankle to the heel, distance from the ankle to the toe, and distance from the toe to the mass center of each foot are denoted as h_a, l_b, l_f, and l_{fc}, respectively. The horizontal and the vertical coordinates of the hip with respect to that of the origin located on the flat ground right below the hip at the beginning are presented

[1]Single-support heel-off occurs when the heel of the stance leg has been lifted from the ground around its toe, while the swing leg is still swinging forward.

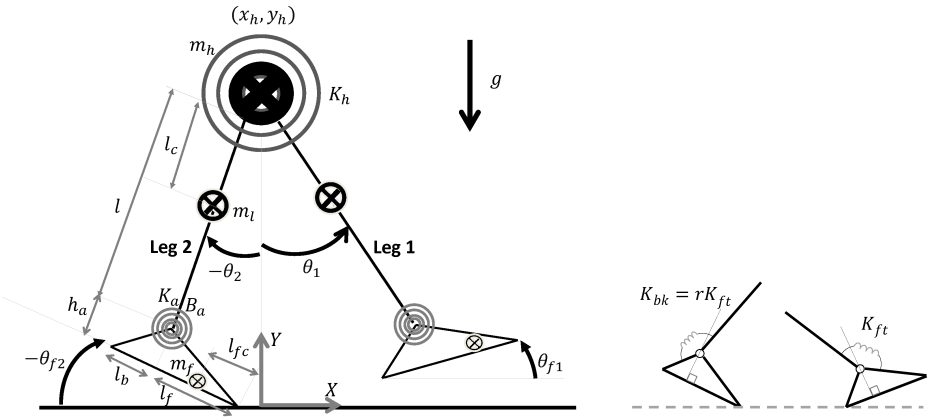

Figure 3.1: (a) Schematic of the actively-assisted compliant-ankle flat-foot bipedal model: the mass and geometrical parameters. (b) Schematic of the two-sided ankle stiffness K_a which means that the ankle spring cuts into two parts the frontside ankle stiffness K_{ft} and the backside ankle stiffness K_{bk}. Note that r is the ratio of the backside ankle stiffness to the frontside.

as x_h and y_h, respectively. The absolute angles of the legs with respect to the positive Y direction are denoted as θ_1 and θ_2, respectively. The absolute angles of the feet with respect to the positive X direction are indicated as θ_{f1} and θ_{f2}, respectively. Noteworthy is that the default direction of all angles are counter clockwise as shown in Figure 3.1a.

The torsional stiffness of the hip spring, torsional stiffness of the ankle spring, and viscous damping of the ankle damper are indicated as K_h, K_a, and B_a, respectively. The neutral position of the hip spring is where two legs are coincident, and the neutral position of the ankle spring is where the leg and the foot are perpendicular.

Two-sided ankle stiffness K_a consists of the frontside ankle stiffness K_{ft} and the backside ankle stiffness K_{bk}, respectively. When the angle between the forefoot and the leg is more than 90^o, the frontside ankle stiffness K_{ft} is in effect, and when the angle is less than or equal to 90^o, the backside stiffness K_{bk} is active, shown in Figure 3.1b. Accordingly, the ankle stiffness K_a is determined by the frontside ankle stiffness K_{ft} and the ankle stiffness

ratio r which is the ratio of K_{bk} and K_{ft} as shown in Figure 3.1b:

$$\begin{cases} K_{ai} = K_{ft} & \theta_i > \theta_{fi} \\ K_{ai} = rK_{ft} & \theta_i \leq \theta_{fi} \end{cases} \tag{3.1}$$

where, index i denotes the leg number.

Several assumptions about the bipedal model are: (a) all masses are concentrated at the centers of mass of the links; (b) knee joints are neglected, allowing the legs scuffing on the ground at the midstance; (c) only viscous damping at the ankle joints is considered; (d) all links are of rigid bodies; (e) friction between the ground and the feet is high enough avoiding sliding on the ground; (f) both heel and foot strikes occur instantaneously, modeled by the rigid-to-rigid impact principles [77]. It is very important to point out that viscous damping at the ankles is necessary to avoid the ankle-lock notion used in [65,69], which unnaturally limits the plantarflexion of the ankles at toe-off and heel-strike.

3.2 New versatile limit-cycle gaits

The gaits of the passive-based compliant-ankle flat-foot bipedal model are novel and more versatile than that of point/round feet models in the literature [12,35,63]. Bipedal gaits of point/round feet bipedal models are mostly comprised of a single series of two gait postures and two gait events sorted in a single gait sequence as the single support, heel-strike, single impact, and heel-off [12,35,63]. However, the gaits of the actively-assisted compliant-ankle flat-foot bipedal model are comprised of a number of gait postures detected among twelve gait postures dictated by the kinetics of the unilateral constraints at the heel, toe, or both.

For example, the single support phase of the bipedal model consists of three different gait postures: the first gait posture is when both the heel and the toe of the stance leg are in contact with the ground; the second posture is when the heel of the stance leg has

been lifted from the ground about the toe, and the last posture is when the toe of the stance leg has been lifted from the ground about the heel. Degrees of freedom of above three gait postures are three, four, and four, respectively. In addition, the double support, single impact, and double impact consist of four, two, and three gait postures, respectively. Please see Table 3.1 for further information on each gait posture such as their gait phase, status of feet, and degrees of freedom.

For example, in the single support phase, when the foot of leg 1 is flat on the ground, and the foot of the leg 2 is swinging forward, there are three independent unilateral constraints. The degrees of freedom for this posture are 3, and is obtained by subtracting the number of the generalized coordinates (6) from the number of the independent unilateral constraints (3). Furthermore, for another posture in the single support phase, when the heel of the leg 1 has been taken off the ground, while the swing leg is swinging forward, the degrees of freedom is 4, and is obtained by subtracting the number of the generalized coordinates (6) from the number of the independent unilateral constraints (in this case 2).

It is very important that the abbreviation of each gait posture shown in Table 3.1 has three parts: gait phase e.g. "DSP" for double support phase; status of the foot of leg 1 e.g. "F" for flat, followed by the last part which is the status of the foot of leg 2 e.g. "HO" for heel-off.

The gait flowchart of Figure 3.2 illustrates the entire walking scenarios of the bipedal model. All twelve gait postures in Table 3.1 progress from one to the next based on the kinetics of the unilateral constraints at the heel, toe, or both. Each compliant-ankle flat-foot in Figure 3.1 interacts with the ground through the unilateral constraints at the heel, toe, and both. Each unilateral constraint lasts if and only if the normal component of the constraint force becomes compressive, otherwise the constraint is lost.

Only independent constraints are considered in deriving dynamic equations of each gait posture to avoid a rank-deficient Jacobian matrix at the time of heel and foot strikes

Table 3.1: Details of the gait phases and the gait postures for the flat-foot bipedal model of Figure 3.1a, corresponding to the multiple walking sequences of Figure 3.2.

Gait phases	Gait postures	Foot of leg 1	Foot of leg 2	degrees of freedom
Single support phase (SSP)	SSP:L_1F:L_2S	Flat (F)	Swing (S)	3
	SSP:L_1HO:L_2S	Heel-off (HO)	Swing (S)	4
	SSP:L_1S:L_2TD	Swing (S)	Toe-down (TD)	4
Double support phase (DSP)	DSP:L_1F:L_2HO	Flat (F)	Heel-off (HO)	1
	DSP:L_1F:L_2TD	Flat (F)	Toe-down (TD)	1
	DSP:L_1HO:L_2HO	Heel-off (HO)	Heel-off (HO)	2
	DSP:L_1HO:L_2TD	Heel-off (HO)	Toe-down (TD)	2
Single impact phase (SIP)	SIP:L_1S:L_2HS	Swing (S)	Heel-strike (HS)	4
	SIP:L_1S:L_2FS	Swing (S)	Foot-strike (FS)	3
Double impact phase (DIP)	DIP:L_1F:L_2HS	Flat (F)	Heel-strike (HS)	1
	DIP:L_1HO:L_2HS	Heel-off (HO)	Heel-strike (HS)	2
	DIP:L_1HO:L_2FS	Heel-off (HO)	Foot-strike (FS)	1

* L1 and L2 in the abbreviation of the gait postures represent the foot of leg 1 and leg 2, respectively.

** To comprehend the name of each gait posture shown in Table 3.1, they are presented in three parts: the first part is the abbreviation of their gait phase e.g. SSP; the second part is the status of the foot of leg 1, followed by the third part that is the status of the foot of leg 2. For example, "SSP:L_1F:L_2S" implies a posture belonging to the single support phase of which the foot of leg 1 is flat on the ground, and the foot of leg 2 is swing forward.

[78,79]. When the foot is flat on the ground, each foot has the maximum of four unilateral constraints which are comprised of the constant tangential and normal positions of the toe and the heel, respectively, relative to the ground. However, out of these four constraints, only three are independent when the foot is flat on the ground (since the foot length is fixed), and only two are independent when it is rotated about either the toe or the heel on the ground. The above aforementioned facts have rigorously been considered into the dynamic equations of twelve gait postures, modeled by the Lagrangian approach based on rigid-to-rigid impact [77].

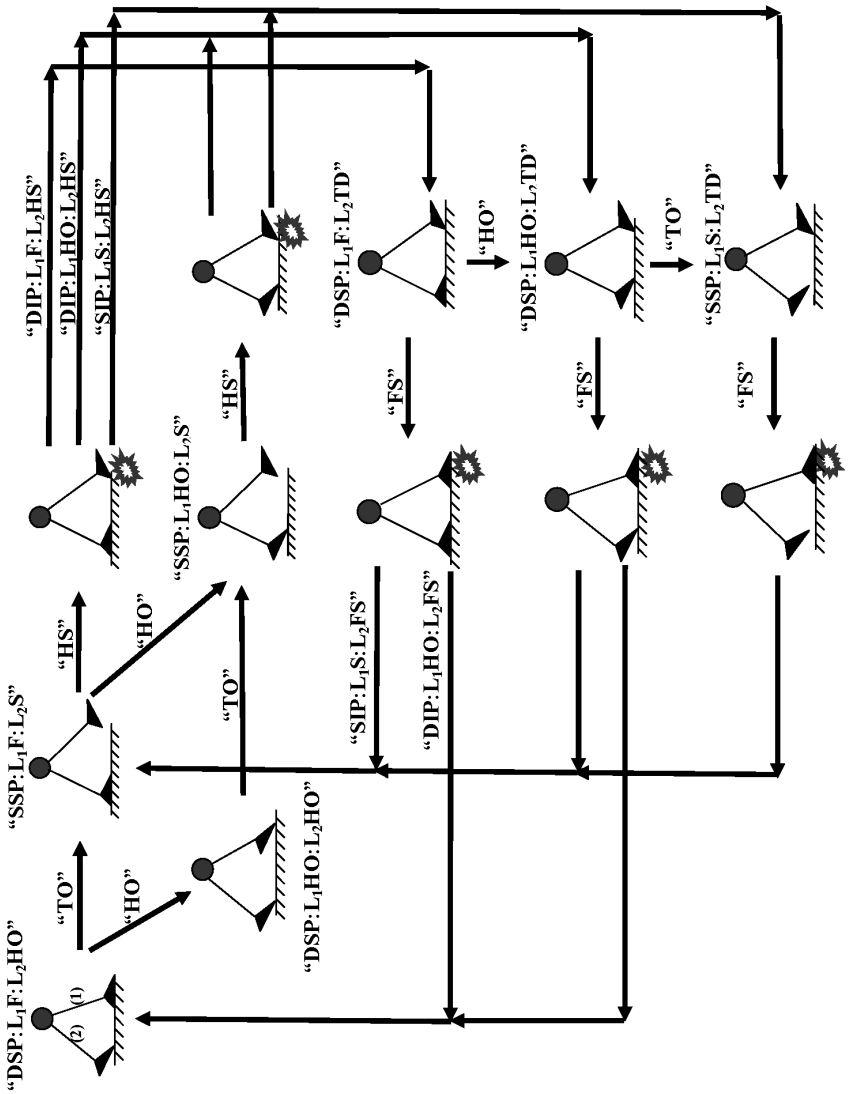

Figure 3.2: Gait flowchart contains all walking sequences resulted in the versatile limit-cycle gait of the compliant-ankle flat-foot bipedal model. Note that each transition from a gait posture to another is dictated by the kinetics of the unilateral constraints at the heel, toe, or both with the ground.

3.3 Dynamic equations of the gait postures

As it was mentioned in the previous section, the actively-assisted compliant-ankle flat-foot bipedal model has a versatile limit-cycle gait which is a sequence detected among twelve gait postures dictated by the kinetics of the unilateral constraints at the heel, toe, or both, shown in Figure 3.2. To extract such a gait, the dynamic equations of twelve gait postures must be derived. Accordingly, the bipedal model is firstly assumed to be lifted from the ground without the feet at the unilateral contact with the ground. Thus, the general form of Lagrange equations is as follows:

$$\frac{d}{dt}\frac{\partial L(\mathbf{q},\dot{\mathbf{q}})}{\partial \dot{q}_i} - \frac{\partial L(\mathbf{q},\dot{\mathbf{q}})}{\partial q_i} + \frac{\partial R(\mathbf{q},\dot{\mathbf{q}})}{\partial \dot{q}_i} = Q_i(\mathbf{q},\dot{\mathbf{q}}) \qquad (i = 1, ..., 6) \tag{3.2}$$

where, $\mathbf{q}$ is the vector of the generalized coordinates of the bipedal model. L, R, and $\mathbf{Q}$ denote the Lagrangian function, Rayleigh's dissipation function, and generalized forces, respectively.

The generalized coordinates of the bipedal model are defined as follows:

$$\mathbf{q} = [x_h, y_h, \theta_1, \theta_2, \theta_{f1}, \theta_{f2}]^T \tag{3.3}$$

The components of the generalized coordinates have already been explained in the previous section. To define the Lagrangian and Rayleigh's dissipation functions, the x- and y- coordinates of all concentrated masses of the bipedal model are defined as follows:

$$\mathbf{X} = \left[x_{m_h},\, x_{m_{l1}},\, x_{m_{l2}},\, x_{m_{f1}},\, x_{m_{f2}}\right] \tag{3.4}$$
$$\mathbf{Y} = \left[y_{m_h},\, y_{m_{l1}},\, y_{m_{l2}},\, y_{m_{f1}},\, y_{m_{f2}}\right]$$

Having defined the mass matrix, $\mathbf{M}$, as Eq. 3.5, the kinetic, E_k, potential-gravity, E_g, and potential-elastic, E_e, energies are written as Eq. 3.6-3.8:

$$\mathbf{M} = \begin{bmatrix} m_h, & m_l, & m_l, & m_f, & m_f \end{bmatrix}^T \tag{3.5}$$

$$E_k = \sum_{j=1}^{5} \frac{1}{2} \mathbf{M}_j (\dot{\mathbf{X}}_j^2 + \dot{\mathbf{Y}}_j^2) \tag{3.6}$$

$$E_g = \sum_{j=1}^{5} (\mathbf{M}_j g) \mathbf{Y}_j \tag{3.7}$$

$$E_e = \frac{1}{2} K_h (\theta_1 - \theta_2)^2 + \sum_{i=j}^{2} \frac{1}{2} K_{aj} (\theta_j - \theta_{fj})^2 \tag{3.8}$$

As a result, the Lagrangian and Rayleigh's dissipation functions are derived as follows:

$$\begin{gathered} L = 0.5 m_h (\dot{x}_h + \dot{y}_h)^2 + \sum 0.5 m_l (\dot{y}_h + l_c \dot{\theta}_i sin(\theta_i))^2 + 0.5 m_l (\dot{x}_h + l_c \dot{\theta}_i cos(\theta_i))^2 \; + \\ \sum 0.5 m_f \left\{ \dot{x} + \dot{\theta}_{fi} (h_a cos(\theta_{fi}) - l_{fc} sin(\theta_{fi})) + l \dot{\theta}_i cos(\theta_i) \right\}^2 \\ + \left\{ \dot{y} + \dot{\theta}_{fi} (h_a sin(\theta_{fi}) + l_{fc} cos(\theta_{fi})) + l \dot{\theta}_i sin(\theta_i) \right\}^2 \\ - g m_h y_h - g m_l (y_h - l_c cos(\theta_1)) \\ + \sum g m_l (y_h - l_c cos\theta_i) - \overset{[}{i} = 1] 2 \sum g m_f (y_h - h_a cos - l cos(\theta_i) + l_{fc} sin(\theta_{fi})) \\ - \sum 0.5 K_a (\theta_i - \theta_{fi})^2 - \sum 0.5 K_h (\theta_1 - \theta_2)^2 \qquad\qquad i = 1, 2 \end{gathered} \tag{3.9}$$

$$R = \sum 0.5 B_a (\dot{\theta}_i - \dot{\theta}_{fi})^2 \qquad\qquad i = 1, 2 \tag{3.10}$$

The vector of the generalized forces applied to the bipedal model is as follows:

$$\mathbf{Q}(\mathbf{q}, \dot{\mathbf{q}}) = \begin{bmatrix} 0, & 0, & -\tau_{hip}, & \tau_{hip}, & 0, & 0 \end{bmatrix}^T \tag{3.11}$$

τ_{hip} is the hip torque applied to the swing leg against the stance leg. This torque is the only constant torque applied to the bipedal model during walking. Having emphasized the fact that the ankles are passive compliant, the hip torque is only to compensate the energy dissipation at the heel and foot strikes, and is necessary only to enable the bipedal model to walk on the ground. The hip torque is zero during the double support phase.

Having substituted the Lagrangian and Rayleigh's dissipation functions into Eq. 3.2, the general form of dynamic equations when the bipedal model is lifted from the ground can be rewritten as:

$$\mathbf{D}(\mathbf{q})\ddot{\mathbf{q}} + \mathbf{C}(\mathbf{q}, \dot{\mathbf{q}})\dot{\mathbf{q}} + \mathbf{G}(\mathbf{q}) = \mathbf{Q}(\mathbf{q}, \dot{\mathbf{q}}) \tag{3.12}$$

where, $\mathbf{D}$, $\mathbf{C}$, and $\mathbf{G}$, are the mass, Coriolis-centrifugal, and gravity matrices, respectively, and are presented in Appendix C. Equation 3.12 contains six differential equations corresponding to six generalized coordinates of Eq. 3.3.

3.3.1 Unilateral constraints at the heel, toe, or both:

Equation (3.3) was derived when the bipedal model is assumed to be lifted from the ground, so it needs revision when the bipedal model is walking on the ground. It is because the heel, toe, or both of each foot are in unilateral contact with the ground during walking. Each unilateral contact means that the contact lasts if and only if the normal component of the constraint forces at that contact point is compressive, otherwise the contact is lost. When a foot is flat on the ground, it has three independent unilateral constraints (since the foot length is fixed), and only two are independent when it is rotated about either the toe or the heel on the ground. As a result, the total unilateral constraints can be varied from minimum 2 to maximum 6. All unilateral constraints are used as independent constraints in deriving dynamic equations to avoid a rank-deficient Jacobian matrix at the

time of heel and foot strikes.

Now, assume that the unilateral constraints during walking are defined as $\varphi \in R^N$ $(N = 2 \ldots 6)$. Thus, Eq. 3.3 is revised as follows:

$$\begin{aligned} &\mathbf{D}(\mathbf{q})\ddot{\mathbf{q}} + \mathbf{C}(\mathbf{q}, \dot{\mathbf{q}})\dot{\mathbf{q}} + \mathbf{G}(\mathbf{q}) = \mathbf{Q}(\mathbf{q}, \dot{\mathbf{q}}) + \left[\frac{\partial \varphi}{\partial \mathbf{q}}\right]^T \mathbf{\Gamma} \\ &\left[\frac{\partial \varphi}{\partial \mathbf{q}}\right]\dot{\mathbf{q}} = \mathbf{0} \end{aligned} \tag{3.13}$$

where, $\mathbf{\Gamma}$ denotes the Lagrangian multipliers vector corresponding to the unilateral constraints vector. The above equations are a combination of six differential equations and N algebraic equations. To integrate Eq. 3.13, a set of independent coordinates the same size as the degrees of freedom of the gait posture are defined as $\beta \in R^{(6-N)}$, and the mapping between the new set of independent coordinates, β, and the generalized coordinates, $\mathbf{q}$, are obtained as follows:

$$\begin{aligned} \dot{\mathbf{q}} &= \mathbf{S}\dot{\beta} \\ \ddot{\mathbf{q}} &= \mathbf{S}\ddot{\beta} + \dot{\mathbf{S}}\dot{\beta} \end{aligned} \tag{3.14}$$

The above mapping is substituted into Eq. 3.13, so the Lagrangian multipliers and the algebraic equations are eliminated, and the differential equations of the same size as the independent coordinates, β, are obtained as follows:

$$\begin{aligned} &\hat{\mathbf{D}}(\mathbf{q})\ddot{\beta} + \hat{\mathbf{C}}(\mathbf{q}, \dot{\mathbf{q}})\dot{\beta} + \hat{\mathbf{G}}(\mathbf{q}) = \hat{\mathbf{Q}}(\mathbf{q}, \dot{\mathbf{q}}) \\ &\hat{\mathbf{D}}(\mathbf{q}) = \mathbf{S}^T\mathbf{D}(\mathbf{q})\mathbf{S},\ \hat{\mathbf{C}}(\mathbf{q}, \dot{\mathbf{q}}) = \mathbf{S}^T\mathbf{D}(\mathbf{q})\dot{\mathbf{S}} + \mathbf{S}^T\mathbf{C}(\mathbf{q}, \dot{\mathbf{q}})\mathbf{S}, \\ &\hat{\mathbf{G}} = \mathbf{S}^T\mathbf{G}(\mathbf{q}) \\ &\hat{\mathbf{Q}}(\mathbf{q}, \dot{\mathbf{q}}) = \mathbf{S}^T\mathbf{Q}(\mathbf{q}, \dot{\mathbf{q}}) \end{aligned} \tag{3.15}$$

Integrating the above equations, the motion of the independent coordinates are obtained. Next, having substituted the above coordinates, β, into Eq. 3.14, all generalized coordinates, $\mathbf{q}$, are then obtained.

3.3.2 Heel and foot strikes:

After heel-strike occurs at the end of the single support phase, the double support phase starts during which the toe of the swing leg rotates about the heel towards the ground until foot-strike takes place. As mentioned in Section 2, the strikes are assumed to be an instantaneous gait event, and their dynamic equations are derived as follows:

$$\begin{aligned} \mathbf{D}(\mathbf{q})(\dot{\mathbf{q}}^{+} - \dot{\mathbf{q}}^{-}) &= \left[\frac{\partial \xi}{\partial \mathbf{q}}\right]^{T} \hat{\mathbf{\Gamma}} \\ \left[\frac{\partial \xi}{\partial \mathbf{q}}\right] \dot{\mathbf{q}}^{+} &= \mathbf{0} \end{aligned} \tag{3.16}$$

where, the superscripts $-$ and $+$ represent the instant right before and after the strikes. ξ represents the unilateral constraints right after the strikes, and $\hat{\mathbf{\Gamma}}$ denotes the impulsive Lagrangian multipliers corresponding to the constraints. To solve the above algebraic-differential equations, the same procedure of defining a set of independent coordinates, β, is applied as the above section. Then, having canceled the impulsive Lagrangian multipliers, the final form of the strike equations are obtained as follows:

$$\dot{\beta}^{+} = (\mathbf{S}^{+T}\mathbf{D}\mathbf{S}^{+})^{-1}\mathbf{S}^{+T}\mathbf{D}\dot{\mathbf{q}}^{-} \tag{3.17}$$

Having the above equation solved, the independent coordinates, β, are obtained. Next, having substituted β into Eq. 3.14, all generalized coordinates, $\mathbf{q}$, are then obtained.

3.4 Numerical programming of the gait flowchart

To achieve reliable and accurate simulations of the compliant-ankle flat-foot bipedal model shown in Figure 3.1, a comprehensive computer program in MATLAB has been developed. The program is based on the gait flowchart shown in Figure 3.2. It starts solving the dynamic equations of ["DSP:L_1F:L_2HO"] which is a gait posture of the double support

phase during which the foot of leg 1 is flat on the ground, while the heel of leg 2 starts being lifted from the ground about the toe.

Having solved the dynamic equations of the above gait posture by the Runge-Kutta method at the step time of $10^{-3}(s)$, the normal components of the unilateral forces at the toe of leg 2 and the heel and the toe of the leg 1 are being calculated, and monitored whether they are compressive or become zero. Following that, the bipedal model at the above gait posture can potentially switch into three different gait postures depending on the kinetics of the toe, heel, or both: (a) "SSP:L_1F:L_2S" when the contact of the toe of leg 2 is lost; (b) "DSP:L_1HO:L_2HO" when the contact of the heel of leg 1 is lost; (c) "DSP:L_1TD:L_2HO" when the contact of the toe of leg 1 is lost. Afterward, this process continues based on the remaining gait scenarios shown in Figure 3.2.

The program keeps running as gait postures are transferring to each others based on the gait flowchart of Figure 3.2 until limit-cycle gait is achieved. Note that the program stops working, when one of the failure events, falling down or running, occurs. Falling down is defined as the angle of the stance leg exceeds the angle of 60^o, and running is considered as the vertical component of the total ground reaction force reaches zero.

It is very important to point out that the performance of the program depends on how accurate the gait events namely, heel-off, toe-off, heel-strike, and foot-strike can be detected otherwise there will be cumulative errors in unilateral constraints that deteriorate the performance of the program. Since the step time has been fixed as $10^{-3}(s)$, the detection of the gait events is not accurate enough. However, it can significantly be improved once the third-order polynomial interpolations are applied to the corresponding unilateral constraints of each gait event, before and after moments at which these gait events are about to occur [80].

3.4.1 Poincare mapping

To systematically extract limit-cycle gaits of the compliant-ankle flat-foot bipedal model, the Newton-Raphson iteration interfaced to the Poincare mapping [80] can be an asset. The algorithm is as follows:

$$\begin{aligned} &\textbf{Repeat } \{\triangle\mathbf{u} = [\mathbf{I} - \mathbf{H}]^{-\mathbf{1}}(\mathbf{f}(\mathbf{u}) - \mathbf{u});\ \mathbf{u} = \mathbf{u} + \triangle\mathbf{u}\} \\ &\textbf{Until } \{|\triangle\mathbf{u}| < \epsilon\} \end{aligned} \tag{3.18}$$

where, $\mathbf{I}$ and $\mathbf{H}$ are the unit matrix and the Jacobian of the Poincare mapping, respectively. $\mathbf{f}$ is the stride function [12] which is the walking sequence detected among twelve gait postures. $\mathbf{u}$ is the vector of three independent states at the Poincare section which is considered right after foot-strike i.e. the beginning of "DSP:L_1F:L_2HO" referring to Table 3.1. The mentioned states contain the angular displacement of leg 1, θ_1, the angular displacement of leg 2, θ_2, and the angular velocity of leg 1, $\dot{\theta}_1$. ε, is defined as the tolerance by which the difference in the independent states at two successive Poincare sections are required to be less than 10^{-10}.

3.4.2 Froude number and active mechanical cost of transport

In this chapter, the gait characteristics are particularly evaluated based on the Froude number, which is a normalized walking speed, and the energy efficiency is evaluated based on the cost of transport, which is a normalized energy cost.

The walking speed is defined as a dimensionless number named the Froude number v. The higher such a number, the faster the bipedal walking is, and vice versa. The maximum value of the Froude number is 1 for bipedal walking [81]. The Froude number is calculated when the step length divided by the step period are normalized by $\sqrt{lg}$, where l is the leg length and g is the gravitational acceleration. The step length is defined as the horizontal distance of the heel of each swing leg between two successive heel-strikes, and the step

period is the time period of each step.

Energy efficiency is attained as a dimensionless number named the active mechanical cost of transport c_{amt} [68]. The higher such a number, lower the energy efficiency is, and vice versa. More specifically, the active mechanical cost of transport is defined by Eq. 3.19 as the amount of the active mechanical energy consumption used per distance traveled per weight of the walker. The active mechanical energy consumption or the energy input W_{act} of the bipedal model is the amount of energy injected by the hip actuation to enable the biped walking on the flat ground. The energy input W_{act} is defined by Eq. 3.20 as the integral of the absolute value of the hip torque multiplied by the relative angular velocity of the two legs during one gait cycle.

$$c_{amt} = \frac{W_{act}}{Weight \times Distanced\,traveled} \tag{3.19}$$

$$W_{act} = \int_0^{Step\,Period} \left| \tau_{hip}(\dot{\theta}_2 - \dot{\theta}_1) \right| dt \tag{3.20}$$

3.5 Simulation results and discussions

Since limit-cycle gaits of the novel passive-based bipedal model contain versatile walking sequences detected among twelve gait postures referred to Figure 3.2 and Table 3.1, it is very challenging to extract such a gait by the algorithm presented in Eq. 3.18. Therefore, it is highly desirable to demonstrate an example of a flat-foot limit-cycle gait and to explain its versatile properties. Following that, the effects of the compliant ankles (two-sided versus uniform) on the gait characteristics (step length, step period, walking speed) and the energy efficiency (active mechanical energy and active cost of transport) are explored. Finally, the effects of a crucial gait event named single-support heel-off on the gait characteristics and the energy efficiency of bipedal walking are studied.

Given the hip torque of 0.5 (N.m) during the single support phase only and the mass and the geometrical parameters of Table 3.2, limit-cycle gaits are achieved for the broad range of the frontside ankle stiffness K_{ft} from 0.10 (N.m/rad) to 0.30 (N.m/rad) by the increment of 0.01 (N.m/rad) as well as the ankle stiffness ratio r of 1 to 10 by the increment of 2.5.

The above range of the frontside ankle stiffness K_{ft} has been chosen since the computer program outlined in Section 3.4 barely converge to a limit-cycle gait when the frontside ankle stiffness K_{ft} is either less than 0.1 (N.m/rad) or greater than 0.3 (N.m/rad). When K_{ft} is less than 0.1 (N.m/rad), the impedance of the foot is not enough to provide a safe landing at heel-strike. In addition, when K_{ft} is greater than 0.3 (N.m/rad), the torque of the ankle spring is too strong making the foot bounce off the ground about the heel at foot-strike.

Table 3.2: Mass and geometrical parameters of the bipedal model of Figure 3.1a.

Parameters	Value	Parameters	Value
hip mass m_h	1.0 (Kg)	mass center of leg l_c	0.40 (m)
leg mass m_l	0.3 (Kg)	mass center of foot l_{fc}	0.04 (m)
foot mass m_f	0.1 (Kg)	ankle to toe l_f	0.07 (m)
leg length l	1.00 (m)	ankle to heel l_b	0.03 (m)
foot length l_f	0.10 (m)	ankle to sole h_a	0.03 (m)

3.5.1 A new versatile gait

A limit-cycle gait of the novel passive-based bipedal model projected on θ_1 and $\dot{\theta}_1$ is shown by Figure 3.3. The ankle stiffness for the gait is the uniform stiffness of 0.2 (N.m/rad). The sequence consists of five gait postures detected among twelve gait postures of Table 3.1 and Figure 3.2, based on the physics of unilateral constraints.

The gait starts at **"1"** representing the gait posture of "DSP:L_1F:L_2HO" during which the foot of leg 1 is flat on the ground, and the heel of leg 2 is just lifted from the ground about its toe. At **"2"**, toe-off occurs at leg 2, so the former gait posture switches to a new gait posture of "SSP:L_1F:L_2S". During this gait posture of the single support phase, the foot of leg 1 is still flat on the ground, and the foot of leg 2 is swinging forward. At **"3"**, heel-strike happens at the foot of leg 2. It is an instantaneous transition from the single support to the double support phase. After impact, the bipedal model is at the gait posture of "DSP:L_1HO:L_2TD". In this gait posture, the heel of the foot of leg 1 starts lifting from the ground about its toe, and the toe of the foot of leg 2 is rotated toward the ground about its heel. At **"4"**, foot-strike occurs at the foot of leg 2. It is an instantaneous transition to another gait posture belonging to the double support phase. This gait posture is "DSP:L_1HO:L_2F" in which the heel of the foot of leg 1 has been lifted from the ground about its toe, and the foot of leg 2 is flat on the ground. Starting at **"5"**, all aforementioned gait postures will be repeated all over again with the only difference, being, leg 1 and leg 2 are switched.

Figure 3.4 shows the stick diagram of the bipedal model, helping visualize the walking sequence shown in Figure 3.3. The independent states of the Poincare section for the gait are θ_1=0.1942 (rad), θ_2=-0.2166 (rad), and $\dot{\theta}_1$=-0.7119 (rad/s). The rest of generalized coordinates of Eq. 3.3 is calculated as follows by satisfying the unilateral constraints of the Poincare section defined in Eq. 3.21:

$$\begin{gathered}\theta_{f1} = 0.0000(rad),\ \theta_{f2} = -0.0665(rad),\ \dot{\theta}_2 = -0.5786(rad/s) \\ \theta_{f1} = 0.0000(rad/s),\ \dot{\theta}_{f2} = -3.8574(rad/s)\end{gathered} \tag{3.21}$$

The normalized step length s_l, normalized step period T, normalized walking velocity (the Froude number) v, active mechanical energy consumption W_{act} of Eq. 3.20, and active cost of transport c_{amt} of Eq. 3.19 are calculated for the gait shown in Figure 3.3 as

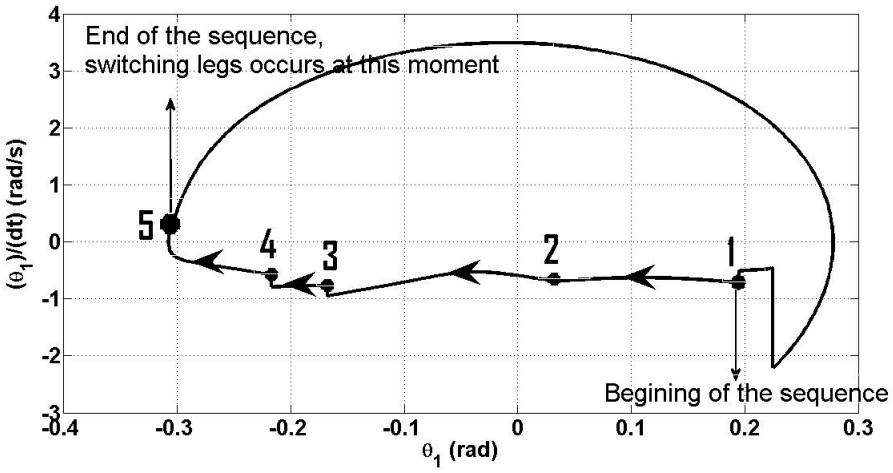

Figure 3.3: Phase portrait of a gait projected on θ_1 and $\dot{\theta}_1$ with the parameters of Table 3.2.

0.82, 1.95, 0.42, 0.3841 (J), and 0.0299, respectively. It is important to point out that the Froude number of the gait, 0.42, assures a higher walking speed of the bipedal model as compared with prototypes in the literature such as Veronica and Meta with the maximum Froude numbers of 0.16 and 0.2, respectively [66]. Furthermore, the active mechanical cost of transport, 0.0299, emphasizes that the bipedal model of Figure 3.1a is certainly energy efficient compared to the mechanical cost of transport for Meta (0.08) and humans (0.04) [18].

3.5.2 Effects of two-sided ankle stiffness versus uniform ankle stiffness on the gait characteristics and the energy efficiency of bipedal walking

Here, the effects of two-sided ankle stiffness versus uniform ankle stiffness on the gait characteristics (the normalized step length s_l, normalized step period T, and Froude number v) and the energy efficiency (active mechanical energy consumption W_{act}, and active cost of transport c_{amt}) are explored through simulations.

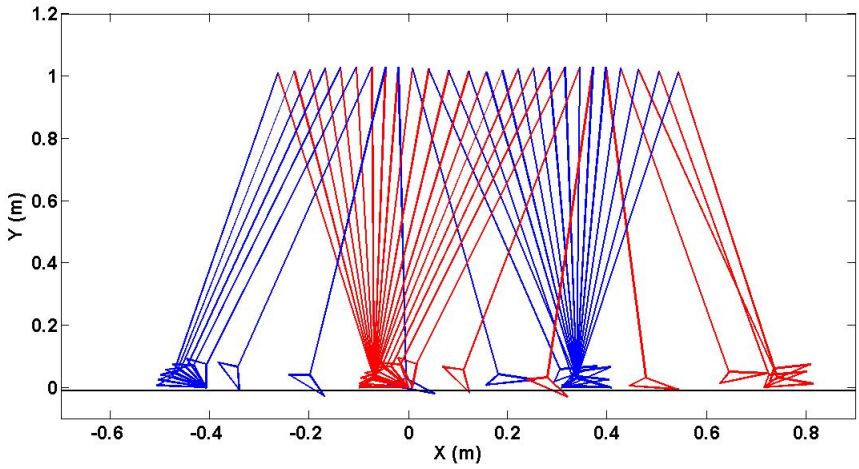

Figure 3.4: Animated a novel passive-based bipedal gait with compliant-ankle flat-foot and compliant hip-actuation.

Noteworthy is that the ankle stiffness is determined by two parameters namely the frontside ankle stiffness K_{ft} and the ankle stiffness ratio r that is the ratio between the backside and the frontside ankle stiffness, explained in details in Section 3.1. The ankle stiffness ratio $r = 1$ represents uniform ankle stiffness, and $r > 1$ denotes two-sided ankle stiffness.

Figure 3.5 shows how the normalized step length s_l, normalized step period T, and normalized walking speed (Froude number) v vary when the frontside ankle stiffness K_{ft} increases from 0.10 (N.m/rad) to 0.30 (N.m/rad) for the ankle stiffness ratio r of 1, 2.5, 5, 7.5, and 10 with the hip torque τ_{hip} of 0.5 (N.m) during the single support phase. The important quantities of Figure 3.5 are also presented in Table 3.3.

Figure 3.6 shows the active mechanical energy consumption W_{act} and the active cost of transport c_{amt} versus the frontside ankle stiffness K_{ft} of 0.10 (N.m/rad) to 0.30 (N.m/rad) for the ankle stiffness ratio r of 1, 2.5, 5, 7.5, and 10 with the hip torque τ_{hip} of 0.5 (N.m) during the single support phase. Furthermore, Table 3.4 presents the important quantities of Figure 3.6.

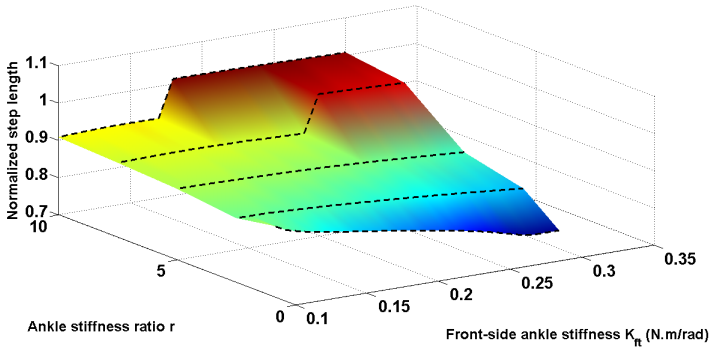

(a)

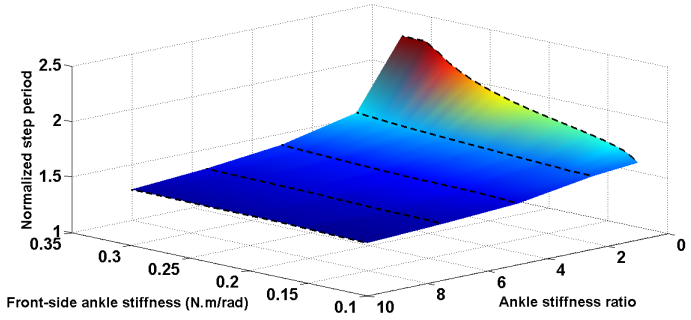

(b)

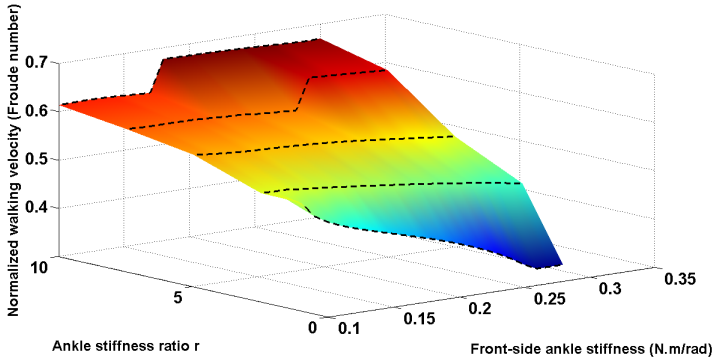

(c)

Figure 3.5: (a) Step length normalized to the leg length. (b) Step period normalized to $\sqrt{(l/g)}$. (c) Walking speed normalized to $\sqrt{lg}$ (Froude number). All parts are presented versus the frontside ankle stiffness K_{ft} and the ankle stiffness ratio r.

Table 3.3: Important quantities about the effects of ankle stiffness on the normalized step length s_l, step period T, and walking speed v.

Gait properties	$K_{ft} = 0.1$	**Change to**	$K_{ft} = 0.2$	**Change to**	$K_{ft} = 0.3$	**Average value**	
	0.88	$\downarrow$ 7%	0.82	$\downarrow$ 9%	0.75	0.82	$r = 1$
	0.87	$\downarrow$ 2%	0.85	$\downarrow$ 4%	0.82	0.85	$r = 2.5$
s_l	0.89	$\downarrow$ 1%	0.88	$\downarrow$ 2%	0.86	0.88	$r = 5$
	0.89	0%	0.90	$\uparrow$ 9%	0.99	0.93	$r = 7.5$
	0.91	$\uparrow$ 11%	1.01	0%	1.01	0.98	$r = 10$
	1.70	$\uparrow$ 18%	2.00	$\uparrow$ 14%	2.28	2.00	$r = 1$
	1.66	$\uparrow$ 3%	1.71	$\uparrow$ 4%	1.78	1.72	$r = 2.5$
T	1.55	$\uparrow$ 1%	1.58	$\uparrow$ 3%	1.63	1.59	$r = 5$
	1.51	$\uparrow$ 2%	1.54	$\uparrow$ 1%	1.55	1.53	$r = 7.5$
	1.48	$\uparrow$ 1%	1.50	$\uparrow$ 1%	1.51	1.50	$r = 10$
	0.52	$\downarrow$ 20%	0.42	$\downarrow$ 21%	0.33	0.42	$r = 1$
	0.53	$\downarrow$ 6%	0.50	$\downarrow$ 8%	0.46	0.50	$r = 2.5$
v	0.57	$\downarrow$ 2%	0.56	$\downarrow$ 5%	0.53	0.55	$r = 5$
	0.60	$\downarrow$ 1%	0.59	$\uparrow$ 9%	0.64	0.61	$r = 7.5$
	0.62	$\uparrow$ 10%	0.68	0%	0.68	0.66	$r = 10$

* To read each quantity, one might need to intersect the desired values of K_{ft} and r. Note that changes have been calculated with respect to two successive values of K_{ft}. For example, under the ankle stiffness ratio r of 5, when the frontside ankle stiffness K_{ft} increases from 0.20 to 0.30 (N.m/rad), the normalized step length s_l decreases about %2 from 0.88 to 0.86, respectively.

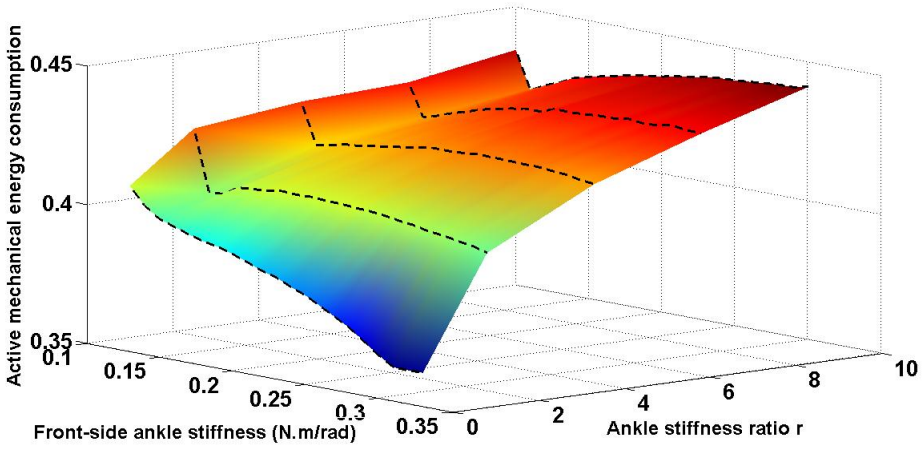

(a)

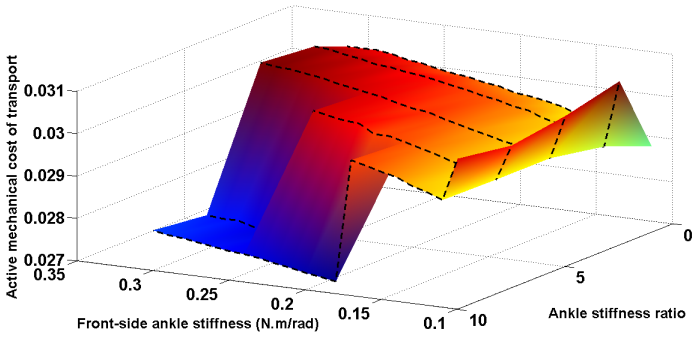

(b)

Figure 3.6: (*a*) Active mechanical energy consumption W_{act}. (*b*) Active cost of transport c_{amt}. All parts are presented versus the frontside ankle stiffness K_{ft} and the ankle stiffness ratio r.

Table 3.4: Important quantities about the effects of ankle stiffness on the active mechanical energy consumption W_{act} and the active mechanical cost of transport c_{amt}.

Gait properties	$K_{ft} = 0.1$	**Change to**	$K_{ft} = 0.2$	**Change to**	$K_{ft} = 0.3$	**Average value**	
	0.40	$\downarrow$ 5%	0.38	$\downarrow$ 5%	0.36	0.38	$r = 1$
	0.42	$\downarrow$ 2%	0.41	$\downarrow$ 5%	0.39	0.41	$r = 2.5$
W_{act}	0.43	$\downarrow$ 2%	0.42	$\downarrow$ 2%	0.41	0.42	$r = 5$
	0.43	0%	0.43	$\uparrow$ 2%	0.44	0.43	$r = 7.5$
	0.44	$\uparrow$ 2%	0.45	$\uparrow$ 2%	0.46	0.45	$r = 10$
	0.0290	$\uparrow$ 3%	0.0299	$\uparrow$ 2%	0.0304	0.0298	$r = 1$
	0.0308	$\downarrow$ 3%	0.0301	$\uparrow$ 2%	0.0307	0.0305	$r = 2.5$
c_{amt}	0.0305	$\downarrow$ 2%	0.0299	$\uparrow$ 4%	0.0310	0.0305	$r = 5$
	0.0303	0%	0.0304	$\downarrow$ 9%	0.0278	0.0295	$r = 7.5$
	0.0305	$\downarrow$ 10%	0.0274	$\uparrow$ 1%	0.0278	0.0286	$r = 10$

* To read each quantity, one might need to intersect the desired values of K_{ft} and r. Note that changes have been calculated with respect to two successive values of K_{ft}. For example, under the ankle stiffness ratio r of 5, when the frontside ankle stiffness K_{ft} increases from 0.20 to 0.30 (N.m/rad), the active mechanical cost of transport c_{amt} increases about %4 from 0.0299 to 0.0310, respectively.

3.5.2.1 Uniform ankle stiffness

Having referred to Figure 3.5 and Table 3.3, one can find that for the ankle stiffness ratio r of 1 (uniform ankle stiffness) for the increase in the frontside ankle stiffness K_{ft} from 0.10 (N.m/rad) to 0.30 (N.m/rad), the normalized step length s_l decreases about 12% from 0.88 to 0.76, while the normalized step period T increases about 35% from 1.70 to 2.28. As a result, the Froude number v decreases about 37% from 0.52 to 0.33.

The aforementioned results indicate that when the ankle stiffness is uniform (the backside ankle stiffness is the same as the frontside ankle stiffness), increasing the ankle stiffness makes the step length and the step period decrease and increase, respectively. As a result, the Froude number decreases. For those conditions, the gait characteristics are very sensitive to any change in ankle stiffness.

Having referred to Figure 3.6 and Table 3.4, one can find that when the frontside ankle stiffness K_{ft} increases from 0.10 (N.m/rad) to 0.30 (N.m/rad) for the ankle stiffness ratio r of 1, the active mechanical energy W_{act} decreases about 12% from 0.405 (J) to 0.362 (J), while the active cost of transport c_{amt} increases about 7% from 0.0290 to 0.0304.

The aforementioned results indicate that for uniform ankle stiffness, when the backside ankle stiffness is the same as the frontside ankle stiffness, increasing the ankle stiffness makes the energy efficiency decrease, although the energy input injected by the hip actuator that is required for the bipedal model to be able to walk on the flat ground decreases too. Under this condition, the active mechanical energy consumption and the active cost of transport are sensitive to any change in ankle stiffness.

The aforementioned results on the effects of uniform ankle stiffness on the gait characteristics and energy efficiency of bipedal walking will be compared with results of two-sided ankle stiffness in the next section.

3.5.2.2 Two-sided ankle stiffness

Having referred to Figure 3.5 and Table 3.3, one can find that for two-sided ankle stiffness with the ankle stiffness ratio r of 2.5, an increase in the frontside ankle stiffness K_{ft} from 0.10 (N.m/rad) to 0.30 (N.m/rad), the average of normalized step length s_l increases about 5%, while the average of normalized step period decreases about 16%. Therefore, the average of Froude number v is about 20% higher. Note that the aforementioned percentages are relative to the same properties for the ankle stiffness ratio r of 1.

When the ankle stiffness is two-sided (the backside ankle stiffness becomes 2.5 and 5 times stiffer, while the frontside ankle stiffness is fixed), increasing the ankle stiffness makes the step length and the step period increase and decrease, respectively. As a result, the Froude number increases. Under this condition, the sensitivity of the gait characteristics to any change in ankle stiffness gradually becomes insignificant.

Having referred to Figure 3.6 and Table 3.4, one can find that for two-sided ankle stiffness with the ankle stiffness ratio r of 2.5, an increase in the frontside ankle stiffness K_{ft} of 0.10 (N.m/rad) to 0.30 (N.m/rad), the average active mechanical energy increases about 8% from 0.386 (J) to 0.414 (J), and the average active cost of transport increases about 2% from 0.0297 to 0.0303. Note that the aforementioned percentages are relative to the same properties for the ankle stiffness ratio r of 1.

For two-sided ankle stiffness, when the backside ankle stiffness increases with the higher ratios, 2.5 and 5, than the frontside ankle stiffness does, increasing the ankle stiffness makes the energy input injected by the hip actuator moderately decreases. Under this condition, the sensitivity of the active mechanical energy consumption and the active cost of transport to any change in ankle stiffness gradually becomes insignificant. The energy efficiency, however, shows two different trends under the aforementioned condition; it moderately increases when the frontside ankle stiffness is low, but it slightly decreases when the frontside ankle stiffness is high.

So far, the effects of two-sided ankle stiffness versus uniform ankle stiffness on the gait characteristics and energy efficiency of bipedal walking have been explored, such that the ankle stiffness ratio r, the ratio between the backside and frontside ankle stiffness, varies from 1 to 5.

However, for the ankle stiffness ratio of 7.5 and 10, a crucial gait event named single-support heel-off occurs, that significantly influences the performance of bipedal walking. In the next section, it is explained how such a gait event occurs, and changes the gait characteristics and the energy efficiency, relative to uniform ankle stiffness.

3.5.3 Single-support heel-off

Single-support heel-off in Figure 3.2 is a crucial gait event in order to achieve a longer step length and a higher walking speed in bipedal walking. Here, two important questions about this crucial gait event are explored: how this gait event can improve the gait characteristics of bipedal walking, and how this gait event can influence the energy efficiency of bipedal walking.

3.5.3.1 How single-support heel-off is achieved

Single-support heel-off occurs when the torque of the ankle spring is sufficient to lift up the heel of the stance leg when the swing leg is still swinging forward. In other words, the torque of the ankle is to overcome the weight of the biped. Such a crucial gait event takes place when the backside ankle spring applies torque after the stance leg passes midstance, because the neutral position of the ankle spring is where the foot and its leg are perpendicular and the distance from the ankle to the toe is more than the distance from the ankle to the heel.

Single-support heel-off does not occur when the frontside and the backside ankle stiffness have the same value for the range of the frontside ankle stiffness K_{ft} from 0.10 (N.m/rad)

to 0.30 (N.m/rad). More importantly, increasing the frontside ankle stiffness even more will not make single-support heel-off occur, but will instead cause the toe of the stance foot to bounce off the ground with heel contact. More specifically, under the same value of the frontside and the backside ankle stiffness, increasing the frontside ankle stiffness K_{ft} from 0.10 (N.m/rad) to 0.30 (N.m/rad) makes the step length s_l decrease to its minimum (normalized value of 0.75), but makes the step period T increase to its maximum (normalized value of 2.28), leading to the minimum normalized walking speed (the Froude number) v of 0.33.

Accordingly, to achieve single-support heel-off, there is a need to increase the backside ankle stiffness more than the frontside ankle stiffness. However, such a gait event still does not occur when the rate of increase in the backside ankle stiffness is 2.5 or 5 times more than the frontside ankle stiffness for the range of the frontside ankle stiffness K_{ft} from 0.10 (N.m/rad) to 0.30 (N.m/rad). The reason is that the torque of the ankle spring still cannot overpower the weight of the bipedal model. More specifically, such an increase in the frontside ankle stiffness K_{ft} for the ankle stiffness ratio r of 2.5 and 5 moderately enlarges the normalized step length s_l to 0.82 and 0.86, respectively, and shortens the normalized step period T to 1.78 and 1.63, respectively. As a result, it leads to a reasonable increase in the normalized walking speed (the Froude number) v up to 0.46 and 0.53, respectively.

Finally, setting the ankle stiffness ratio r to 7.5, single-support heel-off occurs at the frontside ankle stiffness K_{ft} of 0.23 (N.m/rad) since the backside ankle stiffness becomes strong enough to lift up the weight of the biped. With an ankle ratio r of 10, single-support heel-off occurs even earlier at the frontside ankle stiffness K_{ft} of 0.17 (N.m/rad).

In conclusion, it is a very challenging task to produce flat-foot limit-cycle gaits including single-support heel-off, since very specific values are required for the backside and the frontside ankle stiffness.

3.5.3.2 How single-support heel-off improves the gait characteristics of bipedal walking

To determine if single-support heel-off improves the gait characteristics, in particular, the walking speed, it is required to precisely compare the rate of change in the step length, step period, and walking speed of limit-cycles with and without single-support heel-off.

Referring to Figure 3.5, single-support heel-off makes the normalized step length s_l increase significantly to 0.99 and 1.01, for the ankle stiffness ratios r of 7.5 and 10, respectively. It also causes an increase of about 20% in normalized step length s_l, compared to limit-cycle gaits excluding single-support heel-off with the ankle stiffness ratios r of 7.5 and 10, respectively. Furthermore, it shows an increase of about 26% in the minimum value of the normalized step length s_l with the ankle stiffness ratio r of 1 (uniform ankle stiffness). The inclusion of this crucial gait event shortens the normalized step period T to 1.55 and 1.51, with the ankle stiffness ratios r of 7.5 and 10, respectively. This causes the normalized walking speed (the Froude number) v increase significantly to 0.61 and 0.66, respectively. It shows an increase of about 10% in normalized walking speed v of limit-cycle gaits excluding single-support heel-off with the ankle stiffness ratios r of 7.5 and 10, respectively. Furthermore, it shows an increase of 100% in the minimum value of the normalized walking speed v with the ankle stiffness ratio r of 1 (uniform ankle stiffness). Note that the maximum achievable value for the normalized walking speed or the Froude number of bipedal walking is 1.00 [82]. Huang et al. [65] reported a similar significant increase in the step length when single-support heel-off occurs.

To understand the significance of the above results, the key point is the dominant role of the backside ankle stiffness in the timing of the double support phase since such stiffness dominates the vertical component of the ground reaction force of the stance leg. Such timing is inversely proportional to the values of the step length and the walking speed because the unilateral constraints during the double support phase impede the forward

motion. As a result, if the period of the double support phase is longer, the step length and the walking speed will be lower and vice versa.

From Figure 3.7, it can be seen that single-support heel-off makes the period of the double support phase dramatically smaller as it causes the step length and the walking velocity to increase. In addition, when single-support heel-off occurs, the heel of the stance leg has been lifted from the ground, while the stance leg is still pivoting around its toe. Therefore, the effective length of the stance leg increases, so the step length and the walking speed increase.

In conclusion, single-support heel-off significantly increases the step length and the walking velocity, leading to higher walking speed. Such an improvement in the speed of bipedal walking leads to exploration into the energy cost of this gait event in the next subsection.

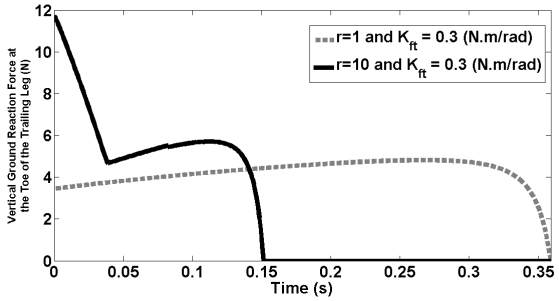

Figure 3.7: Vertical ground reaction force at the toe of the stance foot, which represents the period of the double support phase.

3.5.3.3 How single-support heel-off influences the energy efficiency of bipedal walking

As it was already concluded, to achieve single-support heel-off, the value of the backside stiffness has to be set more than that of the frontside stiffness. Looking at Figure 3.6 and Table 3.4 it can be seen that with the ankle stiffness ratios r of 7.5 and 10, where single-support heel-off occurs, the energy input increases about 16% and 21%, respectively, as

compared with the average of the energy input required when the backside and frontside ankle stiffness is the same.

The energy efficiency defined in Eq. 3.19 is proportional to the ratio of the energy input to the step length. Referring to Figure 3.6 and Table 3.4, when the backside ankle stiffness is set 7.5 and 10 times more than the frontside ankle stiffness, where single-support heel-off takes place; the active cost of transport significantly decreases about 9% and 10%, respectively, as compared with the average of the energy input required when the backside and frontside ankle stiffness is the same. This implies that single-support heel-off significantly improves the energy efficiency. Hobbelen and Wisse [68] reported such an improvement in the energy efficiency for bipedal walking when single-support heel-off occurs.

To understand the significance of the aforementioned behaviors, one should know that when single-support heel-off happens, the step length significantly increases, which increases the maximum elastic energy and the minimum kinetic energy immediately before heel-strike and foot-strike. Since the amount of energy dissipation at the heel and foot strikes is proportional to the amount of kinetic energy immediately before the strikes [35], the higher step length increases the amount of energy dissipation at the strikes. Furthermore, as shown in Figure 3.5, when single-support heel-off takes place, the walking velocity considerably increases. Consequently, the amount of energy dissipation at the ankle increases. Therefore, having single-support heel-off occur, the step length and the walking velocity increase, and due to the above reasoning, the energy input increases.

On the other hand, the active cost of transport has a different trend. Since it is defined as the ratio of the energy input over the step length, its change depends on increase/decrease of the energy input to increase/decrease of the step length. In this particular situation, since the amount of increase in the step length considerably dominates the amount of increase in the energy input, the active cost of transport dramatically

decreases, implying that the energy efficiency of the bipedal model significantly improves.

In conclusion, even though limit-cycle gaits including single-support heel-off require higher energy input as compared with gaits excluding it, single-support heel-off does significantly improve the energy efficiency of bipedal walking since the increase in the step length dominates the increase in the energy input.

3.6 Summary

In this chapter, a novel mathematical model of a passive-based bipedal walking robot with compliant hip-actuation and complaint-ankle flat-foot was developed. Compliant hip-actuation enables the model to walk on the flat ground. The impedance of each ankle was adjusted by two springs, one at the backside and the other at the frontside, and one damper. Poincare mapping was utilized to extract all possible stable limit-cycle gaits for various ankle stiffness. Following that, this chapter made efforts to demonstrate a new type of limit-cycle gaits, and to explain its versatile sequences and rich properties. Such gaits were demonstrated to be versatile, dynamic, and energy-efficient, similar to humans'.

It was then explored how two-sided ankle stiffness influences the performance of bipedal walking, as compared with uniform ankle stiffness. As major conclusions, it was found that:

- for uniform ankle stiffness, when the ankle stiffness increases, the walking speed and the energy efficiency decrease. Furthermore, the sensitivity of gait properties, such as speed and efficiency, to the rate of change in the ankle stiffness is considerable.

- for two-sided ankle stiffness (before single-support heel-off occurs), when the ankle stiffness increases, the walking speed increases, but still the energy efficiency decreases.

- for two-sided ankle stiffness (after single-support heel-off occurs), not only the walking speed increases considerably, but also the energy efficiency improves significantly.

In the next chapter, a physical bipedal robot is designed and developed to experimentally prove the important role of compliant hip-actuation in achieving a highly dynamic and energy efficient walking gait. Note that, the inclusion of compliant-ankle flat-foot in the physical robot remains as future work.

Chapter 4

A highly dynamic and energy-efficient physical bipedal robot

In the previous chapter, a novel mathematical model of a passive-based bipedal walking robot with compliant hip-actuation and compliant-ankle flat-foot was presented to provide mechanical insights into bipedal walking in terms of gait characteristics and energy efficiency. As a result, the mechanical cost of transport and the Froude number of bipedal walking were significantly improved, relative to other passive-based bipedal walkers and humans in the literature [12, 15, 18]. Both compliant hip-actuation and compliant-ankle flat-foot in the above novel model led to such a significant performance of bipedal walking.

Accordingly, this chapter presents the design and development of a physical bipedal robot to experimentally validate the importance of compliant hip-actuation in achieving a highly dynamic and energy efficient walking gait. Note that the inclusion of compliant-ankle flat-foot in the physical bipedal robot remains as future work. This chapter contains the mechanical design, actuation, sensing, coordination, and experimentation of the physical bipedal robot.

The above machine can walk on the flat ground based on the concept of passive-based

dynamic walking. The robot has three internal degrees of freedom: one at the hip and two at the knees. The hip is equipped with a custom-designed compliant hip-actuation mechanism which can inject energy to the system, and enables the bipedal robot to walk on the flat ground. The knees are equipped with two custom-designed spring-loaded knee-latch mechanisms which can lock and unlock the joints.

The main challenge of the design and development of the physical bipedal robot is to replace the gravitational source of energy by another source of energy, while the natural dynamics of the robot is not suppressed by the actuation dynamics. Therefore, the actuation mechanism must allow the coordination between the natural dynamics and the energy injection. However, it is very challenging to experimentally realize such a requirement.

Other than the actuation challenge, to keep the energy consumption low, the knee joints of the prototype are passive. However, having the passive knee joints move desirably during walking is a difficult challenge. The reasons are: firstly, there is no actuation to flex and extend the knees; secondly, when the knees are fully extended, they only stay fully extended for a very short time, almost several milliseconds, due to the gravity. This issue makes the knees to be bent at heel-strike, and since the knees are passive, the stance leg at the next step cannot stay standstill. This eventually causes the robot to fall. As a result, it is highly important to design and develop a smart knee-latch mechanism to latch and unlatch the knees at right time with minimum energy cost, without any interference in the natural dynamics of the robot.

4.1 Passive-based physical bipedal robot

A physical prototype of a passive-based bipedal walking robot shown in Figures 4.1 and 4.2 has been designed and fabricated to walk on the flat ground with a highly dynamic and energy efficient gait. The robot is about $5\,(kg)$, and has two $0.5\,(m)$ long legs. Each

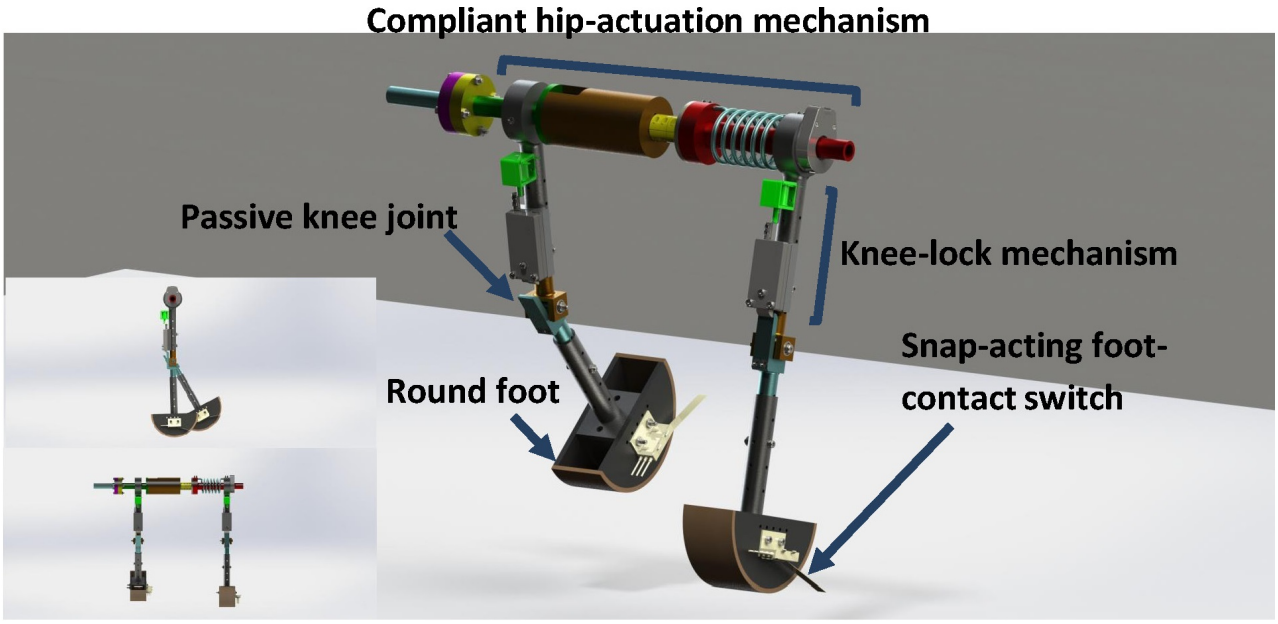

Figure 4.1: Computer-aided design (CAD in SolidWorks) of a passive-based bipedal walking robot.

leg has two parts, a $0.20\,(m)$ long thigh and a $0.25\,(m)$ long shank which are connected by a knee joint. Each ankle is in contact with the ground via a round foot with a radius of $0.05\,(m)$. Two legs are connected by a hip joint. As a result, the robot has 3 internal degrees of freedom: one at the hip joint and two at the knee joints. At the hip joint, a compliant hip-actuation mechanism has been designed to inject energy to the robot. At the knee joints, knee-latch mechanisms have been designed to lock/unlock the knee joints. At the feet, two snap-acting foot-contact switches have been installed to detect the time in which the foot hits the ground, and to coordinate both the hip-actuation and knee-latch mechanisms. The details of these mechanisms will be explained in the next sections.

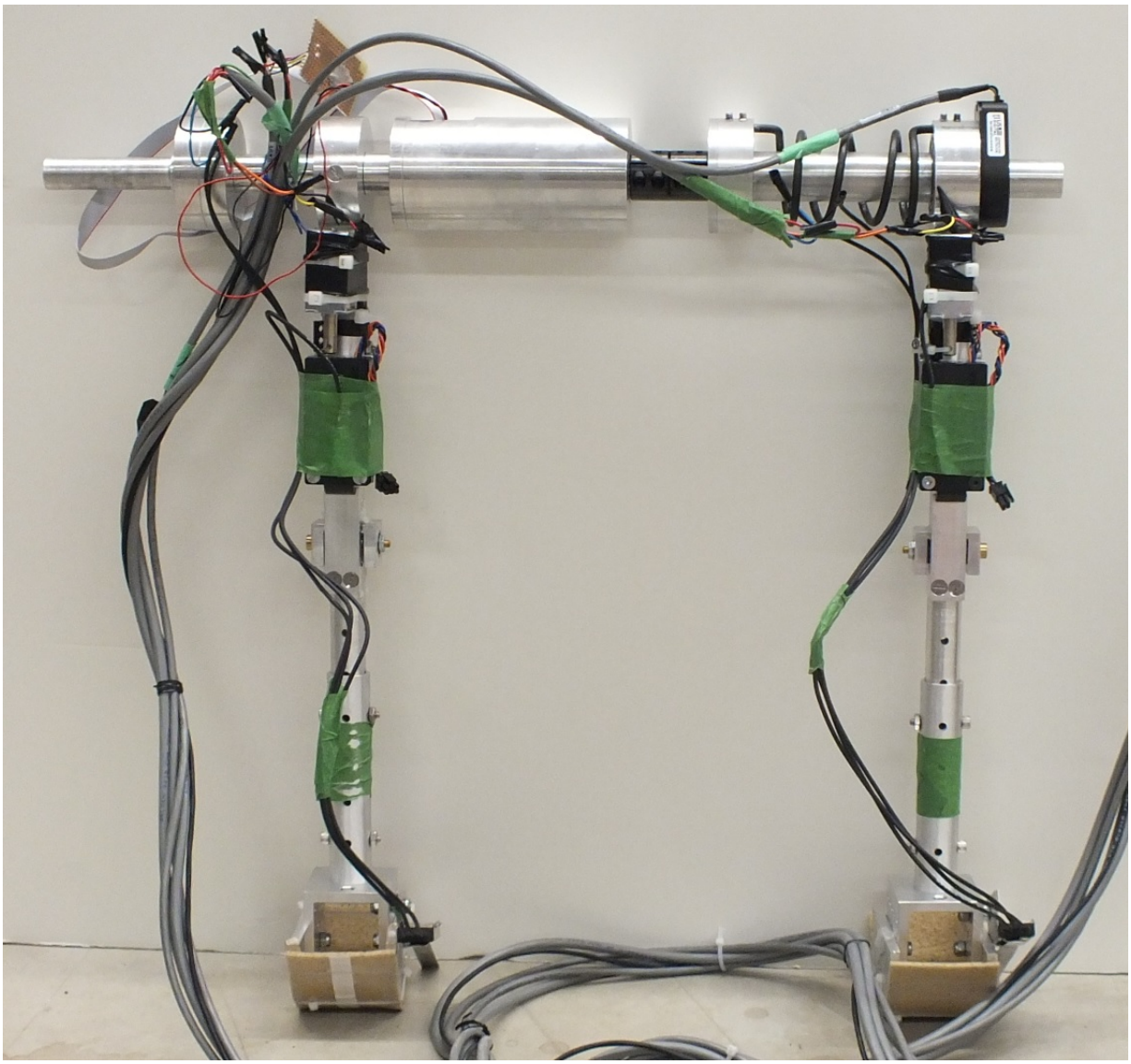

(b)

Figure 4.2: Physical prototype of a passive-based bipedal walking robot.

4.2 Mechanical design, actuation, and sensing

The following sections explain the mechanical design, actuation, and sensing of the physical robot in details.

4.2.1 Compliant hip-actuation mechanism

Figure 4.3 shows the details of the compliant hip-actuation mechanism. This mechanism is expected to:

- coordinate the natural dynamics of the hip joint and the energy input.
- perform energy recovery by storing and releasing the energy input at proper timing, while walking.
- be backdrivable and tolerate shocks due to heel-strikes.

By default, a geared DC electrical motor does not provide any of the aforementioned expectations. Friction and inertia of a DC geared motor at the hip joint dominates the natural dynamics at the joint. Therefore, the joint cannot move freely. In addition, a geared DC motor is not a good choice in terms of energy recovery, since it dissipates energy continually, due to friction. Finally, a geared DC motor with high gear ratio is not backdrivable; when it is directly attached to a joint, it makes the joint to be not backdrivable, either. Thus, any shocks due to heel-strikes are transferred directly to the motor shaft, which can have damaging effects on the shaft.

To resolve all aforementioned issues and meet the above three expectations, a straight-offset torsional spring is installed in series with a geared DC motor. The DC motor controls the neutral angle of the torsional spring, and stores energy as elastic-potential energy. The torsional spring bypasses the high friction and inertia of the geared DC motor; makes the hip actuation backdrivable, and absorbs any shocks due to heel-strike.

Figure 4.3 shows further details about the compliant hip-actuation mechanism. It is comprised of a DC motor, attached by a gearbox at one side and a rotary encoder at the other side. All are covered in the motor housing which is rigidly connected to the right thigh. The gearbox output shaft is attached to the spring shaft via a Mechanical coupling. The other end of the spring shaft is attached to the left thigh via a bearing. So, the spring shaft can rotate relative to the left thigh. Such a relative motion is measured by another rotary encoder.

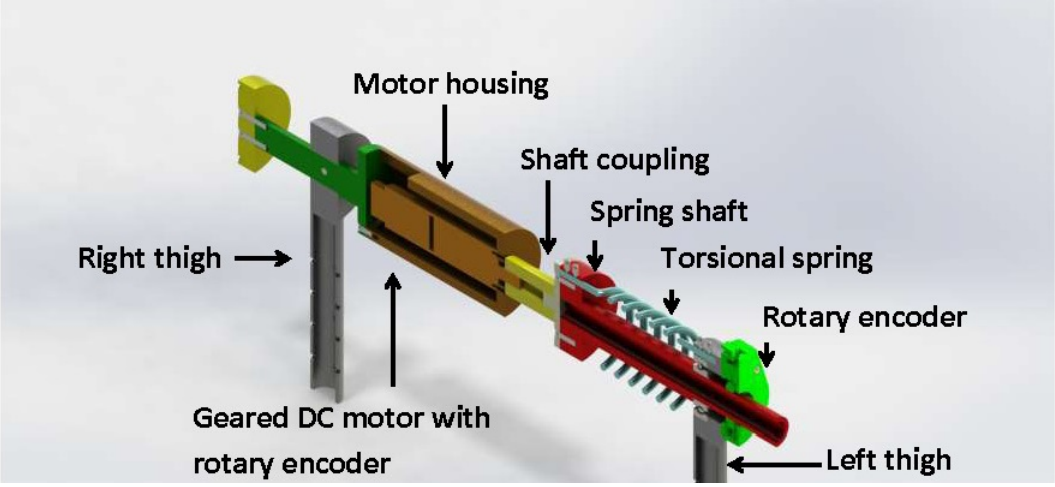

Figure 4.3: Compliant hip-actuation mechanism

4.2.2 Passive knee joints and spring-loaded knee-latches

The knee joints in bipedal walking play a very important role. The knees hinge the thighs to the shanks, and so provide a biped with a reconfigurable leg structure. Such a structure helps the leg to avoid scuffing on the ground during walking. In comparison to trajectory-controlled bipeds [4, 24, 36, 43, 44], in passive-based bipedal walking, for the sake of energy efficiency and natural gait, the knees are passive. However, tuning the knees to move naturally during walking, yet in a desirable way, is a very challenging task [15, 18].

To cope with the above challenge of the passive knees, the physical bipedal robot, shown

in Figure 4.2, uses a spring-loaded knee-latch attached to the thigh and a hyperextension limit attached to the shank, shown in Figure 4.4. The spring-loaded knee-latch is comprised of a compression spring (inside) which is in series with a latch bolt. The rest length of this spring is when the latch bolt is fully extended. When a force pushes up the latch bolt, the spring becomes compressed. At the moment that the force is removed, the compressed spring pushes back the latch bolt in a fully extended position.

The knee joint rotates freely when it is not locked. When the knee reaches full extension midway through swinging, so called "knee-strike", the spring-loaded knee-latch engages. At this moment, the latch bolt is pushed up via the hyperextension limit. After the hyperextension limit passes the latch bolt, the compressed spring clicks, and pushes back the latch bolt in a fully extended position. As a result, the hyperextension limit remains locked in a full extension throughout the rest of the swing phase, and during the upcoming stance phase. But, at the beginning of the next swing, a DC solenoid, which is in series with the spring-loaded latch bolt, through a simple mechanical transmission, disengages the knee-latch by pulling up the latch bolt within a very short time period. The knee joint is then unlocked, and the joint can flex and swing forward freely, to avoid foot-scuffing at midstance.

4.2.3 Round foot and snap-acting foot-contact switch

The foot, shown in Figure 4.5, has been designed as a round-shape foot which is rigidly connected to the shank. The round-shape foot rolls forwards on the ground, and helps the whole biped to progress forwards [12, 15, 18]. The snap-acting foot-contact switches, which has an important role in coordination, are to detect heel-strikes.

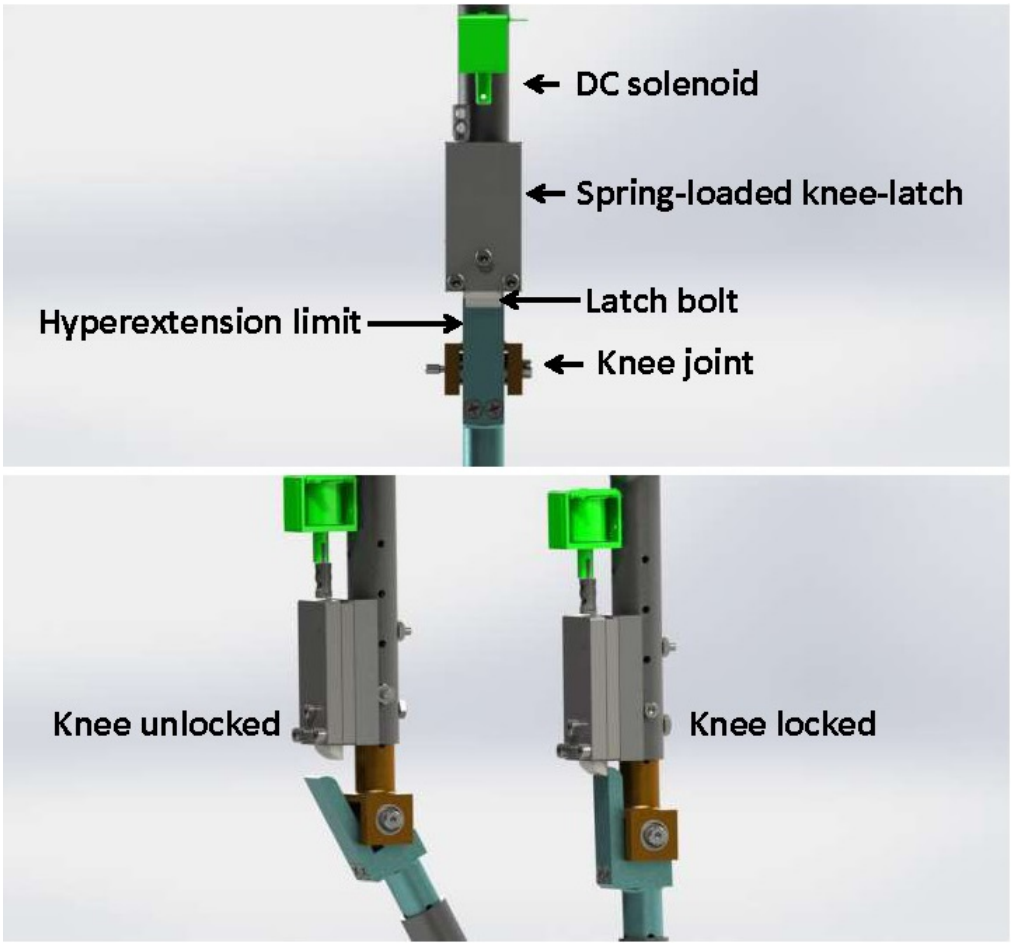

Figure 4.4: (Top) Spring-loaded knee-latch and passive knee joint; (Bottom) Knee joint flexed (unlocked) and fully extended (locked).

Figure 4.5: Round foot and snap-acting contact switch.

4.2.4 Boom

The physical bipedal robot in Figure 4.2 is a 2D walking machine. In the literature, there are two approaches to provide a 2D walking condition for a biped: (1) two pairs of legs [12, 26, 28], (2) a boom [27, 83]. In this thesis, the boom has been selected, to provide a 2D walking condition for the robot.

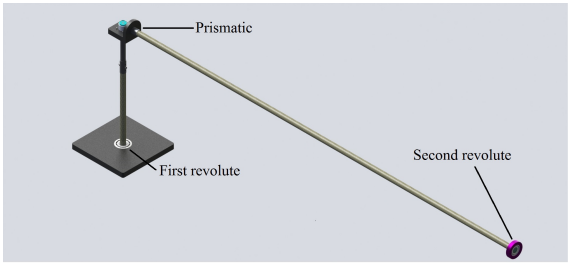

Figure 4.6: Passive boom provides the bipedal robot 2D gait.

The boom has been connected to the hip joint, and has 3 passive degrees of freedom, shown in 4.6. There are two revolute passive joints, and one prismatic passive joint. The first revolute joint allows the robot to walk in a circular path. The prismatic joint allows the robot's hip to have a vertical motion (up and down), and the second revolute allows the robot's hip to have a pitch motion. Therefore, the robot's hip has two translational

and one rotational degrees of freedom. In other words, the robot moves in a 2D plane which is tangential to the circular path at each moment.

4.3 Coordination

Figure 4.7 shows the important postures of a complete gait cycle of the robot, and Figure 4.8 shows the schematic flowchart that clarifies how the robot, its sensing, actuation, and control work.

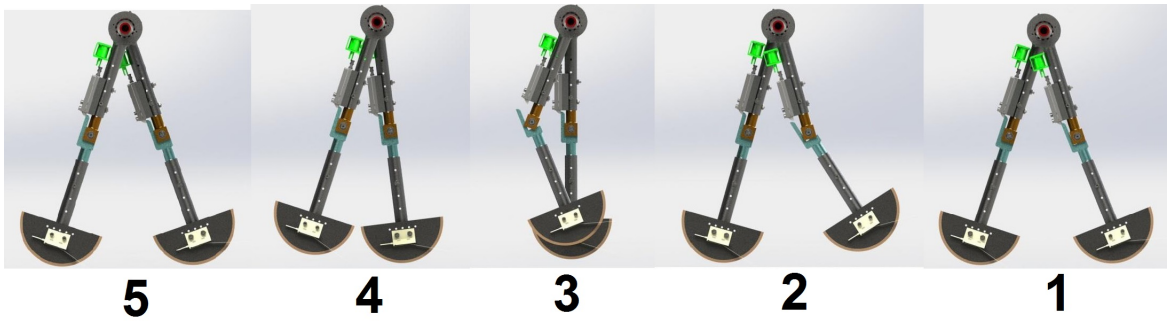

Figure 4.7: Schematic of the passive-based gait on the ground.

Each bipedal gait cycle of the robot starts with posture **"1"**, shown in Figure 4.7, when the foot-contact switch of the swing leg is triggered at heel-strike. A digital signal of the foot-contact switch is then sent to a Microcontroller (Compatible Mega Motor Shield 13A, 5-28V).

During posture **"2"**, the Microcontroller processes the digital signal of the foot-contact switch via C++ programming. It then activates a solid-state relay (PLC Relay Opto-coupler 33V). The relay allows a load current, which comes from a PC power supply (MACRON Power, Model: MPT-301), to activate a linear DC solenoid (Linear Solenoid, Intermittent, Pull,12V DC, 0.5"stroke, 45 Oz Force). The solenoid disengages the knee-latch mechanism almost instantaneously. Thus, the hyperextension limit of the shank of the swing leg is disengaged from the latch bolt of the knee-latch mechanism, and the knee

of the swing leg is then flexed. Right after that, the Microcontroller sends a digital signal as a flag signal to a PC (Model: Dell-Precision T7500 - Processor: Intel (R) Xeon (R) - RAM: 12.0 GB 64 Bit) via a DAQ (Quanser- QPIDe Data Acquisition Device). The flag signal of the Microcontroller triggers a low-level control which has been developed in Simulink (MATLAB) by using QuarC features (Quanser - QUARC® Real-Time Control Software). The controller sends an analog signal as an output to an amplifier (4-Q-DC servo amplifiers). The amplifier, which is powered by a power supply (Power Supply - 60V - 4A - ANALOG), amplifies the analog output of the controller. This signal runs the geared DC motor inside the compliant hip-actuation mechanism, and so injects energy to the bipedal robot.

During posture **"3"**, the input energy injected by the hip-actuation mechanism stores as a potential-elastic energy. Such an energy ensures that the swing leg is swinging forward freely, while the stance leg is progressing forward freely.

Posture **"4"** starts when the hyperextension limit of the swing shank engages with the latch bolt of the knee-latch mechanism, again. The hyperextension limit remains locked in full extension throughout the rest of posture **"4"**. During this posture, the robot moves freely until the heel of the swing leg strikes the ground at instantaneous posture **"5"**. Afterward, the aforementioned five states (**1-5**) will be repeating for the next gait cycle.

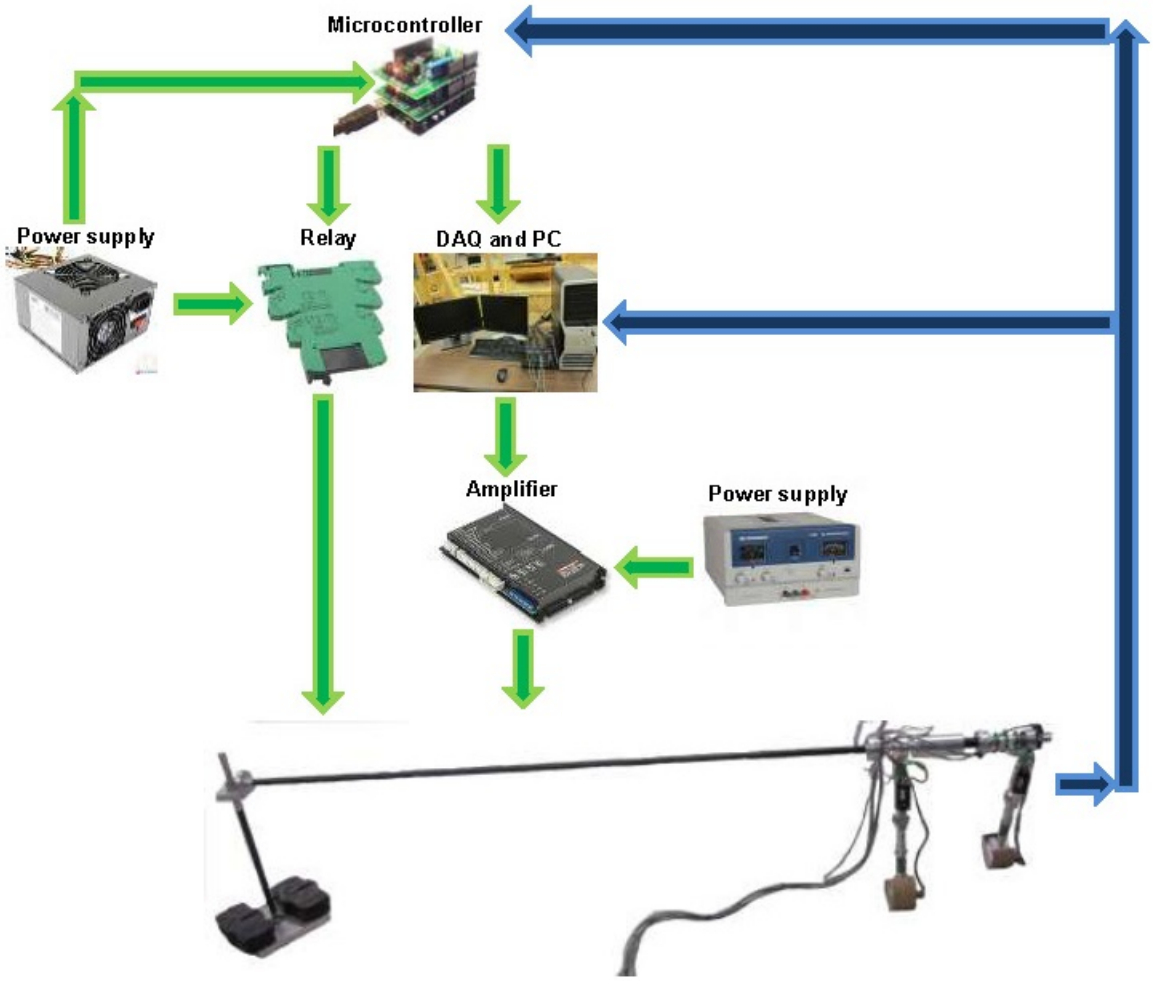

Figure 4.8: Operating flowchart of the passive-based physical bipedal robot.

4.4 Experimentation

Here, the experimental procedure consisting of five parts is explained.

- Coordination between the hip-actuation and the foot-contact switch
- Coordination between the hip-actuation, foot-contact switch, and spring-loaded knee-latch
- Foot size and friction
- Boom effects on the prototype's dynamics and a safety rope
- Prototype walking on the flat ground; gait measurements and properties

4.4.1 Coordination between the hip-actuation and the foot-contact switch

As it was discussed in Section 4.3, the snap-acting foot-contact switch is triggered when heel-strike happens. As a result, a digital signal of the foot-contact switch is used to inject energy into the robot such that the swing leg is swinging forward against the stance leg which itself is progressing forward on the ground.

The sampling time of the coordination between the hip-actuation mechanism and the foot-contact switch is $0.002(sec)$. The output control signal from DAQ to DC amplifier is between $-10\,(V)$ and $+10\,(V)$. Since the nominal voltage of the motor is about $36\,(V)$, the amplifier gain is set at 3.6. The settling time during which the motor stores energy into the spring has been designed to be about $0.2\,(sec)$. Such settling time is important to be as short as possible, because it determines whether the robot can walk forward or fall. For our physical bipedal robot, since the motor power is $22\,(W)$, the aforementioned settling time is the shortest possible settling time.

The amount of total (electrical) and mechanical energy inputs are defined as:

$$E_{iT} = \frac{1}{N_s}\int_0^{T_t} (V_i \times I_i)\, dt \tag{4.1}$$

$$E_{iM} = e_s E_{iT} \tag{4.2}$$

where, E_{iT} is the total (electrical) motor energy input; N_s is the number of walking steps; V_i is the input voltage to the motor; I_i is the input current to the motor, and T_t is the total time of all walking steps. E_{iM} is the mechanical motor energy input, and e_s is the efficiency of the geared DC motor.

4.4.2 Coordination between the hip-actuation, foot-contact switch, and spring-loaded knee-latch

Spring-loaded knee-latch plays a very important role for both the stance and swing legs. For the stance leg, it helps the leg to stay standstill during walking, and prevents the knee of the swing leg from being bent at or after heel-strike. However, at the beginning of each gait, the knee of the swing leg needs to be flexed for the sake of foot clearance, and to avoid foot scuffing at the midstance. Therefore, right after heel-strike is detected by the foot-contact switch, the spring-loaded knee-latch is disengaged by a DC solenoid. Afterward, the hyperextension limit of the shank, which was already locked by the spring-loaded latch bolt, is free to flex.

It is very important that the motor must inject energy after the knee-latch is disengaged. The order is very important, because if the motor injects energy to the system, while the knee-latch is still engaged, both legs will be scuffed on the ground, and the robot will fall.

As a result, when the foot-contact switch is triggered by heel-strike, firstly the DC solenoid of the opposite leg is activated for about $0.15\,(sec)$, and the hip-actuation will

then be activated. Such a timing has been obtained by trials and errors such that: firstly, a proper foot clearance is achieved at about midstance; secondly, posture "**4**" shown in Figure 4.7 is achieved, where the latch bolt is retracted at its default position (after the solenoid is turned off), and the hyperextension limit engages with it. As a result of such an action, the knee is locked at a proper timing which is at right before heel-strike. For about $0.15\,(sec)$, the solenoid needs a voltage of about $12\,(V)$ and a current of about $1.4\,(A)$. As a result, the solenoid consumes $2.52\,(J)$ to function properly.

4.4.3 Foot size and friction

As it was mentioned before, the main reason for the round-shape foot is because it helps the stance leg of a biped rolling forwards on the ground [12,15,18]. However, two challenges about round-foot need to be addressed: firstly, the foot size has to be adjusted; a big foot can cause the leg to slide on the ground, and postpone foot-clearance during walking; secondly, the friction of the foot needs to be adjusted by using a thin-compliant pad underneath the foot where it contacts with the ground.

4.4.4 Boom effects on the prototype's dynamics and a safety rope

The boom restricts the yaw motion of the robot. As a result, the robot can walk along a circular path, similar to a 2D gait. However, the boom introduces uncertainties to the robot motion, particularly the hip joint where the boom is connected to the robot.

The boom is light and weights less than $0.5\,(kg)$. Figure 4.9 shows a snapshot of the robot which is falling on the ground, while is attached to the boom. As a result, there is a safety rope, only attached loosely to the outer end of the hip shaft, in order to avoid the robot hitting the ground, while falling. The rope has no interference on the robot walking. It will be clarified through the analysis of experimental data later in the next section.

Figure 4.9: Snapshot of the robot which is falling on the ground, while is attached to the boom.

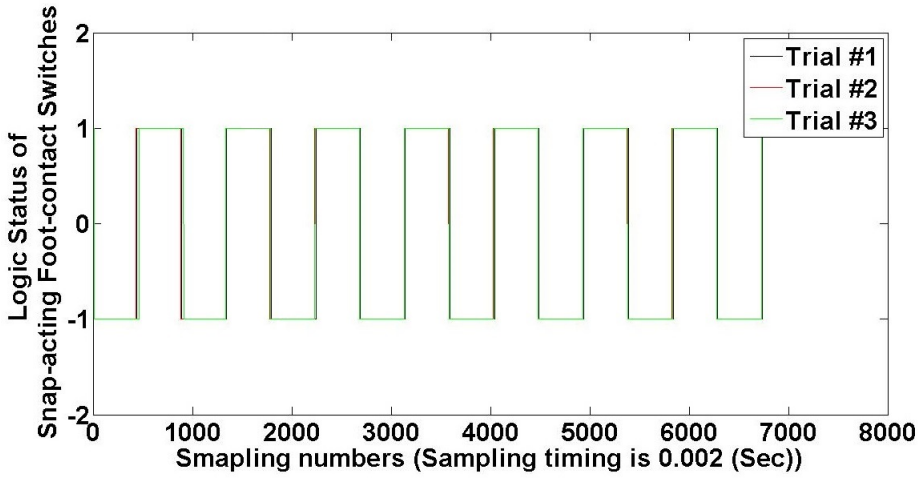

Figure 4.10: Snap-acting foot-contact switches for three experimental walking trails.

4.4.5 Prototype walking on the flat ground; gait measurements and properties

The passive-based bipedal robot, shown in Figure 4.2, has shown multiple successful gaits. Sixteen walking steps of each of three trials have been chosen to be analyzed.

Figure 4.10 shows the timing of the snap-acting foot-contact switches. The digital signal of the switches is indicated by "1", and signs + or − are denoted to the right and the left foot. The horizontal axis shows sampling numbers. Referring to the figure, all

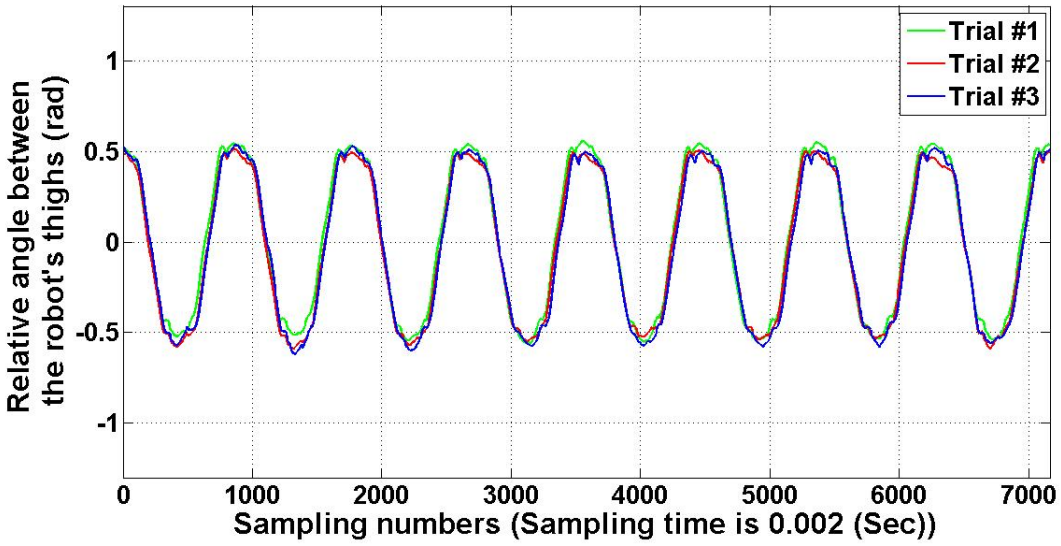

Figure 4.11: Relative angle between the two thighs for three experimental walking trials.

three trials show highly repeatable gaits with an average step period of about $0.90\,(sec)$. The difference in timing of the heel strikes for each walking step for all three trials is less than $0.01(sec)$. Figure 4.11 shows the relative angle between two thighs of the robot for all three trials. This figure shows that all three gaits are of a limit-cycle.

Referring to Figure 4.11 and physical measurements via a tape measure, an average step length of the limit-cycle gait of the three trials is about $0.44\,(m)$. As a result, the average walking speed, which is defined as the average step length divided by the average step period, is about $0.49\,(\frac{m}{s})$. Since the robot height is about $0.5\,(m)$, the Froude number of the prototype[1] is 0.22. This Froude number shows that the gait of our prototype is highly dynamic, compared to Cornell's and Delft's passive-based bipedal robots (their Froude numbers are about 0.16) [18, 19].

Figure 4.12 shows the continuous electrical power of the DC motor. It has been obtained by multiplying the motor input voltage (including amplifier's gain) to the motor input

[1]The Froude number is defined as a nondimensional measure for walking velocity, and is calculated by dividing walking velocity over the square root of the leg length times the gravitational acceleration. Please see Section 3.4.2.

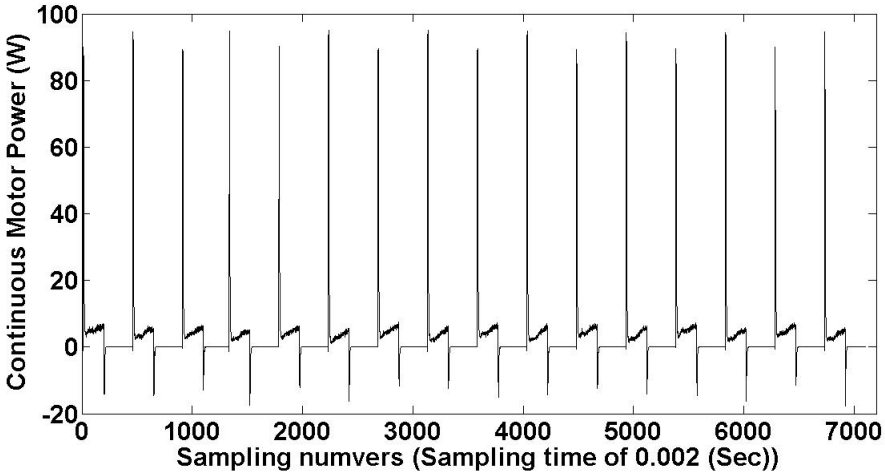

Figure 4.12: Electrical power needed by the compliant hip-actuation mechanism for walking.

current. Figure 4.12 is indeed an experimental proof of the coordination between the natural dynamics and energy. Such a characteristic is the goal of the compliant hip-actuation mechanism. The energy input stores through the hip spring during the first 40% of the gait cycle without suppressing the natural dynamics of the hip joint. The rest of the gait cycle, the robot is walking free of energy cost.

In the literature, the efficiency of bipedal robots is reported via the total (electrical) cost of transport c_{et} and the mechanical cost of transport c_{mt} [4, 12, 15, 18, 19, 28]. Low cost of transport implies high energy efficiency. The mechanical cost of transport is the amount of mechanical power consumption per weight per walking speed, and the total (electrical) cost of transport is the amount of electrical power consumption per weight per walking speed.

After applying Eq. 4.1 in Section 4.4.1 to the data of Figure 4.12, the average electrical energy of the hip actuation during each walking step is about $2.35\,(J)$. Having the motor efficiency of 0.88 and the gearbox efficiency of 0.60, the efficiency of the motor and the gearbox is 0.5280 (the motor efficiency multiplies by the gearbox efficiency [84]). Accordingly, the average mechanical energy required by the motor during each walking step is

about $1.35\,(J)$.

Therefore, the mechanical cost of transport of the passive-based bipedal robot shown in Figure 4.2 is about 0.063. This mechanical cost of transport is the same as that of a passive-based machine [12], walking on a ramp with slope about 3.5 degree. The mechanical cost of transport of Cornell's, Delft's, Honda's ASIMO, and a human are 0.055, 0.08, 1.6, and 0.05, respectively. As a result, our physical robot shows to be highly energy efficient, as compared to humans and other bipedal machines in the literature [4, 12, 15, 18, 19, 28].

The total (electrical) cost of transport of the prototype (the motor and the solenoids) is about 0.226. Note that the total cost of transport of Cornell's, Delft's, Honda's ASIMO, and a human are 0.20, 5.3, 3.2, and 0.2, respectively [18]. The total cost of transport of our prototype shows that it is a highly energy efficient machine, as compared to humans and other bipedal machines in the literature [4, 12, 15, 18, 19, 28]. A video clip of our physical robot walking on the flat ground is available at `http://alghooneh.wix.com/mansooralghooneh#!research-experience/c18h9`.

4.5 Summary

This chapter presented the design and development of a physical bipedal robot to experimentally validate the importance of compliant hip-actuation in achieving a highly dynamic and energy efficient walking gait. In this chapter, the mechanical design, actuation, sensing, coordination, and experimentation of the physical bipedal robot were explained. This bipedal machine walks based on the concept of passive-based dynamic walking. It is equipped with a custom-designed compliant hip-actuation mechanism and a custom-designed spring-loaded knee-latch.

The limit-cycle gait of the physical prototype has a step length of about $0.44\,(m)$, a step period of about $0.9\,(sec)$, a Froude number of about 0.22, a mechanical cost of

transport of about 0.063, and a total (electrical) cost of transport of about 0.226. The physical bipedal robot has shown a highly dynamic and energy efficient gait on the flat ground, in comparison with bipedal machines reported in the literature and a human [4, 12, 15, 18, 19, 28].

In conclusion, it is important to point out that this chapter experimentally validated the importance of compliant hip-actuation in achieving a highly dynamic and energy efficient walking gait. The inclusion of compliant-ankle flat-foot in the physical prototype remains as future work.

It is important to point out that although our physical robot can walk with a high dynamic and energy efficient gait, its versatility is quite limited. Our robot with the current mechanical design and the actuation system cannot handle uneven terrains, nor carry a load while walking. To make our robot enable to perform the aforementioned tasks, there is a need for improvement in its mechanical design and actuation system. For example, using a flat-foot instead of a round-foot as well as an event-based control can be a good start to improve the robot versatility to walk on uneven terrains. Furthermore, using a knee-actuation and a stronger hip-actuation can enable the robot to carry a load while walking. Other strategies can also be studied as future work.

Chapter 5

Conclusions and future work

5.1 Conclusions

Comprehensive simulation and experimental explorations into bipedal walking have been carried out to provide mechanical insights into bipedal walking in terms of gait characteristics and energy efficiency.

The conclusions of this thesis are summarized here:

1. A novel systematic trajectory-controlled gait-planning framework was presented to provide mechanical insights into bipedal walking in terms of gait characteristics (dynamic gait) and energy efficiency. The framework negotiated three biomechanically motivated characteristics: the gait repeatability, postural balance, and highly regulated centroidal angular momentum throughout the gait cycle. The proposed framework improved the energy efficiency of bipedal gaits, relative to available trajectory-controlled approaches [1–11].

2. A novel passive-based bipedal walking mathematical model with complaint-ankle flat-foot was developed to provide mechanical insights into bipedal walking in terms of gait characteristics and energy efficiency. The model was actively assisted by

compliant hip-actuation to enable walking on the flat ground. The impedance of each ankle was adjusted by two springs, one at the backside and the other at the frontside, and one damper. Poincare mapping was utilized to extract all possible stable limit-cycle gaits for various ankle stiffness. New limit-cycle gaits were presented, and all are versatile, dynamic, and energy efficient, similar to humans' [4, 12, 15, 18, 19, 28]. It was then explored how two-sided ankle stiffness influences the performance of bipedal walking, as compared with uniform ankle stiffness. As a result of such an exploration, the following conclusions were drawn:

- for uniform ankle stiffness, when the ankle stiffness increases, the walking speed and the energy efficiency decrease. Furthermore, the sensitivity of gait properties, such as speed and efficiency, to the rate of change in the ankle stiffness is considerable.
- for two-sided ankle stiffness (before single-support heel-off occurs), when the ankle stiffness increases, the walking speed increases, but still the energy efficiency decreases.
- for two-sided ankle stiffness (after single-support heel-off occurs), not only the walking speed increases considerably, but also the energy efficiency improves significantly.

3. Based on mechanical insights that have been achieved by the aforementioned passive-based model, a physical bipedal robot has been designed and fabricated to experimentally validate the importance of compliant hip-actuation in achieving a highly dynamic and energy efficient walking gait. This machine can walk based on the concept of passive-based dynamic walking. The robot is equipped with a custom-designed compliant hip-actuation mechanism and a custom-designed spring-loaded knee-latch. Its gait is on the flat ground, highly dynamic, and energy efficient, as compared with

available bipedal machines in the literature and a human [4, 12, 15, 18, 19, 28]

5.2 Future work

The outlines of future work are described below:

1. The performance of trajectory-controlled gait-planning methods in terms of gait characteristics and energy efficiency can further be improved, if a new stability/balance measure is developed such that stringent restrictions due to ZMP regulation can be removed. Such a new measure can also take advantage of the concept of passive-based bipedal walking. A good start can be the work done in [85].

2. A control algorithm can be developed for the comprehensive mathematical model developed in Chapter 3, such that the algorithm can actively tune the stiffness at the ankles and the hip during motion.

3. A variable compliant hip-actuation mechanism can be designed and developed for the physical robot in Chapter 4. Such a mechanism can tune and control the properties of gaits in real-time, changing the hip spring stiffness, while walking.

4. A compliant knee-actuation mechanism can be designed and developed for the knee of the physical robot in Chapter 4. This mechanism can actively tune the knee motion, while using the knee natural dynamics and keeping energy cost low.

5. A compliant-ankle flat-foot can be designed and developed for the physical robot in Chapter 4. Such a foot can experimentally validate the interesting results achieved in Chapter 3.

6. An upper body structure can be added to the robot to explore the effects of higher degrees of freedom on the gait characteristics and the energy efficiency.

7. Improvement in the physical prototype to walk on uneven terrains or to walk while carrying a load, using the concept of passive-based walking, can be explored.

Bibliography

[1] G. Cabodevila and G. Abba, "Quasi optimal gait for a biped robot using genetic algorithm," in *IEEE International Conference on Systems, Man, and Cybernetics*, vol. 4, oct 1997, pp. 3960–3965.

[2] T. Arakawa and T. Fukuda, "Natural motion generation of biped locomotion robot using hierarchical trajectory generation method consisting of ga, ep layers," in *IEEE International Conference on Robotics and Automation*, vol. 1, apr 1997, pp. 211–216.

[3] Y. Hurmuzlu, "Dynamics of bipedal gait; part i: Objective functions and the contact event of a planar five-link biped," *ASME Journal of Applied Mechanics*, vol. 60, pp. 331–336, 1993.

[4] K. Hirai, M. Hirose, Y. Haikawa, and T. Takenaka, "The development of honda humanoid robot," in *IEEE International Conference on Robotics and Automation*, vol. 2, may 1998, pp. 1321–1326.

[5] D. Tlalolini, C. Chevallereau, and Y. Aoustin, "Comparison of different gaits with rotation of the feet for a planar biped," *Robotics and Autonomous Systems*, vol. 57, no. 4, pp. 371–383, 2009.

[6] C. Chevallereau and Y. Aoustin, "Optimal reference trajectories for walking and running of a biped robot," *Robotica*, vol. 19, pp. 557–569, August 2001.

[7] Q. Huang, K. Yokoi, S. Kajita, K. Kaneko, H. Arai, N. Koyachi, and K. Tanie, "Planning walking patterns for a biped robot," *IEEE Transactions on Robotics and Automation*, vol. 17, no. 3, pp. 280–289, jun 2001.

[8] S. Kajita, F. Kanehiro, K. Kaneko, K. Fujiwara, K. Harada, K. Yokoi, and H. Hirukawa, "Biped walking pattern generation by using preview control of zero-moment point," in *Proceedings IEEE International Conference on Robotics and Automation*, vol. 2, sept. 2003, pp. 1620–1626.

[9] B. Vanderborght, B. Verrelst, R. V. Ham, M. V. Damme, D. Lefeber, B. M. Y. Duran, and P. Beyl, "Exploiting natural dynamics to reduce energy consumption by controlling the compliance of soft actuators," *The International Journal of Robotics Research*, vol. 25, no. 4, 2006.

[10] G. Dip, V. Prahlad, and P. Kien, "Genetic algorithm-based optimal bipedal walking gait synthesis considering tradeoff between stability margin and speed," *Robotica*, vol. 27, pp. 355–365, 2008.

[11] G. Dip, V. Prahlad, and P. D. Kien, "Genetic algorithm-based optimal bipedal walking gait synthesis considering tradeoff between stability margin and speed," *Robotica*, vol. 27, no. 03, pp. 355–365, 2009.

[12] T. McGeer, "Passive dynamic walking," *International Journal of Robotics Research*, vol. 9, pp. 68–82, 1990.

[13] K. Hirai, M. Hirose, Y. Haikawa, and T. Takenaka, "The development of the honda humanoid robot," in *IEEE International Conference Robotics and Automation,*, 1998, pp. 1321–1326.

[14] "Asimo is climbing stairs: https://www.youtube.com/watch?v=mnhchs13wji," http://advanced-education.com/educators/products/nao-robot/?gclid=CMXWssGWk8ACFQszaQodrCoAZg.

[15] S. Collins, M. Wisse, and A. Ruina, "A three-dimensional passive-dynamic walking robot with two legs and knees," *International Journal of Robotics Research*, vol. 20, no. 7, pp. 607–615, 2001.

[16] S. Hashimoto, S. Narita, H. Kasahara, H. Shirai, and T. Kobayashi, "Humanoid robots in waseda university hadaly-2 and wabian," *Autonomous Robots*, vol. 12, no. 1, pp. 25–38, 2002.

[17] M. Wisse and J. van Frankenhuyzen, "Design and construction of mike; a 2d autonomous biped based on passive dynamic walking," in *Conference Adaptive Motion of Animals and Machines*, 2003.

[18] S. Collins and A. Ruina, "A bipedal walking robot with efficient and human-like gait," in *Proceedings of IEEE International Conference on Robotics and Automation*, 2005, pp. 1983 – 1988.

[19] M. Wisse, G. Feliksdal, J. Van Frankkenhuyzen, and B. Moyer, "Passive-based walking robot; denise, a simple, efficient and lightweight biped," *IEEE Robotics Automation Magazine*, vol. 14, no. 2, pp. 52–62, 2007.

[20] M. Alghooneh and C. Wu, "A systematic gait-planning framework negotiating biomechanically motivated characteristics of a planar bipedal robot," *International Journal of Humanoid Robotics*, vol. 9, no. 4, 2012.

[21] ——, "Single-support heel-off, a crucial gait event helps achieving energy efficient and agile bipedal walking," *Robotica*, vol. in press, 2014.

[22] ——, "A systematic framework for the gait planning of a five-link bipedal robot," *CSME congress*, 2012.

[23] M. Alghooneh and C. Q. Wu, "Effects of compliant ankles on gait characteristics of flat-feet limit-cycle walkers," in *Dynamic Walking*, 2013.

[24] K. Kaneko, F. Kanehiro, and S. Kajita, "Humanoid robot hrp-2," *IEEE International Conference on Robotics and Automation*, pp. 1083–1090, 2004.

[25] J. Anderson, J. Baltes, and C. T. Cheng, "Robotics competitions as benchmarks for ai research," *The Knowledge Engineering Review*, vol. 26, pp. 11–17, 2011.

[26] K. Rushdi, D. Koop, and C. Q. Wu, "Experimental study on passive dynamic bipedal walking: Comparing test platforms and effects of parameter changes on gait patterns," in *ASME Dynamic Systems and Control Conference*, 2011, pp. 87–94.

[27] G. Pratt, "Low impedance walking robots," *Integrative and Comparative Biology*, vol. 42, pp. 174–181, 2002.

[28] T. McGeer, "Low-bandwidth reflex-based control for lower power walking: 65 km on a single battery charge," *International Journal of Robotics Research*, vol. in press, 2014.

[29] M. Vukobratovic, B. Borovac, D. Surla, and D. Stokic, *Biped Locomotion Dynamic, Stability, Control and Application*. springer-verlag, 1990.

[30] C. Iverach-Brereton, J. Baltes, J. Anderson, A. Winton, and D. Carrier, "Gait design for an ice skating humanoid robot," *Robotics and Autonomous Systems*, vol. 62, pp. 306–318, 2014.

[31] "Nao bipedal robot: http://advanced-education.com/educators/products/nao-robot/?gclid=cmxwssgwk8acfqszaqodrcoazg," http://advanced-education.com/educators/products/nao-robot/?gclid=CMXWssGWk8ACFQszaQodrCoAZg.

[32] H. Elftman, "The measurment of the external force in walking," *Science*, vol. 88, no. 2276, pp. 152–153, 1938.

[33] M. Vukobratovic, A. A. Frank, and D. Juricic, "On the stahility of biped locomotion," *IEEE Transactions on Biomedical Engineering*, vol. 17, no. 1, pp. 25–36, 1970.

[34] M. Vukobratovic and B. Borovac, "Zero-moment point, thirty five years of its life," *International Journal of Humanoid Robotics*, vol. 1, no. 1, pp. 147–173, 2004.

[35] A. D. Kuo, "Energetics of actively powered locomotion using the simplest walking model," *Journal of Biomedical Engineering*, vol. 124, no. 1, pp. 113–120, 2002.

[36] A. Takhmar, M. Alghooneh, K. Alipour, and S. A. A. Moosavian, "Mhs measure for postural stability monitoring and control of biped robots," in *IEEE/ASME International Conference on Advanced Intelligent Mechatronics*, july 2008, pp. 400–405.

[37] P. V. D. M. D. A. v. H. R. L. D. Versluys, Rino; Beyl, "Prosthetic feet: State-of-the-art review and the importance of mimicking human ankle-foot biomechanics," *Disability and Rehabilitation: Assistive Technology*, vol. 4, no. 2, pp. 65–75, 2009.

[38] "Asimo is walking on level ground with bent knees: https://www.youtube.com/watch?v=xftlje1uw14," http://advanced-education.com/educators/products/nao-robot/?gclid=CMXWssGWk8ACFQszaQodrCoAZg.

[39] S. Kajita, F. Kanehiro, K. Kaneko, K. Fujiwara, K. Harada, K. Yokoi, and H. Hirukawa, "Resolved momentum control: humanoid motion planning based on the

linear and angular momentum," in *Proceedings. IEEE/RSJ International Conference onIntelligent Robots and Systems*, vol. 2, oct. 2003, pp. 1644–1650.

[40] H. Hemami and R. L. Rarnsworth, "Postural and gait stability of a planar five link biped by simulation," *IEEE Transactions on Automatic Control*, vol. 22, pp. 452–458, 1977.

[41] D. Tolani, A. Goswami, and N. I. Badler, "Real-time inverse kinematics techniques for anthropomorphic limbs," *Graphical Models*, vol. 62, pp. 353–388, 2000.

[42] J. Kierzenka and L. F. Shampine, "A bvp solver based on residual control and the matlab pse," *ACM TOMS*, vol. 27, no. 3, pp. 299–316, 2001.

[43] S. A. A. Moosavian, M. Alghooneh, and A. Takhmar, "Cartesian approach for gait planning and control of biped robots on irregular surfaces," *International Journal of Humanoid Robotics*, vol. 6, no. 4, pp. 675–697, 2009.

[44] S. A. A. Moosavian, A. Takhmar, and M. Alghooneh, "Regulated sliding mode control of a biped robot," in *International Conference on Mechatronics and Automation*, aug. 2007, pp. 1547–1552.

[45] J. H. Choi and J. W. Grizzle, "Planar bipedal walking with foot rotation," in *Proceedings of the American Control Conference*, vol. 7, june 2005, pp. 4909–4916.

[46] J. Vermeulen, B. Verrelst, B. Vanderborght, D. Lefeber, and P. Guillaume, "Trajectory planning for the walking biped "lucy"," *International Journal of Robotics Research*, vol. 25, no. 9, pp. 867–887, 2006.

[47] B. Ma and Q. Wu, "Parametric study of repeatable gait for a planar five-link biped," *Robotica*, vol. 20, pp. 493–498, September 2002.

[48] Q. Wu and C. Y. Chan, "Design of joint angle profiles for a planar five-link bipedal system," *ASME the Dynamic Systems, Measurement, and Control*, vol. 127, pp. 192–196, 2005.

[49] X. Mu and Q. Wu, "On impact dynamics and contact events for biped robots via impact effects," *IEEE Transactions on Systems, Man, and Cybernetics, Part B*, vol. 36, no. 6, pp. 1364–1372, dec. 2006.

[50] A. Goswami, "Postural stability of biped robots and the foot-rotation indicator (fri) point," *The International Journal of Robotics Research*, vol. 18, no. 6, pp. 523–533, 1999.

[51] M. Vukobratovic and B. Borovac, "Zero-moment point, thirty five years of its life," *International Journal of Humanoid Robotics*, vol. 1, no. 1, pp. 147–173, 2004.

[52] M. B. Popovic, A. Goswami, and H. Herr, "Ground reference points in legged locomotion: Definitions, biological trajectories and control implications," *The International Journal of Robotics Research*, vol. 24, no. 12, pp. 1013–1032, 2005.

[53] M. Popovic, A. Hofmann, and H. Herr, "Angular momentum regulation during human walking: biomechanics and control," in *Proceedings of the IEEE International Conference on Robotics and Automation*, 2004, pp. 2405–2411.

[54] M. Popovic, W. Gu, and H. Herr, "conservation of angular momentum in human movement," *Research Abstract*, pp. 264–265, 2002.

[55] A. Goswami and V. Kallem, "Rate of change of angular momentum and balance maintenance of biped robots," in *Proceedings of the 2004 IEEE International Conference on Robotics and Automation*, april 2004, pp. 3785–3790.

[56] M. Popovic, A. Hofmann, and H. Herr, "Zero spin angular momentum control: definition and applicability," in *Proceedings of the IEEE-RAS/RSJ International Conference on Humanoid Robots*, 2004, pp. 478–493.

[57] J. Pratt, J. Carff, S. Drakunov, and A. Goswami, "Capture point: A step toward humanoid push recovery," in *6th IEEE-RAS International Conference on Humanoid Robots*, dec. 2006, pp. 200–207.

[58] J. H. Park, "Impedance control for biped robot locomotion," *IEEE Transactions on Robotics and Automation*, vol. 17, pp. 870–882, dec. 2001.

[59] A. Goswami, B. Espiau, and A. Keramane, "Limit cycles in a passive compass gait biped and passivity-mimicking control laws," *Autonomous Robots*, vol. 4, no. 3, pp. 273–286, 1997.

[60] M. Garcia, A. Chatterjee, A. Ruina, and M. Coleman, "The simplest walking model: Stability, complexity, and scaling," *Journal of Biomedical Engineering*, vol. 120, no. 2, pp. 281–288, 1998.

[61] A. D. Kuo, "Choosing your steps carefully," *IEEE Robotics and Automation Magazine*, vol. 14, no. 2, pp. 18–29, 2007.

[62] M. Kwan and M. Hubbard, "Optimal foot shape for a passive dynamic biped," *Journal of Theoretical Biology*, vol. 248, no. 2, pp. 331–339, 2007.

[63] D. Koop and C. Q. Wu, "Passive dynamic biped walking-part i: Development and validation of an advanced model," *Journal of Computational and Nonlinear Dynamics*, vol. 8, no. 4, 2013.

[64] ——, "Passive dynamic biped walking-part ii: Stability analysis of the passive dynamic gait," *Journal of Computational and Nonlinear Dynamics*, vol. 8, no. 4, 2013.

[65] Y. Huang, L. Wang, B. Chen, G. Xie, and L. Wang, "Modeling and gait selection of passivity-based seven-link bipeds with dynamic series of walking phases," *Robotica*, vol. 30, pp. 39–51, 2012.

[66] Y. Huang, B. Vanderborght, R. Van Ham, Q. Wang, M. Van Damme, G. Xie, and D. Lefeber, "Step length and velocity control of a dynamic bipedal walking robot with adaptable compliant joints," *IEEE/ASME Transactions on Mechatronics*, pp. 1–14, 2012.

[67] Y. Huang and Q. Wang, "Gait selection and transition of passivity-based bipeds with adaptable ankle stiffness," *International Journal of Advanced Robotic Systems*, vol. 9, 2012.

[68] D. Hobbelen and M. Wisse, "Ankle actuation for limit cycle walkers," *International Journal of Robotics Research*, vol. 27, no. 6, pp. 709–735, 2008.

[69] Q. Wang, Y. Haikawa, and L. Wang, "Passive dynamic walking with flat feet and ankle compliance," *Robotica*, vol. 28, pp. 413–425, 2010.

[70] Q. Li, A. Takanishi, and I. Kato, "Learning control for a biped walking robot with a trunk," in *IEEE/RSJ International Conference on Intelligent Robots and Systems*, vol. 3, jul 1993, pp. 1771–1777.

[71] B. Vanderborght, B. Verrelst, R. V. Ham, M. V. Damme, and D. Lefeber, "Objective locomotion parameters based inverted pendulum trajectory generator," *Robotics and Autonomous Systems*, vol. 56, no. 9, pp. 738–750, 2008.

[72] O. Stasse, B. Verrelst, B. Vanderborght, and K. Yokoi, "Strategies for humanoid robots to dynamically walk over large obstacles," *IEEE Transactions on Robotics*, vol. 25, no. 4, pp. 960–967, aug. 2009.

[73] S. Tzafestas, M. Raibert, and C. Tzafestas, "Robust sling-mode control applied to a 5-link biped robot," *Journal of Intelligent and Robotic Systems*, vol. 15, pp. 67–133, 1996.

[74] C. Zhu, Y. Tomizawa, X. Luo, and A. Kawamura, "Biped walking with variable zmp, frictional constraint, and inverted pendulum model," in *IEEE International Conference on Robotics and Biomimetics*, aug. 2004, pp. 425–430.

[75] G. S. Sawicki, C. L. Lewis, and D. P. Ferris, "It pays to have a spring in your step," *Exercise and Sport Sciences Reviews*, vol. 37, pp. 130–150, 2009.

[76] G. P. Ostermeyer, "On the dynamics of the friction coefficient," *Wear*, vol. 254, pp. 852–858, May 2003.

[77] D. T. Greenwood, *Advanced Dynamics*. Cambridge University Press, 2003.

[78] X. Mu and C. Q. Wu, "On impact dynamics and contact events for biped robots via impact effects," *IEEE Transactions on Systems, Man and Cybernetics*, vol. 36, no. 6, pp. 1364–1372, 2006.

[79] ——, "On post-impact angular velocities and resultant impulses with rank-deficient jacobian matrices using newton impact law," *International Journal of Applied Mechanics*, vol. 2, no. 3, 2010.

[80] M. Wisse and A. L. Schwab, "First steps in passive dynamic walking," pp. 745–756, 2005.

[81] D. Hobbelen and M. Wisse, "Controlling the walking speed in limit cycle walking," *International Journal of Robotics Research*, vol. 27, no. 9, pp. 989–1005, 2008.

[82] M. Wisse, A. L. Schwab, R. Q. van der Linde, and F. C. T. van der Helm, "How to keep from falling forward: Elementary swing leg action for passive dynamic walkers," *IEEE Transactions on Robotics*, vol. 21, no. 3, pp. 393–401, 2005.

[83] E. R. Westervelt, J. W. Grizzle, and D. E. Koditschek, "Hybrid zero dynamics of planar biped walkers," *IEEE Transactions on Automatic Control*, vol. 48, no. 1, pp. 42–56, 2003.

[84] S. Cetinkunt, *Mechatronics*. John Wiley, 2007.

[85] F. Firmani and E. Park, "Theoretical analysis of the state of balance in bipedal walking," *Journal of Biomechanical Engineering*, vol. 135, 2013.

Appendix A.

The general form of the dynamic equations of the bipedal model explained in Chapter 2 have already presented in Section 2.1. Here, the details of the matrices D, H, and G are presented. The size of all three matrices are of 5×5.

$$D = \begin{bmatrix} D_{11} & D_{12} & D_{13} & D_{14} & D_{15} \\ D_{21} & D_{22} & D_{23} & D_{24} & D_{25} \\ D_{31} & D_{32} & D_{33} & D_{34} & D_{35} \\ D_{41} & D_{42} & D_{43} & D_{44} & D_{45} \\ D_{51} & D_{52} & D_{53} & D_{54} & D_{55} \end{bmatrix}$$

$$D_{11} = I_1 + l_1^2 m_2 + l_1^2 m_3 + l_1^2 m_4 + l_1^2 m_5 + d_1^2 m_1$$

$$D_{12} = l_1 cos(\theta_1 - \theta_2)(l_2 m_3 + l_2 m_4 + l_2 m_5 + d_2 m_2)$$

$$D_{13} = l_1 d_3 m_3 cos(\theta_1 - \theta_3)$$

$$D_{14} = l_1 cos(\theta_1 - \theta_4)(l_4 m_5 + d_4 m_4)$$

$$D_{15} = l_1 d_5 m_5 cos(\theta_1 - \theta_5)$$

$$D_{21} = D_{12}$$

$$D_{22} = I_2 + l_2^2 m_3 + l_2^2 m_4 + l_2^2 m_5 + d_2^2 m_2$$

$$D_{23} = l_2 d_3 m_3 cos(\theta_2 - \theta_3)$$

$$D_{24} = l_2 cos(\theta_2 - \theta_4)(l_4 m_5 + d_4 m_4)$$

$$D_{25} = l_2 d_5 m_5 cos(\theta_2 - \theta_5)$$

$$D_{31} = D_{13}$$

$$D_{32} = D_{23}$$

$$D_{33} = m3 * lc3^2 + I3$$

$$D_{34} = 0$$

$$D_{35} = 0$$

$$D_{41} = D_{14}$$

$$D_{42} = D_{24}$$

$$D_{43} = D_{34}$$

$$D_{44} = m_5 l_4^2 + m_4 d_4^2 + I_4$$

$$D_{45} = l_4 d_5 m_5 cos(\theta_4 - \theta_5)$$

$$D_{51} = D_{15}$$

$$D_{52} = D_{25}$$

$$D_{53} = D_{35}$$

$$D_{54} = D_{45}$$

$$D_{55} = D_{55}$$

$$H = \begin{bmatrix} H_{11} & H_{12} & H_{13} & H_{14} & H_{15} \\ H_{21} & H_{22} & H_{23} & H_{24} & H_{25} \\ H_{31} & H_{32} & H_{33} & H_{34} & H_{35} \\ H_{41} & H_{42} & H_{43} & H_{44} & H_{45} \\ H_{51} & H_{52} & H_{53} & H_{54} & H_{55} \end{bmatrix}$$

$$H_{11} = 0$$

$$H_{12} = \dot{\theta}_2 l_1 sin(\theta_1 - \theta_2)(l_2 m_3 + l_2 m_4 + l_2 m_5 + d_2 m_2)$$

$$H_{13} = \dot{\theta}_3 l_1 d_3 m_3 sin(\theta_1 - \theta_3)$$

$$H_{14} = \dot{\theta}_4 l_1 sin(\theta_1 - \theta_4)(l_4 m_5 + d_4 m_4)$$

$$H_{15} = \dot{\theta}_5 l_1 d_5 m_5 sin(\theta_1 - \theta_5)$$

$$H_{21} = -\dot{\theta}_1 l_1 sin(\theta_1 - \theta_2)(l_2 m_3 + l_2 m_4 + l_2 m_5 + d_2 m_2)$$

$$H_{22} = 0$$

$$H_{23} = \dot{\theta}_3 l_2 d_3 m_3 sin(\theta_2 - \theta_3)$$

$$H_{24} = \dot{\theta}_4 l_2 sin(\theta_2 - \theta_4)(l_4 m_5 + d_4 m_4)$$

$$H_{25} = \dot{\theta}_5 l_2 d_5 m_5 sin(\theta_2 - \theta_5)$$

$$H_{31} = -\dot{\theta}_1 l_1 d_3 m_3 sin(\theta_1 - \theta_3)$$

$$H_{32} = -\dot{\theta}_2 l_2 d_3 m_3 sin(\theta_2 - \theta_3)$$

$$H_{33} = 0$$

$$H_{34} = 0$$

$$H_{35} = 0$$

$$H_{41} = -\dot{\theta}_1 l_1 sin(\theta_1 - \theta_4)(l_4 m_5 + d_4 m_4)$$

$$H_{42} = -\dot{\theta}_2 l_2 sin(\theta_2 - \theta_4)(l_4 m_5 + d_4 m_4)$$

$$H_{43} = 0$$

$$H_{44} = 0$$

$$H_{45} = \dot{\theta}_5 l_4 d_5 m_5 sin(\theta_4 - \theta_5)$$

$$H_{51} = -\dot{\theta}_1 l_1 d_5 m_5 sin(\theta_1 - \theta_5)$$

$$H_{52} = -\dot{\theta}_2 l_2 d_5 m_5 sin(\theta_2 - \theta_5)$$

$$H_{53} = 0$$

$$H_{54} = -\dot{\theta}_4 l_4 d_5 m_5 sin(\theta_4 - \theta_5)$$

$$H_{55} = 0$$

$$G = \begin{bmatrix} G_{11} \\ G_{21} \\ G_{31} \\ G_{41} \\ G_{51} \end{bmatrix}$$

$$G_{11} = -gsin(\theta_1)(l_1 m_2 + l_1 m_3 + l_1 m_4 + l_1 m_5 + d_1 m_1)$$

$$G_{21} = -gsin(\theta_2)(l_2 m_3 + l_2 m_4 + l_2 m_5 + d_2 m_2)$$

$$G_{31} = -gd_3m_3sin(\theta_3)$$

$$G_{41} = -gsin(\theta_4)(l_4m_5 + d_4m_4)$$

$$G_{51} = -gd_5m_5sin(\theta_5)$$

Here, the details of the matrix A are presented:

$$A_{ij} = \begin{cases} I_i + m_i(a_il_i - d_i)^2 + \left(\sum_{k=1}^{i-1} m_k\right) a_il_i & i = j \\ -\left[\left(\sum_{k=1}^{i} m_k\right) a_il_ia_jl_j - m_id_ia_jl_j\right] cos(\theta_i - \theta_j) & j > i \\ \left[\left(\sum_{k=1}^{j} m_k\right) a_il_ia_jl_j - m_jd_ja_il_i\right] cos(\theta_i - \theta_j) & j < i \end{cases}$$

Appendix B.

In Section 2.2.4, the ZMP is a point where the horizontal components of the resultant moment of all gravitational and inertial force, applied to a bipedal robot, become zero. [51] The ZMP equation is presented as follows for the bipedal robot shown in Figure 2.1: [51,52]

$$\sum_{i=1}^{N}\left[(\overrightarrow{r_i}-\overrightarrow{r_{zmp}})\times m_i\overrightarrow{a_i}+\frac{d(\overleftrightarrow{I_i}\overrightarrow{\omega_i})}{dt}\right]_{horizontal}$$

$$=[(\overrightarrow{r_{CM}}-\overrightarrow{r_{zmp}})\times M\overrightarrow{g}]_{horizontal}$$

where, $\overrightarrow{r_{zmp}}$ is the position of the ZMP, and $\overrightarrow{r_i}$ is the position of the center of mass of ith link. $\overrightarrow{r_{CM}}$ is the position of the center of mass of the biped. $\overleftrightarrow{I_i}$ is the mass inertia matrix about the center of mass of ith link. ω_i is the angular velocity of ith link. M is the total mass of the bipedal robot, and m_i is the mass of ith link. $\overrightarrow{a_i}$ is the acceleration of the center of mass of ith link, and $\ddot{Z}_{cm}$ is the Z-component of $\overrightarrow{a_i}$. $\overrightarrow{g}$ is the gravitational vector $(-g\,\overrightarrow{k})$.

In Section 2.2.5, the CMP is a point where the ground reaction force would have to act to keep CAM conserved. [52] The CMP equation is presented as follows for the bipedal robot shown in Figure 2.1: [52]

$$(\overrightarrow{r_{cmp}}-\overrightarrow{r_{CM}})\times\overrightarrow{R}=\overrightarrow{0}$$

where, $\overrightarrow{r_{cmp}}$ is the position of the CMP, and $\overrightarrow{R}$ is the ground reaction force. The relation

between the CMP and the ZMP is also as: [52]

$$X_{cmp} = X_{zmp} + \frac{\dot{H}_{Gy}}{R_z}$$

$$Y_{cmp} = Y_{zmp} - \frac{\dot{H}_{Gx}}{R_z}$$

$$\overrightarrow{\dot{H}_G} = \sum_{i}^{N} \overrightarrow{\dot{H}_{Gi}} + \sum_{i}^{N} (\overrightarrow{r_{CM}} - \overrightarrow{r_{CMi}}) \times m_i \overrightarrow{a_i}$$

where, X_{zmp}, Y_{zmp}, X_{cmp}, and Y_{cmp} are the X- and Z-components of the ZMP and the CMP, respectively. $\dot{H}_{Gx}$ and $\dot{H}_{Gy}$ are the X- and Z- components of the rate of change of CAM of the biped, respectively. $\overrightarrow{\dot{H}_G}$ and $\overrightarrow{\dot{H}_{Gi}}$ are the rate of change of CAM of the biped and ith link, projected to the inertia coordinate frame, respectively. R_z is the Z-component of the ground reaction force. $\overrightarrow{r_{CMi}}$ is the position of center of mass of ith link.

In Section2.2.6, M^*_{ij}, C^*_{ij}, and G^*_{ij} are presented as follows:

$$M^*_{11} = (X_{hip} - X_{zmp})\, M\, (3AX^2_{hip} + 2BX_{hip} + C) - M\, Z_{hip}$$

$$M^*_{12} = (x_{ankle} - X_{zmp})\, m\, (4Ax^3_{ankle} + 3B^{'} x^2_{ankle} + 2C^{'} x_{ankle} + D^{'}) - m\, z_{ankle}$$

$$M^*_{21} = -(X_{hip} - X_G)\, M\, (3AX^2_{hip} + 2BX_{hip}) + (Z_{hip} - Z_G)\, M$$

$$M^*_{22} = -(x_{ankle} - X_G)\, m\, (4A^{'} x^3_{ankle} + 3B^{'} x^2 + 2C^{'} x + D^{'}) + (z_{ankle} - Z_G)$$

$$C^*_{11} = (X_{hip} - X_{zmp})\, M\, (6AX_{hip} + 2B)$$

$$C_{12}^{*} = (x_{ankle} - X_{zmp})\, m\, (12A^{'} x_{ankle}^{2} + 6B^{'} x_{ankle} + 2C^{'})$$

$$C_{21}^{*} = (X_{hip} - X_{G})\, M\, (3AX_{hip} + 2B + C)\, \dot{X}_{hip}$$

$$C_{22}^{*} = (x_{ankle} - X_{G})\, m\, (12A^{'} x_{ankle}^{2} + 6B^{'} x_{ankle} + 2C^{'})$$

$$G_{11}^{*} = M\, g\, (X_{hip} - X_{zmp}) + m\, g\, (x_{ankle} - X_{zmp}) - mgX_{zmp}$$

$$G_{21}^{*} = -\dot{H}_{G}$$

Appendix C.

The general form of the dynamic equations of the bipedal model explained in Chapter 3 have already presented in Section 3.3. Here, the details of the matrices M, C, and G are presented. The size of all three matrices are of 6×6.

$$M = \begin{bmatrix} M_{11} & M_{12} & M_{13} & M_{14} & M_{15} & M_{16} \\ M_{21} & M_{22} & M_{23} & M_{24} & M_{25} & M_{26} \\ M_{31} & M_{32} & M_{33} & M_{34} & M_{35} & M_{36} \\ M_{41} & M_{42} & M_{43} & M_{44} & M_{45} & M_{46} \\ M_{51} & M_{52} & M_{53} & M_{54} & M_{55} & M_{56} \\ M_{61} & M_{62} & M_{63} & M_{64} & M_{65} & M_{66} \end{bmatrix}$$

$$M_{11} = 2m_f + m_h + 2m_l l$$

$$M_{12} = 0$$

$$M_{13} = cos(\theta_1)(lm_f + l_c m_l)$$

$$M_{14} = cos(\theta_2)(lm_f + l_c m_l)$$

$$M_{15} = m_f(h_a cos(\theta_{f1}) - c_f sin(\theta_{f1}))$$

$$M_{16} = m_f(h_a cos(\theta_{f2}) - c_f sin(\theta_{f2}))$$

$$M_{21} = M_{12}$$

$$M_{22} = 2m_f + m_h + 2m_l$$

$$M_{23} = sin(\theta_1)(lm_f + l_c m_l)$$

$$M_{24} = sin(\theta_2)(lm_f + l_c m_l)$$

$$M_{25} = m_f(c_f cos(\theta_{f1}) + h_a sin(\theta_{f1}))$$

$$M_{26} = m_f(c_f cos(\theta_{f2}) + h_a sin(\theta_{f2}))$$

$$M_{31} = M_{13}$$

$$M_{32} = M_{23}$$

$$M_{33} = m_f l^2 + m_l l_c^2$$

$$M_{34} = 0$$

$$M_{35} = lm_f(h_a cos(\theta_1 - \theta_{f1}) + c_f sin(\theta_1 - \theta_{f1}))$$

$$M_{36} = 0$$

$$M_{41} = M_{14}$$

$$M_{42} = M_{24}$$

$$M_{43} = M_{34}$$

$$M_{44} = m_f l^2 + m_l l_c^2$$

$$M_{45} = 0$$

$$M_{46} = lm_f(h_a cos(\theta_2 - \theta_{f2}) + c_f sin(\theta_2 - \theta_{f2}))$$

$$M_{51} = M_{15}$$

$$M_{52} = M_{25}$$

$$M_{53} = M_{35}$$

$$M_{54} = M_{45}$$

$$M_{55} = m_f(c_f^2 + h_a^2)$$

$$M_{56} = 0$$

$$M_{61} = M_{16}$$

$$M_{62} = M_{26}$$

$$M_{63} = M_{36}$$

$$M_{64} = M_{46}$$

$$M_{65} = M_{56}$$

$$M_{66} = m_f(c_f^2 + h_a^2)$$

$$C = \begin{bmatrix} C_{11} & C_{12} & C_{13} & C_{14} & C_{15} & C_{16} \\ C_{21} & C_{22} & C_{23} & C_{24} & C_{25} & C_{26} \\ C_{31} & C_{32} & C_{33} & C_{34} & C_{35} & C_{36} \\ C_{41} & C_{42} & C_{43} & C_{44} & C_{45} & C_{46} \\ C_{51} & C_{52} & C_{53} & C_{54} & C_{55} & C_{56} \\ C_{61} & C_{62} & C_{63} & C_{64} & C_{65} & C_{66} \end{bmatrix}$$

$$C_{11} = 0$$

$$C_{12} = 0$$

$$C_{13} = -\dot{\theta}_1 sin(\theta_1)(lm_f + l_c m_l)$$

$$C_{14} = -\dot{\theta}_2 sin(\theta_2)(lm_f + l_c m_l)$$

$$C_{15} = -m_f \dot{\theta}_{f1}(c_f cos(\theta_{f1}) + h_a sin(\theta_{f1}))$$

$$C_{16} = -m_f \dot{\theta}_{f2}(c_f cos(\theta_{f2}) + h_a sin(\theta_{f2}))$$

$$C_{21} = 0$$

$$C_{22} = 0$$

$$C_{23} = \dot{\theta}_1 cos(\theta_1)(lm_f + l_c m_l)$$

$$C_{24} = \dot{\theta}_2 cos(\theta_2)(lm_f + l_c m_l)$$

$$C_{25} = m_f \dot{\theta}_{f1}(h_a cos(\theta_{f1}) - c_f sin(\theta_{f1}))$$

$$C_{26} = m_f \theta_{f2}(h_a cos(\theta_{f2}) - c_f sin(\theta_{f2}))$$

$$C_{31} = 0$$

$$C_{32} = 0$$

$$C_{33} = B_a$$

$$C_{34} = 0$$

$$C_{35} = -lm_f \dot{\theta}_{f1}(c_f cos(\theta_1 - \theta_{f1}) - h_a sin(\theta_1 - \theta_{f1})) - B_a$$

$$C_{36} = 0$$

$$C_{41} = 0$$

$$C_{42} = 0$$

$$C_{43} = 0$$

$$C_{44} = B_a$$

$$C_{45} = 0$$

$$C_{46} = -lm_f\dot{\theta}_{f2}(c_f cos(\theta_2 - \theta_{f2}) - h_a)sin(\theta_2 - \theta_{f2})) - B_a$$

$$C_{51} = 0$$

$$C_{52} = 0$$

$$C_{53} = lm_f\dot{\theta}_1(c_f cos(\theta_1 - \theta_{f1}) - h_a sin(\theta_1 - \theta_{f1})) - B_a$$

$$C_{54} = 0$$

$$C_{55} = +B_a$$

$$C_{56} = 0$$

$$C_{61} = 0$$

$$C_{62} = 0$$

$$C_{63} = 0$$

$$C_{64} = lm_f\dot{\theta}_2(c_f cos(\theta_2 - \theta_{f2}) - h_a sin(\theta_2 - \theta_{f2})) - B_a$$

$$C_{65} = 0$$

$$C_{66} = B_a$$

$$G = \begin{bmatrix} G_{11} \\ G_{21} \\ G_{31} \\ G_{41} \\ G_{51} \\ G_{61} \end{bmatrix}$$

$$G_{11} = 0$$

$$G_{21} = g(2m_f + m_h + 2m_l)$$

$$G_{31} = K_a\theta_1 + K_h\theta_1 - K_h\theta_2 - K_a\theta_{f1} + glm_f sin(\theta_1) + gl_c m_l sin(\theta_1)$$

$$G_{41} = K_a\theta_2 - K_h\theta_1 + K_h\theta_2 - K_a\theta_{f2} + glm_f sin(\theta_2) + gl_c m_l sin(\theta_2)$$

$$G_{51} = K_a\theta_{f1} - K_a\theta_1 + c_f g m_f cos(\theta_{f1}) + gh_a m_f sin(\theta_{f1})$$

$$G_{61} = K_a\theta_{f2} - K_a\theta_2 + c_f g m_f cos(\theta_2) + gh_a m_f sin(\theta_{f2})$$